ELASTOHYDRODYNAMIC FILM THICKNESS AND TRACTION IN A ROLLING, SPINNING AND SLIDING POINT CONTACT

by

ROBIN RUFUS DUCKWORTH

A thesis submitted for the degree of Doctor of Philosophy of the University of London and also for the Diploma of Imperial College

December, 1976

Department of Mechanical Engineering
Imperial College
London SW7

A B S T R A C T

Measurements of elastohydrodynamic oil film thickness and traction have been obtained for a range of temperatures, loads and bearing material combinations for varying amounts of spinning, sliding and rolling in a point contact.

The use of optical interferometry has permitted a more detailed analysis of traction effects than previously possible.

These investigations provide further support for the hypothesis that at high pressures (0.4→1.6 GPa) in elastohydrodynamic traction, fluids exhibit elastic shear behaviour for small amounts of sliding.

Further evidence is found for limiting shear stress behaviour of fluids under elastohydrodynamic conditions for small amounts of sliding corresponding to mean shear strains of the fluid film in excess of 0.15. A strong correlation is found between the derived mean elastic shear modulus and mean limiting shear stress and it is found that these may be approximately related by a simple theoretical shear strength model.

Strong correlation is found between these results and those for glassy polymers, and it is suggested that the field of solid polymer physics is more closely related to EHD traction than previously assumed.

A C K N O W L E D G E M E N T S

I would like to express my thanks to the following people for their help and advice during the course of this work.

Professor A. Cameron (my supervisor) for his constant encouragement and willingness to discuss problems.

Dr. G.R. Paul, Dr. C.R Gentle and Dr. P.B. Macpherson for their friendly help and interest in this work.

Dr. K.L. Johnson for several interesting discussions of this work.

Mr. R. Dobson and Mr. T. Wymark for their practical help with technical problems.

Miss R. Willox for the care and skill with which she has typed this thesis.

My dear wife, Jane, and Ben, for their sympathy and tolerance.

C O N T E N T S

INDEX TO FIGURES

N O M E N C L A T U R E

Symbols used infrequently are defined in the text.

a	Hertz contact radius
A	area of EHD contact
C	specific heat
E	compressive elastic modulus
G	elastic shear modulus
$\bar{G}$	derived mean effective elastic shear modulus
h	EHD film thickness
h_c	EHD central film thickness
$\bar{h}$	mean EHD film thickness
K	thermal conductivity
m_α	initial gradient of spin traction curve i.e. $m_\alpha = \dfrac{(T_\alpha/N)}{(\omega_s a/N)}$
m_β	initial gradient of sideslip traction curve i.e. $m_\beta = \dfrac{(T_\beta/N)}{(\Delta V/U)}$
n	refractive index
N	normal load
P	pressure
Pmax	maximum Hertz pressure
r	the radius of the ball
R	distance from the centre of the Hertzian contact to the centre of the disc
T	traction force
T_α	traction force arising from spin
T_β	traction force arising from sideslip

U_1, U_2	surface velocities
U	mean rolling speed
V	sideslip velocity
W	weight of ball shaft
x	displacement in the rolling direction
y	displacement at right angles to the rolling direction in the contact plane
z	displacement normal to the contact plane
α	the angle between the axis of rotation of the ball and the plane of the disc (see fig. 2.8)
α'	pressure viscosity coefficient
β	sideslip angle (see fig. 2.8)
γ	shear strain
$\dot{\gamma}$	shear strain rate
η_o	inlet viscosity
$\bar{\eta}$	derived mean effective viscosity
θ	temperature
λ	wavelength of light
ρ	density
σ	Poisson's ratio
τ	shear stress
$\bar{\tau}$	mean limiting shear stress
ω_s	differential spin in the EHD contact
Ω	angular velocity of the disc

INTRODUCTION AND LITERATURE SURVEY

1.1 INTRODUCTION

Lubrication is concerned with the understanding and control of friction and failure in machine elements. In both of these areas the film thickness of the lubricant film formed between bearing surfaces is a very important factor. This is particularly true for elastohydrodynamic conditions where the film thickness is often of the same order as the irregularities of the bearing surfaces.

The present state of knowledge in elastohydrodynamics is such that the formation of elastohydrodynamic oil films is now understood more or less fully, and theory and practice agree quite well up to pressures of about 7×10^8 Pa (10^5 p.s.i.). Current work and the work over the last ten years has been involved with the extension of experimental methods to new arrangements such as "in situ" observation of bearing contacts, or they are to do with explanations of discrepancies between theory and experiment.

Of these discrepancies, the most striking is the fact that traction forces transmitted across EHD lubricant films during sliding of one element relative to the other cannot be predicted. Since the phenomenon of traction is of primary importance in the functioning of rolling contact friction drives such as the Kopp variator and the Perpury gear, an ability to predict the traction for a specific lubricant is important.

1.2 EXPERIMENTAL WORK

Much experimental work has now been completed in the field of traction but little compared with the amount completed on EHD film thickness investigations. A table has been drawn up (see fig.1.1 to show some of the various experimental approaches adopted by researchers and used by theoreticians in this field.

The main categories are as follows:

A. Pure traction

B. Supplementary work on fluids

C. Supplementary traction

A. Pure traction

The standard apparatus for studies of pure elastohydrodynamic traction in line contact, until recently, has been the two disc machine. This apparatus consists of two cylindrical discs pressed together to form what is known as a line contact hertzian deformation of the surfaces. Oil is provided at the inlet and is drawn into the conjunction at the mean peripheral speed of the discs. A difference of speed of the discs shears the oil film in the conjunction. The tangential force at the periphery of the discs is determined by spring dynamometers for different temperatures (θ), pressures (p), and $\overline{U}$ rolling and sliding speeds. Typical traction curves are shown in fig. 1.2. They are obtained by keeping θ, p, U constant and measuring the variation of the traction force T with the sliding speed.

FIG. 1.1

TABLE OE EXPERIMENTAL WORK RELEVANT TO ELASTOHYDRODYNAMIC TRACTION

A PURE TRACTION

(a) LINE CONTACT

CROOK
BELL
JOHNSON
HIRST
DOWSON

(b) POINT CONTACT

SMITH
PLINT
GENTLE

B SUPPLEMENTARY WORK ON FLUIDS

VISCOELASTICITY
BARLOW ET AL

HIGH PRESSURE VISCOMETRY
PAUL
HUTTON

SOLIDIFICATION
JACOBSON

C SUPPLEMENTARY TRACTION

SPINNING POINT CONTACT
POON
JOHNSON
LINGARD

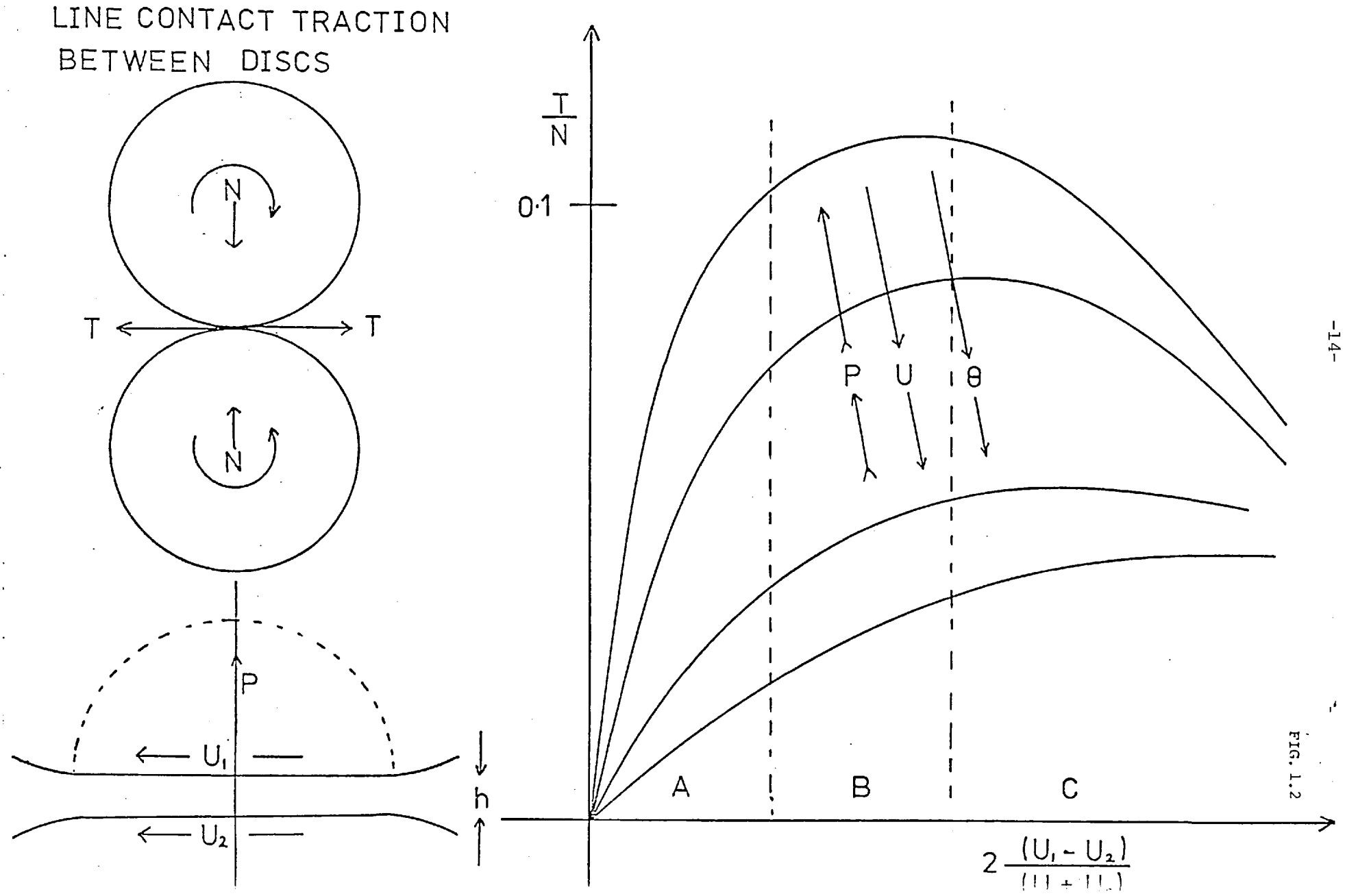
LINE CONTACT TRACTION
BETWEEN DISCS
N
T
T
N
P
U_1
U_2
h
$\frac{T}{N}$
0·1
P
U
θ
A
B
C
$2\frac{(U_1 - U_2)}{(U_1 + U_2)}$

FIG. 1.2

POINT CONTACT TRACTION

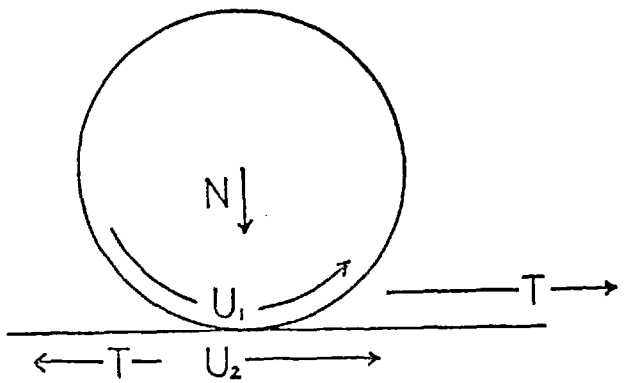

BALL ON PLATE

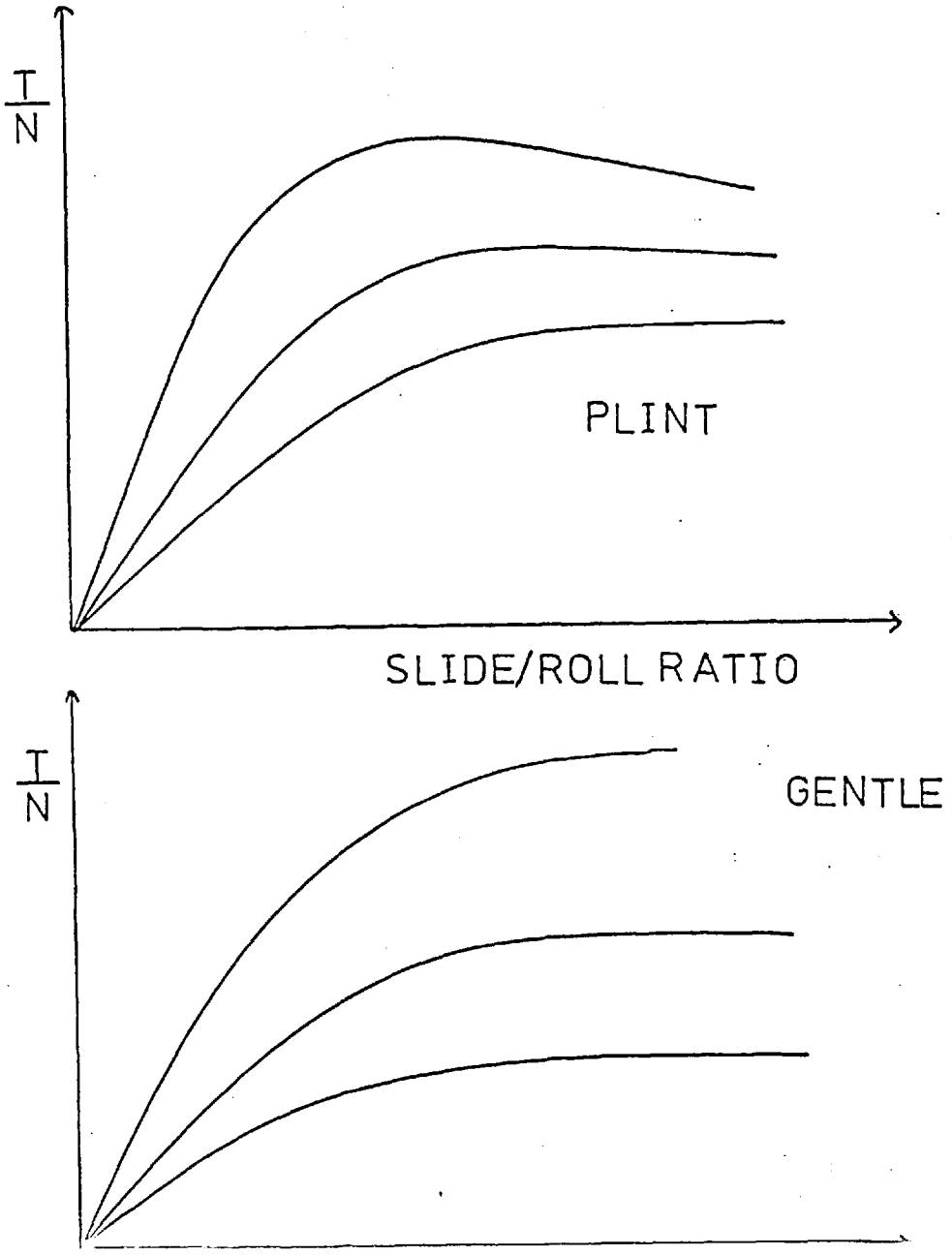

FIG. 1.3

Much controversy was caused by Crook(1) and Smith(2), and to a certain extent by Sasaki, Okomo and Isogai(3). Crook's experiments were performed up to a maximum hertz pressure of 6.9×10^8 NM^{-2} (10^5 p.s.i.) which was much less than that normally encountered in roller bearings, etc. Smith(2) used a point contact arrangement (see fig. 1.3) with one of the discs crowned, thus making higher hertz contact pressures obtainable but also less amenable to theoretical treatment. The Japanese work dealt mostly with rolling friction and only to relatively small extent with sliding friction.

In spite of the diversity and scarcity of experimental results, there was apparently a large discrepancy between experiment and theory. The natural assumption of Newtonian behaviour combined with an exponential pressure variation led to theoretical predictions that were several orders of magnitude too high, even when thermal effects were included. Much data was subsequently produced by Plint(4), Poon and Haines(5), Johnson and Cameron(6), Allen, Townsend and Zaretsky(7), Adams and Hirst(8) and Gentle(9) in order to resolve this embarrassment. Traction results of a similar nature to those of Crook(1) and Smith(2) were obtained.

The traction curves have a distinct shape in that at low sliding speeds they are linear, increased sliding gives rise to increasing non linearity to a maximum of 5→10% of the normal contact force in high pressure contacts and then it falls off with increasing sliding speed.

From the gradient of the initial part of a traction curve, a mean effective 'viscosity' of the oil in the contact may be found by:

$$\tau = \bar{\eta} \frac{\partial u}{\partial z} \quad , \quad \frac{\partial u}{\partial z} = \frac{U_1 - U_2}{\bar{h}}$$

$$\tau = \frac{T}{A}$$

$$\therefore \quad \bar{\eta} = \frac{T}{A} \frac{\bar{h}}{(U_1 - U_2)} \qquad (0)$$

Plots could then be made of the variation in mean effective 'viscosity' with pressure, temperature, for various rolling speeds as shown in fig. 4. At constant pressure the mean effective viscosity is seen to fall with rolling speed. At moderate pressures (0.4 GPa) the mean effective viscosity varied approximately exponentially with pressure ($\eta_o e^{\alpha' p}$) and was found to have values consistent with low pressure measurements, using 'falling plungers', close to equilibrium state, viscometry. Johnson and Cameron(6) confirmed the fall of viscosity with rolling speed but found that at pressures higher (0.5 GPa) than Crook(1) used, there is a tailing off of viscosity, see fig.1.4. Bell, Kannel, and Allen(10) showed that above pressures of 0.7 GPa the curves start to flatten off to a plateau region,

i.e. $\frac{\partial \bar{\eta}}{\partial p} \rightarrow 0$ assympotic

B. Supplementary work on fluids

While the above work was being performed and in the wake of it, there was much discussion and controversy over the real behaviour of oils under elastohydrodynamic traction. The finer details of the extreme physical conditions prevailing in EHD were not clear and nor were the variations with temperature, pressure and shear rate of the physical properties of the oils known. This, combined with a somewhat crude type of experiment, led to an excess of hypotheses,

FIG. 1.4

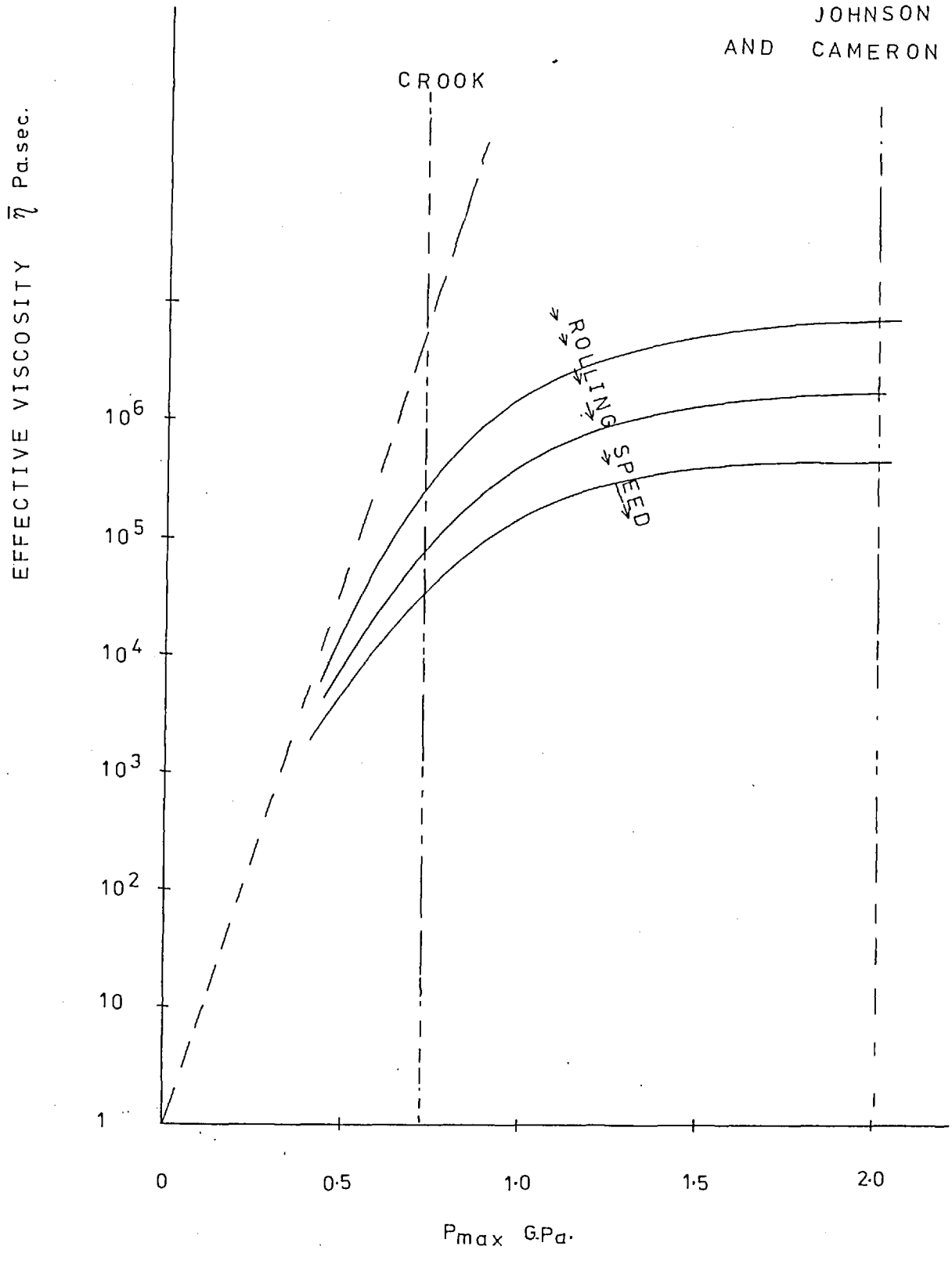
JOHNSON
AND CAMERON
CROOK
ROLLING
SPEED
EFFECTIVE VISCOSITY $\bar{\eta}$ Pa.sec.
10^6
10^5
10^4
10^3
10^2
10
1
0
0·5
1·0
1·5
2·0
P_{max} G.Pa.

i.e. Thermal Newtonian

Viscoelastic shear hypothesis

Compressional viscoelasticity

Plastic shear hypothesis

The Granular model

These various models prompted theoreticians to search for more rheologically orientated experiments. The work of Barlow, Ergintslav and Lamb(12) provided evidence for the viscoelastic shear nature of liquids in oscillatory shear at low pressures on various fluids. This work was used by Dyson(13) to explain traction data with some success, considering the change in environment from one experiment to the other. The impact microviscometer of Paul and Cameron(14) demonstrated that oils certainly exhibit a time dependent viscosity following pressure step from atmospheric pressure to 1 GPa in about 20 milliseconds, which was quite a lot longer than typical EHD transit times. This work lent credence to the compressional viscoelastic theory, argued by Fein(15), which was subsequently used in a modified form to explain the results of Harrison and Trachman(16).

Hutton and Phillips(17) used a Couette viscometer to measure the viscosity/pressure relationship for various oils and found that the conventional equation

$$\eta = \eta_o e^{\alpha' p}$$

fitted the results but this was interpreted as an equilibrium viscosity by Paul(14) since it took a very long time to reach high pressure in the Couette viscometer experiments.

Following his early work in which he developed a theory for EHD film formation using the idea that the oil behaves like an elastic solid in the high pressure part of an EHD contact, Jacobson(18) made simple measurements of shear modulus of a lubricant, solidified under hydrostatic pressure. More recently, Jacobson(19) has tried to measure the solidification velocity and found that at a pressure of 2 GPa, 90% of the hertz contact becomes solidified in 5μS. This work would seem to point to the viscoelastic shear model proposed by Dyson(13).

All of these ancillary experiments were of great interest to EHD investigators, but none of them resolved the problem as to which of the models best described EHD traction.

C. Supplementary traction work

Johnson and Roberts(20) recognised that if spin were present in a rolling point contact, that this would lead to a net shear strain of the oil film at right angles to the rolling direction even when there was no sideslip to contribute to this (see fig. 1.5). They also noted that the net integrated shear strain rate through such a contact would be zero if the deformed surfaces were assumed to be flat and rigid. This offered an opportunity to distinguish the viscoelastic shear theory,which would show a force at right angles to the rolling direction,from the compressional viscoelastic theory which would show a force in the opposite direction and the Newtonian theory which would show no net force. They used the Poon and Haines(21) apparatus and concluded that above pressures of about 0.7 GPa, their oil (Shell turbo 70) showed strong elastic shear behaviour even when compliance of the surfaces had been taken into account.

1.3 THEORETICAL APPROACHES

From the start of theoretical analyses of traction curves, it was soon realised that the use of classical Newtonian fluid concepts to explain the results was not correct. This was shown by Cameron(22) who applied Newton's viscosity relation

$$\tau = \eta \frac{\partial u}{\partial z} \quad (1)$$ Shear Stress = Visc. X Shear Rate

By considering the contact to be a parallel film of constant thickness h and edge velocities of U_1 and U_2 the velocity gradient or shear rate is found to be

$$\frac{\partial u}{\partial z} = \frac{(U_1 - U_2)}{h} \quad (2)$$

By integration over the whole contact of known geometry, the total friction force T can be found if the viscosity can be expressed at at each point in contact,

$$\text{i.e.} \quad T = \frac{U_1 - U_2}{h} \cdot L \int_{-a}^{+a} \eta dx \quad (3)$$

$$\text{i.e.} \quad dT = \tau L dx$$

By using

$$\eta = \eta_o e^{\alpha' p} \quad (4)$$

and approximating to the pressure distribution across the conjunction to a parabola, a traction coefficient $\frac{T}{N}$ could be found.

$$\text{i.e.} \quad \frac{T}{N} = L \frac{(U_1 - U_2)}{h N} \eta_o \exp(\alpha' p_{max}) \; a \sqrt{\frac{\pi}{\alpha' p_{max}}} \quad (5)$$

N = load

p_{max} = maximum hertz pressure

a = half contact width

FIG. 1.5

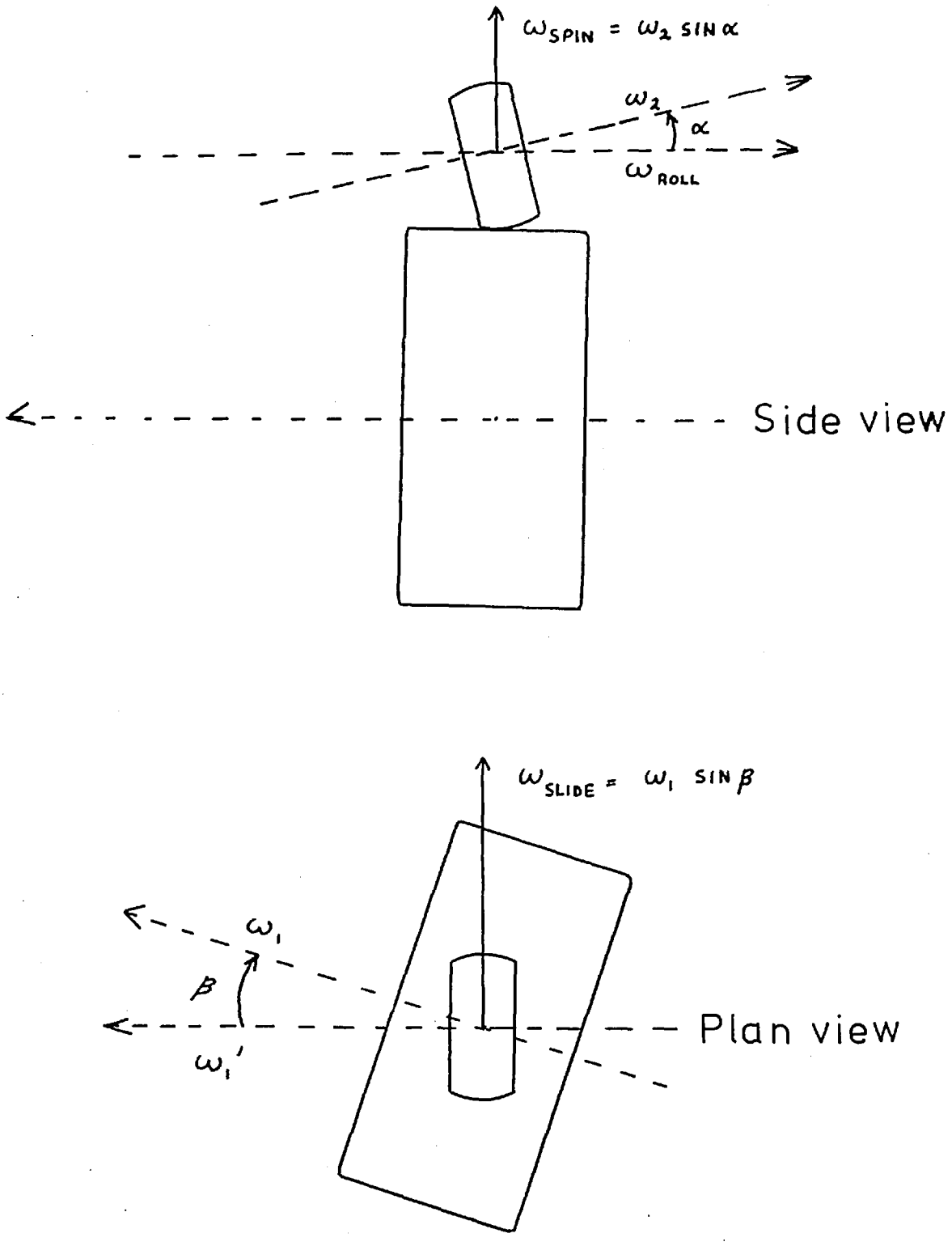

The kinematic diagrams of the Poon and Haines apparatus used by Johnson and Roberts.

Both a and h can be calculated or measured optically and so by using typical values for all the parameters it is possible to calculate the traction coefficient. The result is a traction coefficient several hundred times too large. This cannot be put down to inaccuracies in a, h, η_o, p_{max}, pressure distribution or film shape. The only other alternative is the shape of the viscosity distribution. No significant improvement can be gained by using other pressure-viscosity relationships and so the omission of thermal effects was thought to be the major factor affecting the results.

The effect of considerable frictional heating has the double effect of lowering the overall viscosity of the lubricant inside the contact and also making the viscosity a variable across the thickness of the film.

Consider now the equation for dissipation of energy.

$$\eta \left(\frac{\partial u}{\partial z}\right)^2 = -K \frac{d^2\theta}{dz^2} \qquad (6)$$

Generation Conduction

Cameron(22), p. 223.

Therefore from $\tau = \eta \frac{\partial u}{\partial z}$ (1)

$$\frac{d^2\theta}{dz^2} = \frac{-\tau^2}{\eta K} \qquad (7)$$

K is the thermal conductivity

A first integration was performed by Grubin(23) who used a specialisation of the Slotte viscosity relation

$$\eta = \frac{S}{(\theta'+C)^M} \qquad (8)$$

θ' = temperature in any scale

S,C,M constants for any fluid

The use of this equation has been justified by Cameron(24), who showed it to be suitable for determining temperature distributions across oil films. It is preferred to the more accurate Vogel equation, since it is more mathematically tractable. Crook(25) used Reynold's viscosity relation but this has been shown to be very inaccurate. There are several other viscosity-temperature relationships, but they are rather more involved mathematically than the equation of Slotte and of comparable accuracy.

Since θ' can be in any temperature scale, then define θ with origin at -C

$$\eta = \frac{S}{\theta^M} \tag{9}$$

$$\frac{d^2\theta}{dz^2} = -\frac{\tau^2\theta^M}{SK} \tag{10}$$

if τ is constant w.r.t. z

$$\text{i.e.} \quad \frac{d\tau}{dz} = 0 \tag{11}$$

Then it can be integrated easily.

The basic relationship for fluid equilibrium is

$$\frac{\partial\tau}{\partial z} = -\frac{\partial p}{\partial x} \tag{12}$$

and so the equation can only be integrated at the pressure maximum where $\frac{\partial p}{\partial x} = 0$. The fact that the variation of τ with z is ignored over the whole of the contact is justified because $\frac{\partial p}{\partial x}$ is the term which causes rolling friction . Since rolling friction is negligible compared with sliding friction, it is argued that the variation of $\frac{\partial p}{\partial x}$ is also neglgible and can be taken as zero throughout, thus making τ independent of z.

Unfortunately typical values of $\frac{\partial p}{\partial x}$ away from the centre point are about $(3 \times 10^{12}\ NM^{-3})$ and so it is difficult to believe that τ is invariant across the film.

However, this approach has been used on thermal Newtonian theories of Crook(25), Grubin(23), Hingley and Cameron(26), Cheng(27) and Kannel and Walowit(28).

The first estimate of the central plane film temperature and viscosity was given by Grubin(23) as

$$\frac{\theta_c}{\eta_c} = (U_2-U_1)^2 \frac{(M+1)}{8K} + \frac{\theta_x}{\eta_x} \qquad (13)$$

where θ_c and η_c are the temperature and viscosity at the central plane of the film and θ_x and η_x are the temperature and viscosity at the bearing surfaces respectively.

Using measured values of S,M,K it is possible to calculate θ_c since $\frac{\theta^M}{S} = \frac{1}{\eta}$ Slotte (9)

A knowledge of θ_c and η_c means that a value for the overall traction can be calculated, which includes thermal effects. The accuracy is limited by the problem raised above, and also by the fact that S,M,K are measured at atmospheric pressure. The conductivity K varies considerably - it is primarily a function of density increasing with increasing density.

$$K = (\beta/\alpha^*)\rho^{4/3} \qquad (14)$$

where β depends upon molecular weight

α^* varies slowly with temperature

ρ is the density

Also S and M vary with pressure, but it is difficult to describe the functions mathematically. Crook has shown, however, that a thermal Newtonian interpretation does lead to a peak in the traction curve but the fact that it was an order of magnitude too high could be explained by the uncertainty in the properties of oils at high pressures. All other workers have also managed to fit thermal theories to give some explanation of the traction peak by adjusting values of the fluid properties to fit the curves.

The indication of the way in which thermal conductivity of oils varies with pressure has been given by Naylor(29), who found an increase in conductivity with pressure which far outweighs the decrease with temperature described by Cragoe(30).

$$K = \frac{0.28}{\rho} (1 - 0.000540) \times 10^{-3} \text{ c.g.s. units} \qquad (15)$$

This increase in conductivity lowers the temperature rise of the oil since the heat flows out more easily to the bearing surfaces. Crook's thermal Newtonian theory is therefore even less accurate than he presumed for predicting traction forces quantitatively. Hingley(26) fitted the experimental facts more closely than Crook by using a different viscosity-temperature relationship in his calculation. The objection, first raised by Johnson and Cameron concerning the increasing of conductivity with pressure, still holds though. There is no mention of the traction ceiling or the linear section of the curve for small slide/roll ratios close to the origin. The complicated numerical solution of Cheng(27) has been simplified by Kannel and Walowit(28) and has been used as a fairly quick method of comparing various pressure/viscosity/temperature

relationships. Smith, Walowit and McGrew(67) used a similar method and found that the Newtonian model will only give a good quantitative fit if a pressure viscosity coefficient of 5.42 GPa^{-1} for 5P4E is used, whereas a typical value would be about 43 GPa^{-1}. It would seem that by this kind of calculation all physical meaning is lost, although it may prove useful from an engineering design standpoint, where parametric relationships are more important in the short term. Gentle and Cameron(61) found that all the fluids over the range of conditions tested gave traction curves of a similar shape when plotted against slide/roll ratio. The gradients of the initial linear parts were found to be independent of rolling speed. This was in agreement with Johnson and Cameron(33), but implied further criticism of Newtonian theories of EHD traction in that this implied a mean effective viscosity that was a function of rolling speed, i.e. $\bar{\eta}_{\alpha}(U)^{-0.3}$

Gentle and Cameron argued that at very low sliding speeds, thermal effects would be insignificant and so the above relation ($\bar{\eta}_{\alpha}U^{-0.3}$) could be used as direct evidence for non-Newtonian behaviour of fluids in EHD traction. This conclusion was reached by Crook(32) and Smith(2) and was later explained by Johnson and Cameron(33) who brought out another criticism. They showed that thermal theory predicts that a temperature rise would reduce the film thickness to such an extent that the traction rises in spite of the reduced viscosity. This is completely at odds with the experimental facts.

From an analysis of the work of Hamilton and Moore(34), in which a manganin strip pressure transducer was used to study EHD pressure distribution, Adams and Hirst(35) showed that the apparent variation of mean effective viscosity of mineral oils may be explained by the

modification of the pressure distribution with rolling speed. They concluded that if account was taken of this effect, the viscosity was not a function of rolling speed. This would be expected, however, since the peak hertz pressure, for the results quoted by Adams and Hirst(35), was only 0.44 GPa (62 K.p.s.i.) where Newtonian behaviour for low shear rates would be expected.

Another possible factor affecting the apparent rolling speed dependence of viscosity has been suggested by Miller(65), who proposed that transient temperature excursions can be obtained because of nearly adiabatic and irreversible, compressional heating occurring even in pure rolling contact. Miller used an equation of state, developed by Walsh and Christian(57) and improved by Shaw(58) to calculate a temperature rise as a function of pressure and concluded that temperature rises of the order of 150^{o}C or in a 1.75 GPa (250 K.p.s.i.) high speed EHD contact might be possible for 5P4E (5 phenyl 4 ether).

1.41 Possible Rheological Models

The failure of thermal Newtonian fluid theories to explain and predict quantitatively the traction forces, transmitted through elasto-hydrodynamic contacts in sliding led to the postulation of various rheological models for fluid behaviour under these unique conditions of shear rate, pressure, time and temperature.

The basic models proposed were:

(1) Viscoelastic shear

(2) Compressional viscoelastic shear

(3) Plastic shear

(4) Granular behaviour

These will now be discussed in order.

1.42 Viscoelastic shear behaviour

All real solid or liquid materials will show viscoelastic behaviour depending upon the rate of shear or in other words the time scale over which shear deformations upon them are observed. Obvious examples of this are pitch, glass, and plastics which over short periods of time appear to be elastic solids, but over long periods of time (years or 100's of years) creep in such a way as to appear to be liquids.

Clear experimental evidence of non-Newtonian behaviour of mineral oils in a comparable experimental situation to that encountered in elastohydrodynamic traction was difficult to find. The basic difficulty being that temperature effects generated during the shearing of an oil obscured the more fundamental shear behaviour and also the hydrostatic pressures attainable in conventional falling ball or rotational viscometers were quite low (0.2 GPa). There was some work done by Norton, Knott and Muenger (36) on mineral oils, using a capillary viscometer which was analysed by Hahn, Eyring, Higuchi and Ree(1958,37). The results implied non-Newtonian behaviour at shear stresses of the order of $10^4 \rightarrow 10^6$pa at pressures of 0.2 GPa but no corrections were made for temperature. Hahn later showed that temperature correction could definitely reduce the non-Newtonian effects significantly.

The simplest model of viscoelastic behaviour is the Maxwell fluid model which considers a fluid element to consist of an elastic component and a viscous component in series. The total strain is then the sum of the elastic and viscous strains at any instant.

This leads to:

$$\gamma = \gamma_{el} + \gamma_{visc} \tag{16}$$

$$\dot{\gamma} = \dot{\gamma}_{el} + \dot{\gamma}_{visc} \tag{17}$$

$$\dot{\gamma} = \frac{\dot{\tau}}{G} + \frac{\tau}{\eta} \tag{18}$$

where $\dot{\gamma}$ = The shear rate

τ = The shear stress

G = The limiting shear modulus for infinite shear rate

η = The limiting viscosity for an infinitesimal shear rate

Milne(38) was the first to analyse this concept following on suggestion of Cameron(39). It was applied to a contact by Crouch and Cameron(39).

If in the Maxwell model the reference axes are assumed to translate then the viscoelastic effects become important when the transit time of an oil through an EHD contact approaches the relaxation time of the fluid

$$\text{i.e. if } \frac{2a}{\bar{U}} \approx \frac{\eta}{G} \tag{19}$$

Where a = ½ hertzian width

$\bar{U}$ = mean rolling speed

Using typical values

$G = 10^9$ Pa

$\bar{U} = 10\ MS^{-1}$

$2a = 10^{-4}M$

$\eta = 10^5$ Pa.sec

Then for $h = 10^{-6}M$, $U_1 - U_2 = 0.1\ MS^{-1}$. This would imply a shear stress of 10 Gpa. which is far removed from practice.

Several authors - Fromm(40), Oldroyd(41) - have pointed out that Maxwell's equation cannot be applied in a system of axes which maintains its orientation relative to the planes of shear, the reason being that even simple shear involves some component of rotation. This rotation is $\frac{\gamma}{2}\ sec^{-1}$ where $\gamma\ sec^{-1}$ is the rate of simple shear. Tanner (42) discussed this in detail and put viscoelasticity back into the picture but as Dyson(43) showed, the Maxwell model has certain shortcomings.

(1) For shear stresses of the same order as the elastic modulus G there will be large strains but the Maxwell model is restricted to small strains and so is not applicable to EHD traction.

(2) The predicted normal stresses do not agree with observation (Jobling and Roberts, 1953, 44), (Russell, 1946, 45), (Roberts, 1953, 46).

(3) The model is only valid up to the shear stress maximum.

Dyson(13) suggested that a better model for viscoelastic behaviour would be the Barlow and Lamb model.

1.43 The Barlow and Lamb Model

The exact form of the Barlow and Lamb model is similar in concept to that of Maxwell in that it combines the viscous properties of a Newtonian fluid with the elastic properties of a Hookean solid but it leads to better practical results. It combines the admittances of the viscous and elastic components instead of the compliances used by Maxwell. The justification for this lies in the fact that the temperature viscosity dependence would then be governed by the equation

$$\eta = A + \frac{B}{\theta - \theta_o} \qquad A, B, \theta_o \text{ constants} \qquad (20)$$

where viscosity temperature dependence is limited by free volume. Most practical lubricants would be expected to behave in this way and in fact this has been verified by tests made on a wide range of chemically defined fluids such as di (2 ethyl Hexyl) phthalate. Some strange behaviour has been noticed in some mixtures, but the model is obeyed closely by mineral oils (Hutton(47)).

Dyson(43) applied the Barlow-Lamb model to the mineral oil results of Johnson and Cameron(33), using the Bolzmann principle of linear superposition to transform from the oscillatory shear results of Barlow and Lamb to continuous shear. The results of his work met with mixed success.

(1) The Barlow-Lamb model predicts a fall in effective viscosity with rolling speed, but indicates that the amount is dependent on the viscosity and other properties of the fluid.

Experimentally $\bar{\eta} \propto (\bar{U})^{-0.3}$ (21)

(2) Secondly, the traction curve is predictable, but quantitative fits can only be obtained by parameter adjustment.

(3) The traction ceiling is not explained.

(4) The Barlow-Lamb model predicts a plateau region of effective viscosity, as the actual viscosity under static conditions is increased. Since this corresponds to a tailing off with pressure it can be fitted to the results of Johnson and Cameron(33) roughly.

(5) By including thermal effects, the theory predicts the temperature and shear stress of the central plane of the fluid film, and these are shown to agree with those of Johnson and Cameron(33) taken to the right of the traction curve maximum.

The fact that the Dyson solution leads to a prediction of the whole traction curve is taken as evidence against discontinuity in the fluid properties causing the peak. This discontinuity has been suggested by Smith(2,48) and Plint(4).

1.44 The Compressional Viscoelastic Model

The maximum pressures encountered in elastohydrodynamic oil films can be as high as 2 GPa (300 k.p.s.i.). The lubrucant film is therefore subjected to a very large transient pressure, as it passes through a contact, leading to large changes in the viscosity of the oil through the contact (10 to 10^5 pa.secs.). Fein(15) suggested that the failure of an oil to respond to a rapidly changing pressure could explain the rolling speed dependence of derived mean effective viscosity from EHD traction curves. His analysis showed that at high rolling speeds, the time of transit of oil through the contact zone could be small compared with the time required for the oil to reach an equilibrium viscosity value. The result of this would be that an increase in rolling speed could lead to a lower mean effective viscosity. This type of fluid behaviour has been obtained by Paul and Cameron(14) (see fig.1.6) for periods of time greater than 2×10^{-2} secs. Trachman and Cheng(49) used a non linear model, proposed by Kovacs(50) to explain the rolling speed dependence of the gradient of the initial part of traction curves. The model was changed slightly by Trachman(51) where the density of a liquid was assumed to respond to a rapid change of pressure with an instantaneous volume change attributable to the elastic compression of a liquid lattice, followed by a time dependent volume change due to changes in molecular ordering. The result of this effect on the viscosity is

FIG. 1.6

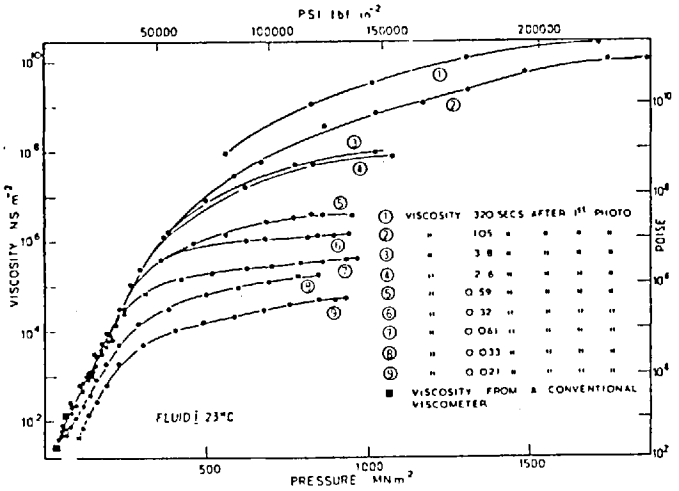

Fig. 2—Viscosity against pressure for fluid I

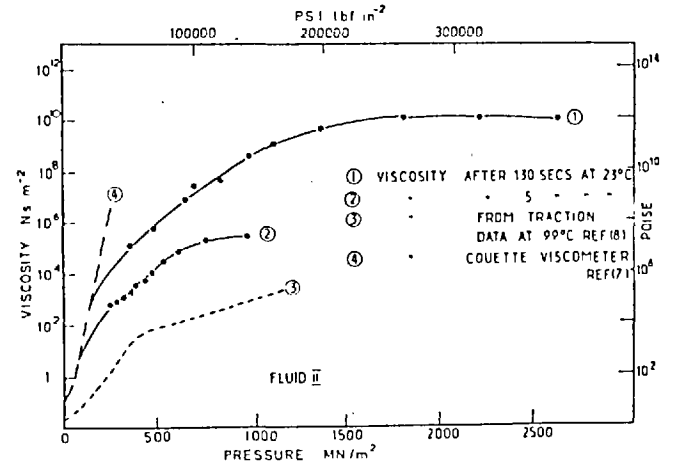

Fig. 3—Viscosity against pressure for fluid II

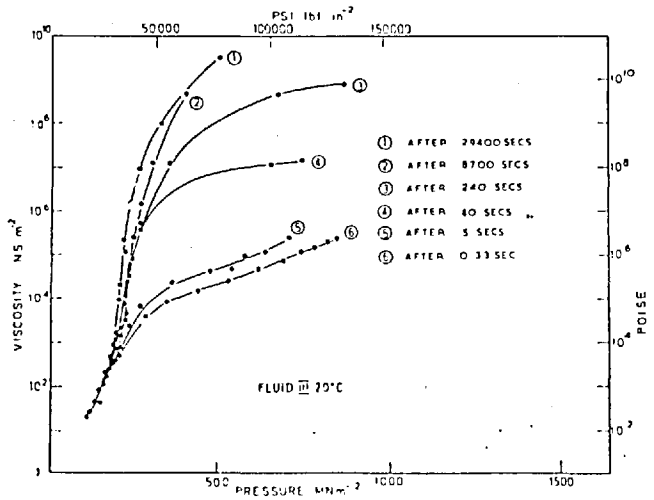

Fig. 4—Viscosity against pressure for fluid III

TABLE 1—FLUID I PARAFFINIC CYLINDER STOCK; FLUID II 5-PHENYL 4-ETHER; FLUID III PERFLUORALKYL ETHER

	VISCOSITY	TEMPERATURE
Fluid 1.....	0.045 NSm^{-2}	99 C
	1.49 NSm^{-2}	40 C
	4.5 NSm^{-2}	20 C
Fluid 2.....	0.017 NSm^{-2}	99 C
	.419 NSm^{-2}	40 C
Fluid 3.....	.15 NSm^{-2}	99 C
	.014 NSm^{-2}	40 C

FIG. 1.7

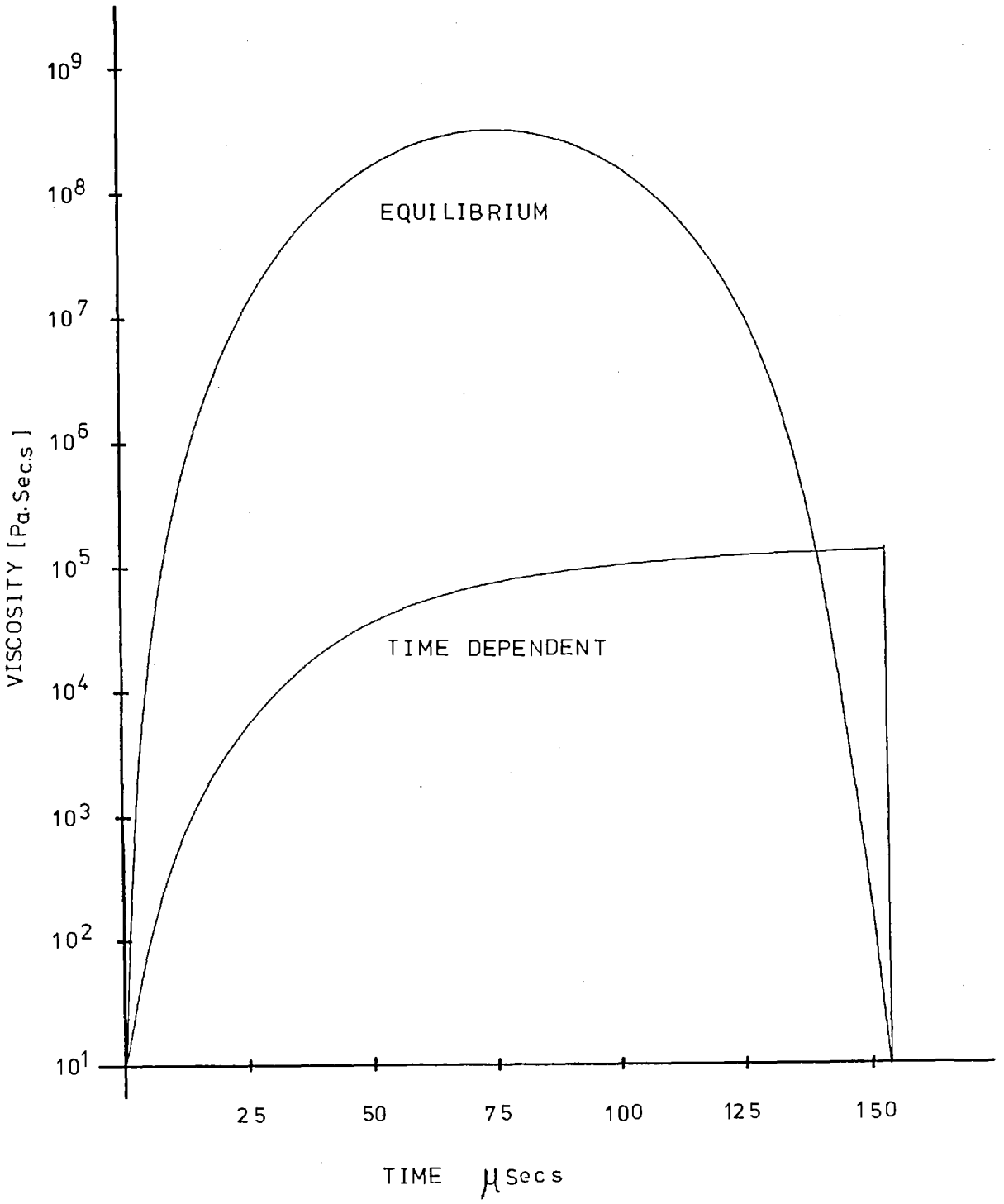

A comparison between the transient viscosity values in a concentrated contact and the equilibrium viscosity values corresponding to the Hertzian pressure profile

FIG. 1.8

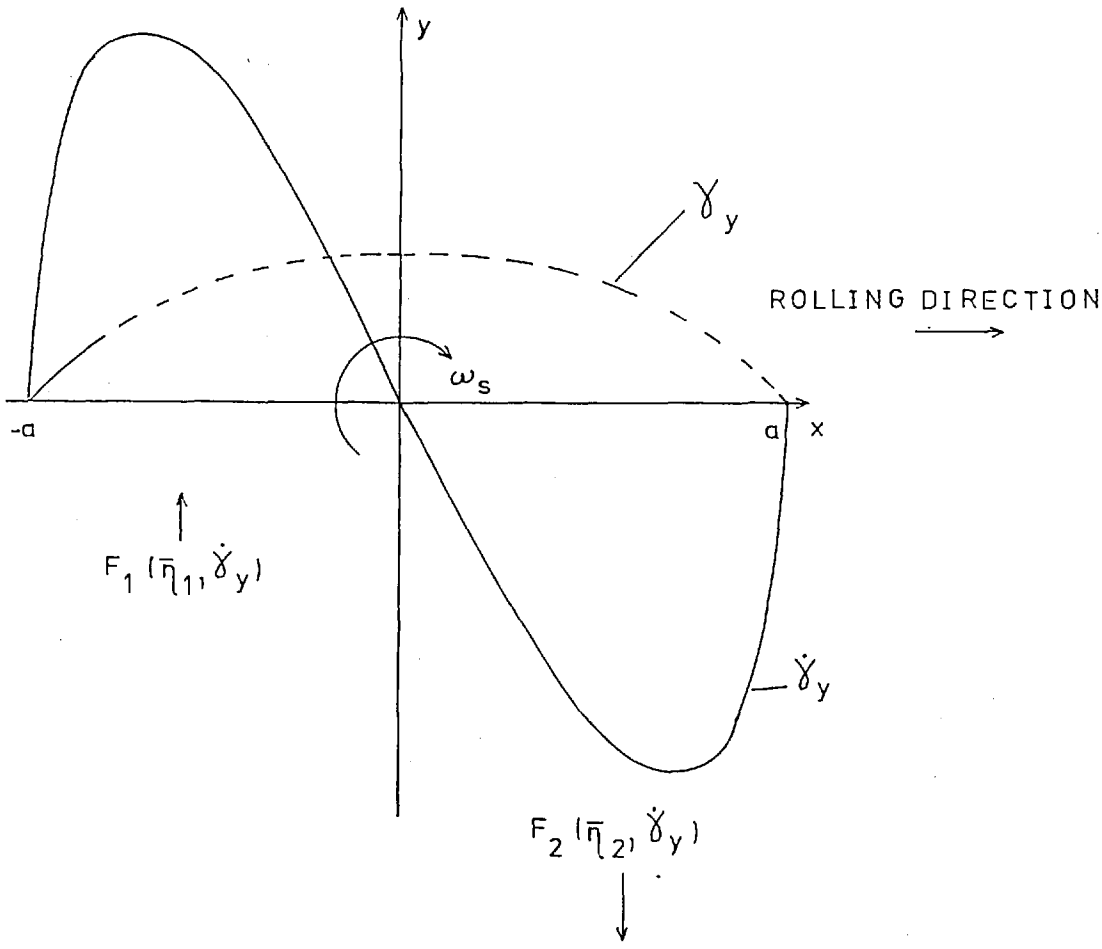

The variation of the components of shear strain and shear strain rate at right angles to the rolling direction in a point contact with spin present.

$\bar{\eta}_1$ and $\bar{\eta}_2$ are the mean effective viscosities in the inlet and outlet halves of the contact respectively.

F_1 and F_2 are the forces arising from the shear conditions prevailing in the inlet and outlet halves of the contact respectively.

If viscosity is time dependent

$$\bar{\eta}_2 > \bar{\eta}_1 \quad \text{and so} \quad F_2 > F_1$$

and an external force in the -y direction is expected.

If film behaves in a pure elastic manner, a force will be expected in the +y direction as observed by Johnson and Roberts(20).

to cause a sharp initial rise in viscosity followed by a gradually flatter response with time (see fig. 1.7).

Although this type of model offers an explanation of the initial part of the traction curves in terms of a physically credible model, supported by the specific viscometry work of Paul and Cameron(14), it predicts a spin traction force in the opposite direction to that observed by Johnson and Roberts(20).

This would have been due to the assymetrical shear rate distribution in pure rolling with pure spin shear resulting in a greater shear stress contribution from the outlet half of the contact resulting from a higher viscosity in that region (see fig. 1.8).

1.45 The plastic solid theory

The first plastic solid theory was put forward by Smith(2) and followed by Plint(4) to explain the fact that elastohydrodynamic traction curves increase to a maximum shear stress with sliding for a given pressure, temperature and shear rate. Simple fluid models would predict a continuous increasing of shear stress with shear rate and so this effect was thought to be the result of a discontinuity in the fluid properties of oils in EHD lubrication. This apparent discontinuity was highlighted by the semi-logarithmic plotting of the traction curves of Plint(4), following the earlier failure of Smith(2) and Crook(1) to obtain quantitative agreement between their thermal Newtonian theories with experiment.

Smith(2) postulated that fluids would behave in a Newtonian manner up to a critical shear stress, beyond which point the shear stress would continue to rise up to a limiting shear stress,like the behaviour of a plastic solid.

The primary assumption of Newtonian behaviour seems most unlikely in view of the variation of derived mean effective viscosity, with rolling speed which implies that

$$\bar{\eta} \alpha (U^{-0.3}) \tag{21}$$

but the critical shear stress model has been discussed at length by Johnson and Cameron(6). Johnson and Cameron(6) attempted to interpret their traction ceiling results by using the flash temperature relation of Crook(1) with a parabolic heating distribution function together with the shear plane temperature equation of Archard(52), which assumed that all the heat was generated in a central shear plane, to plot mean limiting shear stress as a function of mean shear plane temperature and mean pressure.

This obtained quite good straight lines for the function:

$$\frac{\tau_c}{\bar{P}} = 0.083\left(\frac{\bar{P}}{139,000}\right)^{0.2}\left(\frac{\bar{\theta}_c}{30}\right)^{-0.4} \tag{22}$$

τ_c = mean critical shear stress

$\bar{P}$ = mean pressure

$\bar{\theta}_c$ = mean shear plane temperature

This showed that the critical shear stress was probably only dependent upon pressure and temperature.

Recent work has been performed by Hirst and Moore(53), using the critical shear stress model to explain their traction results at low sliding speeds where thermal effects were thought to be insignificant. They attempted to relate the critical shear stress to the average size of molecules of four chemically well defined liquids. This involved the application of the energy barrier theory of Eyring(54) which treats shear stress as the dominant variable affecting the viscosity of a fluid above a certain shear stress. They concluded that the critical shear stress of the fluids tested was approximately inversely proportional to the molecular volume which was thought to lend support to an Eyring(54) model for fluid behaviour.

Since there is much controversy over the behaviour of fluids at very low shear rates, most of which is over which non-Newtonian model to apply, it seems fortuitous that an Eyring(54) model, that assumes Newtonian behaviour at low shear stresses,should fit the traction results at higher shear stresses. It would also seem more probable that an elastic solid would show plastic behaviour under large deformations than a viscous liquid, at large shear stresses. The apparent experimental fit may be due to some of the more basic assumptions of Eyring's model which do not distinguish a highly stressed viscous liquid from a highly stressed elastic solid.

1.46 The Eyring model

Apart from those models which attempt to describe fluid properties in terms of macroscopic elastic solid and viscous liquid properties, there exists the Eyring(54) significant structures theory

which endeavours to describe the transport properties of liquids in molecular terms. Eyring et al.(55,56) suggest that molecular translation in a liquid occurs when a molecule moves from its equilibrium position in a quasi-crystalline structure to an adjacent site or hole. This is an activated process and a proportion of the molecules possess sufficient activation energy by virtue of a Boltzmann thermal energy distribution. In the absence of any external force, as many move in one direction as the other so leading to no net flow. When a shear stress is applied, the barrier to molecules moving in the shear stress direction is effectively lowered by an amount equal to the mechanical work done on the flowing molecules and for the opposite direction the barrier is raised by the same amount.

The result of the type of approach is that the viscosity η is given by

$$\eta = \frac{\exp(E'/kT')}{2A'\sinh(\tau\alpha''\lambda/2kT')} \qquad (23)$$

τ = the shear stress

E' = the height of the energy barrier

α'' = the area of a molecule

λ = the average intermolecular distance

A' = a frequency term proportional to temperature

T' = the absolute temperature

It may be seen that for small shear stresses that the viscosity becomes independent of τ but that the point of departure from Newtonian behaviour occurs when

$$\frac{\tau\alpha\lambda}{2kT} \approx 1 \qquad (24)$$

Hirst and Moore(53) develop this argument to relate molecular volume to a limiting shear stress

Bell, Kannel and Allen(10) have adopted this model to explain film thickness generation

The main disadvantages of this approach are as follows:-

(a) This model assumes Newtonian behaviour at low shear stresses which is not borne out by most experimental work.

(b) It is extremely difficult to put definite figures into the equation except for very simple low viscosity fluids.

(c) The "constants" are complicated functions of temperature, pressure, etc.

1.47 The granular theory

Following in the footsteps of Bernal(59) and Scott(60), Gentle and Cameron(61) attempted to use a model which described a fluid as a collection of spheres. Bernal(59) used this concept to relate the variation of the viscosity of a fluid with temperature and free volume in terms of the packing arrangements of spheres. Gentle(9) recognised the similarity in form, of typical traction curves with those found by Golden(62), shearing a bed of sand. Gentle proposed that under the high pressure (2 GPa, 300 k.p.s.i.) conditions of EHD that the onset of a vitrification of a fluid might be characterised by the formation of aggregates of molecules forming around nucleation centres which he called granules. By consideration of the degree of packing of these granules associated with different pressures and shear rates, he

succeeded in describing qualitatively the shape of traction curves for the low pressure and high pressure regimes (ref. Gentle and Cameron(61)).

Apart from the apparent qualitative success of this model, there would seem to be few ways of proving or disproving it from more specific experiments, apart from by testing the prediction of a 20% decrease in density with increased shear rate, arising from a transition from close packing to loose packing configurations with shear. This type of behaviour may be inferred from the recent work by Paul(66), in which the refractive index of a polyphenyl ether is found to drop with shearing at pressures of about 2 GPa since density would be expected to fall with refractive index.

1.48 Conclusions

It would seem that thermal Newtonian theories of fluid behaviour neither quantitatively nor qualitatively explain elastohydrodynamic traction results. The various complicated rheological models, although physically credible, can easily lead to curve fitting without a detailed knowledge of the parameters included in them.

Of the rheological models, the main contenders for an overall phenomenological explanation, which are open to direct experimental investigation, are the "viscoelastic shear model" and the "compressional viscoelastic model"which both have some specific experimental support.

Model	Support
Viscoelastic shear	Johnson and Roberts(20) Jacobson(18,19) Barlow et al.(12)
Compressional viscoelasticity	Paul(63) Paul and Cameron(14) Doolittle(64) Constantinescu(31)

For these reasons it was considered that experiments of a similar kind to those of Johnson and Roberts(20) would lead to elucidation of the state of the fluid between contacts, if they were performed in such a way that the film thickness could be measured interferometrically and the materials parameters (rolling elements and fluids) varied.

This experimental approach could lead to sufficient evidence to decide which of the above processes is the more dominant in and relevant to the behaviour of liquids in elastohydrodynamic lubrication.

1.5 References

1. CROOK, A.W., 1963, Phil. Trans. A 255, 281

2. SMITH, F.W., 1960, Rep. Nat. Res. Labs., Ottawa, Canada, MP-17

3. SASAKI, T., OKAMURA, K. and ISOGAI, R., Fundamental Research on Gear Lubrication, Bull. Jap. Soc. Mech. Eng., 1961, 4, 382-394

4. PLINT, M.A., Ph.D. Thesis, London University 1967

5. POON, S.Y. and HAINES, D.J., Frictional Behaviour of Lubricated Rolling Contact Elements, Proc. Inst. Mech. Engrs., 1966-67, 181 I, 363

6. JOHNSON, K.L. and CAMERON, R., 1967 Proc. Inst. Mech. Engrs, 182 pt.1

7. ALLEN, C.W., TOWNSEND, D.P. and ZARETSKY, E.V., EHD Lubrication of a Spinning Ball on a non-Conforming Groove, J. Lub. Tech., Jan 1970, 89

8. ADAMS, D.R. and HIRST, W., "Frictional Traction in EHD Lubrication", Proc. R. Soc. Lond., A 332, 505-525 1973

9. GENTLE, C.R., Ph.D. Thesis, London University 1971

10. BELL, J.C., KANNEL, J.W. and ALLEN, C.M., "The Rheological Behaviour of the Lubricant in the Contact Zone of a Rolling Contact System", Trans. ASME, Series D, vol. 86, 1964, pp 423-432

12. BARLOW, A.J., ERGINSTAV, A. and LAMB, J., "Viscoelastic Relaxation of Supercooled Liquids, 11", Proc. Roy. Soc., London, Series A, vol. 298, 1967, pp. 481-494

13. DYSON, A., Flow Properties of Mineral Oils in EHD Lubrication, Phil Trans. Roy. Soc., 1965, 258, 529, 564

14. PAUL, G.R. and CAMERON, A., "Time-dependent Viscosity Effects measured in an Impact Microviscometer", Nature vol. 248, No. 5445, pp. 219-220, March 15, 1974

15. FEIN, R.S., J. Lubrication Technology, Trans ASME, Series F, 89, 127-131, 1967

16. HARRISON, G. and TRACHMAN, E.G., "The Role of Compressional Viscoelasticity in the Lubrication of Rolling Contacts", General Motors Research Publication GMR-1162, Jan. 1972

17. HUTTON, J.F. and PHILLIPS, M.C., 1973 Nature, London, 245, 15-16

18. JACOBSON, B., "On the Lubrication of Heavily Loaded Spherical Surfaces Considering Surface Deformations and Solidification of the Lubricant", Acta Polytechnica Scandinavica, Mech. Eng. series 54, Stockholm 1970

19. JACOBSON, B., "An Experimental Determination of the Solidification Velocity for Mineral Oils", Trans ASLE 17, 4, 290-294

20. JOHNSON, K.L. and ROBERTS, A.D., "Observations of Viscoelastic Behaviour of an EHD Film", Proc. Roy. Soc., London, A 337, 217-242, 1972

21. POON, S.Y. and HAINES, D.J., Frictional Behaviour of Lubricated Rolling Contact Elements, Proc. Inst. Mech. Engrs. 1966-67, 181, I, 363

22. CAMERON, A., Principles of Lubrication, Longmans, 1966

23. GRUBIN, A.N., "Contact Stresses in Toothed Gears and Work Gears", Cen. Sci. Res. Inst. for Tech. and Mech. Eng., 1949, Book 30

24. CAMERON, A., Hydrodynamic Lubrication of Rotating Discs in Pure Sliding - A New Type of Oil Film Formation, J. Inst. Petroleum, 37, 1951, p. 471

25. CROOK, A.W., The Lubrication of Rollers II, Film Thickness with Relation to Viscosity and Speed, Phil Trans. Roy. Soc., (A) 1961, 254 , pp. 223-236

26. HINGLEY, G.G., Ph.D. Thesis, London University (1964)

27. CHENG, H.S., A Refined Solution to the Thermal EHD Lubrication of Rolling and Sliding Cylinders, ASLE Trans 1965, 8, pp. 397-410

28. KANNEL, J.W. and WALOWIT, J.A., Simplified Analysis for Traction between Rolling/Sliding EHD Contacts, ASME 70-Lub S-13

29. See ref. 6

30. CRAGOE, C.S., Miscellaneous Publications No. 97 (U.S. Bureau of Standards)

31. CONSTANTINESCU, V.N., PAN, C.H.T., CHIANG, T. and WACHMANN, C., On the Possibility of Measuring Viscosity during a Rapid Pressure Pulse, ASME J. Basic Eng.

32. CROOK, A.W., The Lubrication of Rollers IV. Measurements of Friction and Effective Viscosity, Phil Trans. Roy. Soc. (A) 1963, 49, pp. 295-307

33. JOHNSON, K.L. and CAMERON, R., Shear Behaviour of EHD Oil Films at High Rolling Contact Pressures, Proc. Inst. Mech. Engrs., 67-68, 182, I, 14, paper 4

34. HAMILTON, G.M. and MOORE, S.L., 1971, Proc. Roy. Soc., London, (A) 322, 313

35. ADAMS, D.R. and HIRST, W., 1973, Proc. Roy. Soc., London (A), 332, 505

36. NORTON, A.E., KNOTT, M.J. and MUENGER, J.R., 1941, Trans ASME, 63, 631

37. HAHN, S.J., EYRING, H., HIGUCHI, I and LEE, T., 1959, NLGI Spokesm. 22, 121

38. MILNE, A.A., 1957, Proc. Conf. on Lubrication and Wear, I. Mech. E., London, p. 61, paper no. 41

39. CAMERON, A. and CROUCH, R.F., J. Inst. Petr., 1960, 46, p. 118-125

40. FROMM, H., 1948 Z. Angew Math. Mech. 28, 43

41. OLDROYD, J.C., 1950, Proc. Roy. Soc. (A), 200, 523

42. TANNER, R.I., 1960, Int. J. Mech. Sci., 1, 206

43. DYSON, A. "Frictional Traction and Lubricant Rheology in Elastohydrodynamic Lubrication", Phil Trans Soc., (A), 1971, 266

44. JOBLING, A. and ROBERTS, J.E., 1958, Rheology Theory and Applications (Ed. F. Eirich), Vol. 2, chapter 13, p. 503-535

45. RUSSELL, R.J., 1946 Ph.D. Thesis, University of London, "The Determination of the Basic Rheological Constants Governing the Flow of Pseudo-plastic Substances"

46. ROBERTS, J.E., 1953, 2nd Int. Congress on Rheology, Oxford, Preprints, p. AA 161

47. HATTON, J.F., Visco-elastic Relexation Spectra of Lubricating Oils and their Component Fractions", Proc. Roy. Soc. (A), 304, 1968, 65

48. Smith, F.W., "The Effect of Temperature in Concentrated Contact Lubrication", Trans ASLE 1962, 5, 142

49. TRACHMAN, E.G. and CHENG, H.S., "Thermal and non-Newtonian Effects on Traction in EHD Contacts", I. Mech. Eng., EHL Symposium, paper 37/72 (1972)

50. KOVACS, A.J., "Bulk Creep and Recovery in Systems with Viscosity dependent upon Free Volume", Trans of Soc. of Rheology, vol. 5, p. 285-296, 1961

51. TRACHMAN, E.G., "The Short Time Viscosity Behaviour of a Lubricant in a Hertzian Pressure Zone", Trans ASME, Paper No. 74-Lub-8

52. ARCHARD, J.F., "The Temperature of Rubbing Surfaces", Wear 1959, 2, 438

53. HIRST, W. and MOORE, A.J., "Non-Newtonian Behaviour in Elasto-hydrodynamic Lubrication", Proc. Roy. Soc., London (A), 337, 101-121, 1974

54. EYRING, H., 1936, J. Chem. Phys., 4, 283

55. EYRING, H., REE, T. and HIRAI, N., "Significant Structures in the Liquid State", Proc. Nat. Acad. Sci., 44, 1958, p. 683

56. EYRING, H. and JHON, M.S., Significant Structures of Liquids, Wiley and Sons, Inc. 1969

57. WALSH, J.M. and CHRISTIAN, R.H., "Equation of State of Metals from Shock Waves Measurements", Physical Review, vol. 97, no. 6, p. 1544-1556, 1955

58. SHAW, R., "Calculated Shock Temperature of Liquid TNT, Nitromethane and four Liquid Bis (Diflouroamino) Alkanes", J. of Chem. Phys., vol. 54, no. 8, p. 3657-3658, 1971

59. BERNAL, J.D., (1959), Nature, 183, 141; (1960), 185, 68

60. SCOTT, G.D. (196)), Nature, 188, 908

61. GENTLE, L.R. and CAMERON, A., Wear, 27 (1974), 71-81

62. GOLDER, H.Q., Engineering 153 June 26, 1942, p. 501-503

63. PAUL, G., "Time Dependent Viscosity following a Pressure Rise measured on an Impact Microviscometer", ASLE/ASME Lubrication Conference, Montreal Canada (1970), Preprint No. 74LC-5B-1

64. Doolittle, A.K., "Studies in Newtonian Flow"

I. The Dependence of the Viscosity of Liquids on Temperature, Journal of Applied Physics, vol. 22, no. 3, p. 1031-1035, (1951)

II. The Dependence of Viscosity of Liquids on Free Space, Journal of Applied Physics, vol. 22, no. 12, p. 1471-1475, (1951)

III. The Dependence of Viscosity of Liquids on Molecular Weight and Free Space (in Homologous Series), vol. 23, no. 2, (1952)

65. MILLER, R.S. "On the mechanical behaviour of entrained materials of concentrated contacts", ASLE/ASME Lubrication Conference, Montreal, Paper 74LC-2A-2 (1974)

66. PAUL, G.R., Private communication

67. SMITH, R.L., WALOWIT, J.A., McGREW, J.M., "Elastohydrodynamic traction characteristics of 5P4E polyphenyl ether", Trans. ASLE (72-LUB 40(A)) 1973, p. 353

C H A P T E R 2

THE MECHANICAL SYSTEM

2.1 APPARATUS CHOSEN

The purpose of the apparatus was to introduce very small amounts of sideslip and spin into a rolling point contact and measure the resultant traction forces and film thickness (see fig. 2.1).

It was realised that spin shear was usually present in a rolling point contact between a sphere and disc due to the variation of surface velocity with radius. It was also noticed that sideslip could be introduced by skewing the axis of the ball in the plane of the plate.

These facts formed the basis of a rig in which traction forces arising from spin and sideslip could be measured.

The amount of spin was found to depend upon the vertical component of the angular velocity of the ball, the radius of the ball and the track radius on the disc surface.

The test ball was contained in and loaded by a nest of rollers. To each ball was attached a shaft to control and vary its axis of rotation.

A range of ball types and sizes were employed to vary the pressure distributions and contact widths over a wide range. Facility was provided for varying the load on the ball, the ambient temperature and the speed.

FIG. 2.1

PHOTO OF THE OPTICAL ELASTOHYDRODYNAMIC
TRACTION RIG

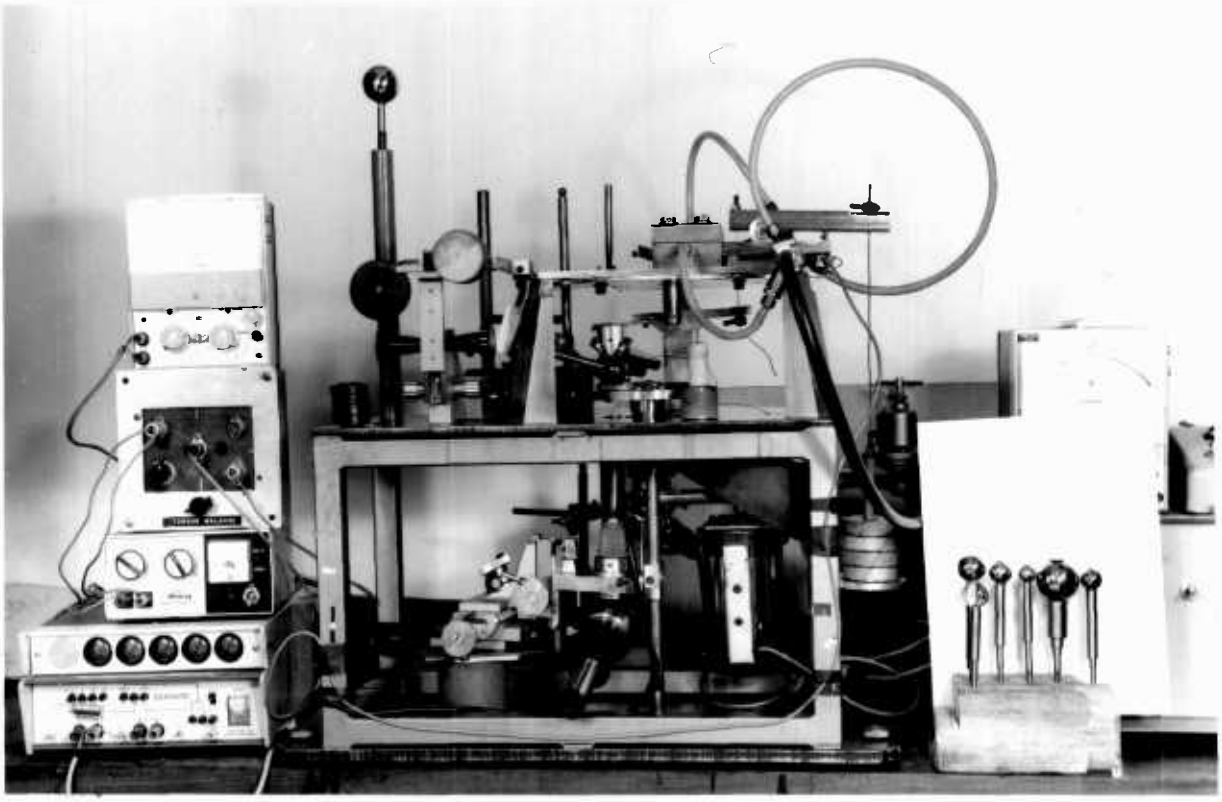

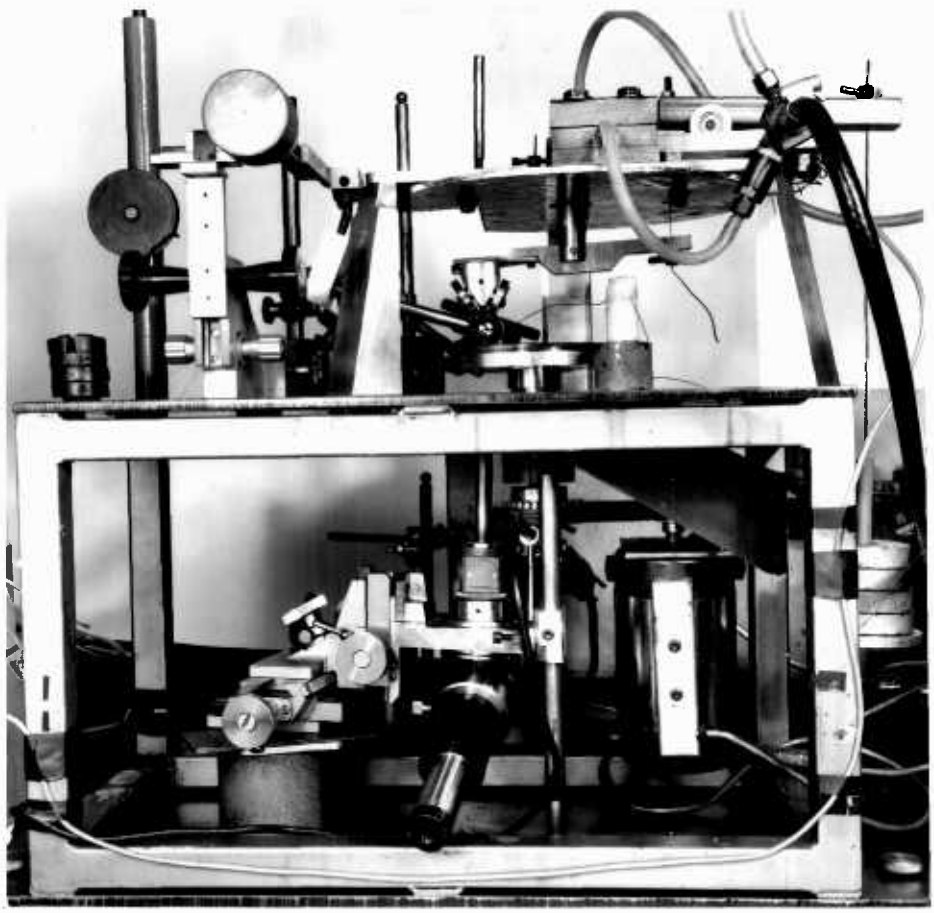

FIG. 2.2

THE DISC LOCATION

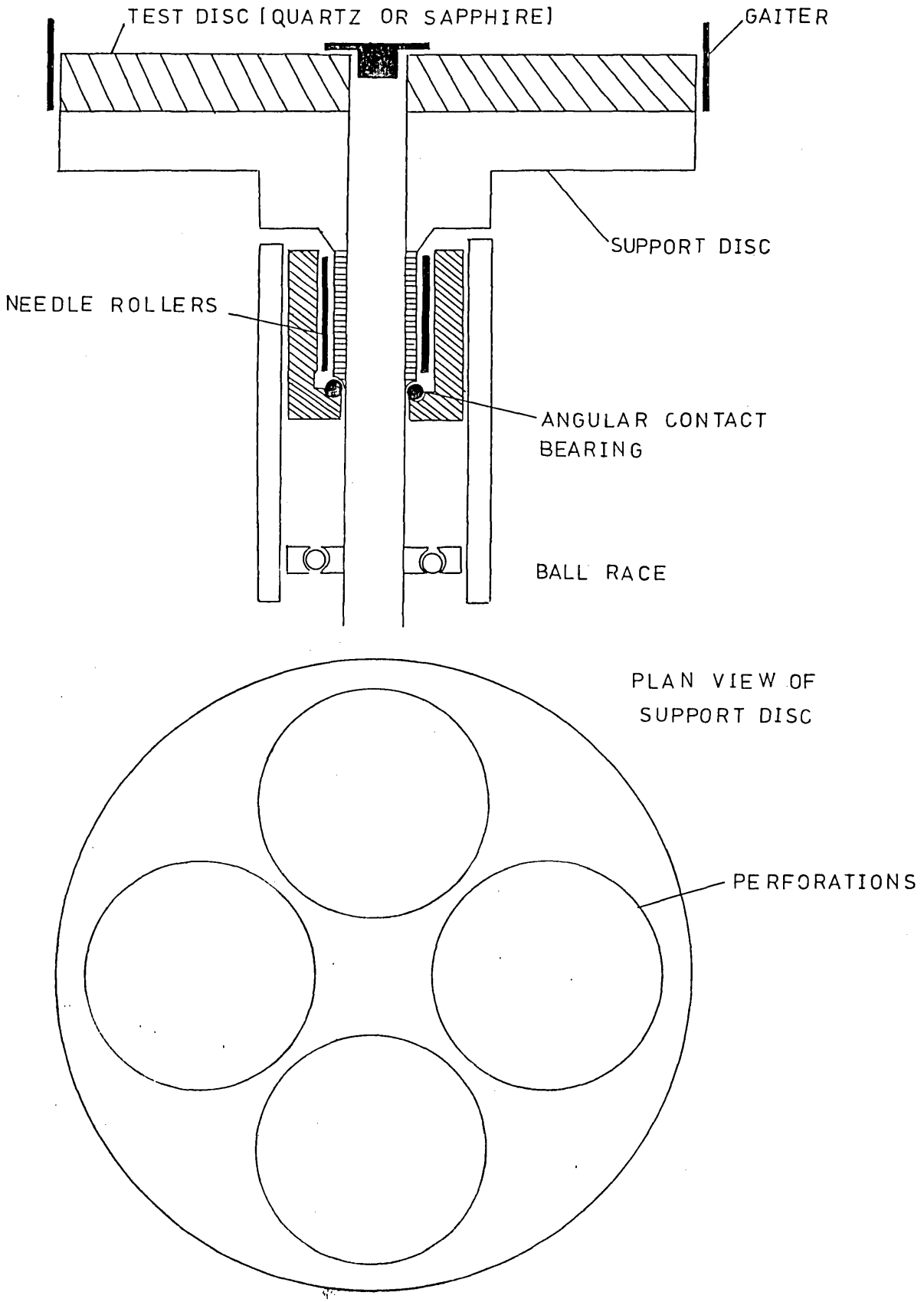

The resulting traction forces at right angles to the rolling direction were measured using a strain gauge bridge.

2.2 THE DISCS

Both of the discs were 0.102 M (4") in diameter and ground and polished to be optically flat. It was most important that each disc was optically flat for successful interferometry. Each disc, when used, was supported by a perforated duralumin disc which was machined flat on its shaft to better than 5×10^{-6} M. This was essential since any vertical component of the motion of the disc surface was found to lead to irritating periodic variations in the traction force measurement.

Duralumin was used because it was easier to machine than steel and sufficiently strong for this application. The support disc was perforated with four 1" diameter holes to allow optical film thickness measurements to be made through it. This disc was mounted on a half inch diameter shaft, running in a combination of spherical and needle roller bearings for the sake of rigidity. Each test disc was centrally held and located by a bush with a bolt screwed into the main driving shaft (see fig. 2.2).

During experiments where high disc speeds were required, the oil on the surface of the disc tended to be thrown off by centrifugal force and so a gaiter was placed around the edge of the disc as an oil retainer.

The main advantage of this apparatus was its flexibility in that, if desired, any type of disc could be easily fitted in a short time.

2.3 THE DRIVE SYSTEM

The requirements of the apparatus were for rotation of the disc over a wide speed range (1:100) with very good speed constancy for a wide range of torques. This facility was provided by a variable speed direct current motor operating on 30V.D.C. with an integral tacho-generator and control unit with a ten turn variable potentiometer to vary the speed from 2 → 2000 r.p.m. This was found to hold any set speed to better than ± 1% for the range of torque loads encountered in the experiments.

As shown in the diagram (fig. 2.3) the motor was mounted on the same structure as the disc support and was connected to the shaft of the support disc via two toothed pulleys and an inextensible fibre glass reinforced toothed belt. Provision was made to slide the motor laterally to accommodate various combinations of pulleys and so vary the drive ratios. The complete motor and support disc could be moved sideways in order to change the ball track radius. This was useful from an experimental point of view and also essential because from time to time the surface coating of chromium on a disc would become worn or scratched and so a different track had to be used.

2.4 THE LOADING SYSTEM

As may be seen from fig.2.4 the test ball is loaded and held in position by a special carriage. The carriage consisted of a prism shaped piece of steel with two rollers fixed to it in one plane and one in another. The rollers rotated on deep groove spherical roller bearings, built to aircraft specification for accuracy and low friction.

FIG. 2.3

THE DRIVE SYSTEM

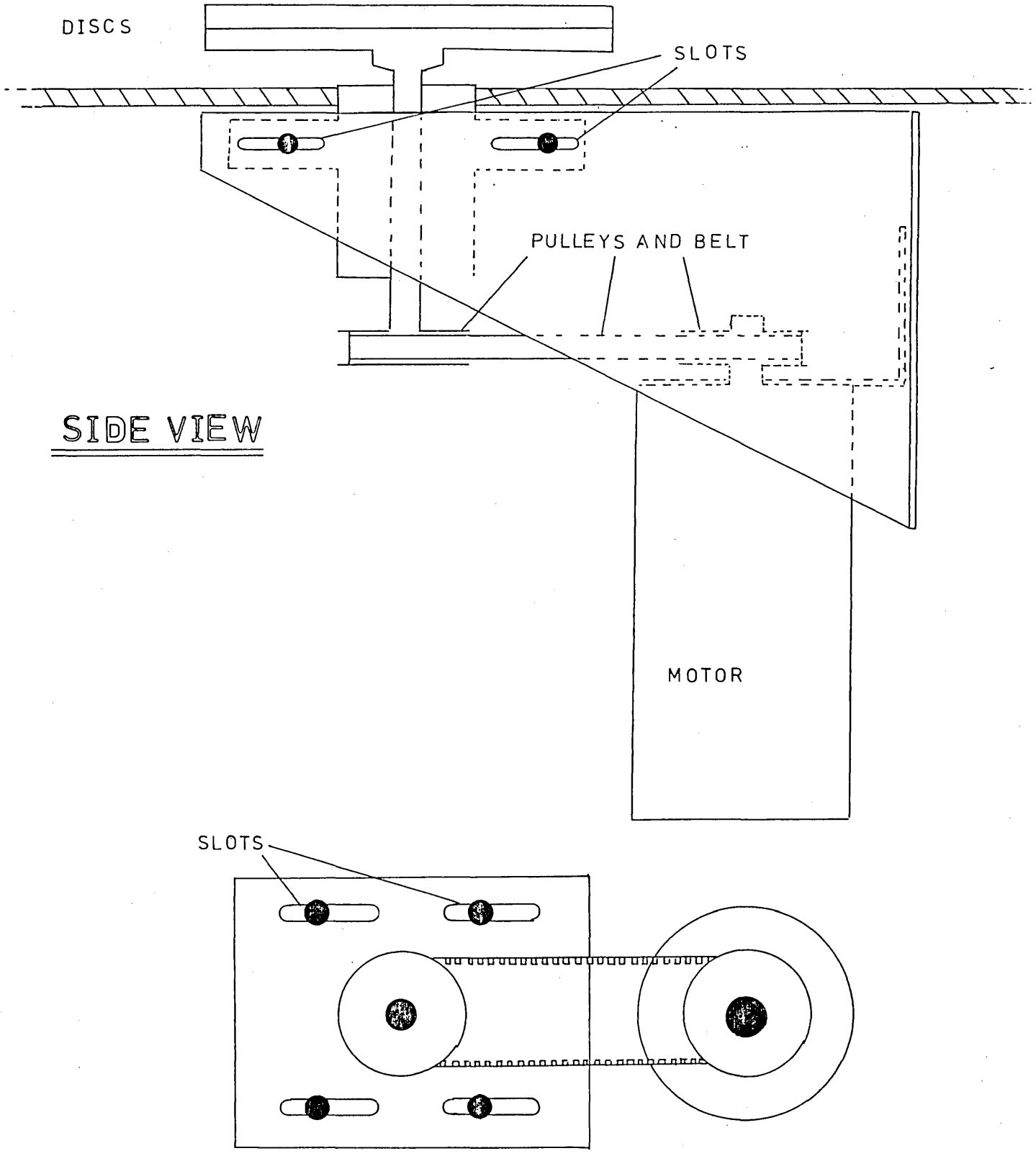

FIG. 2.4

THE LOADING SYSTEM

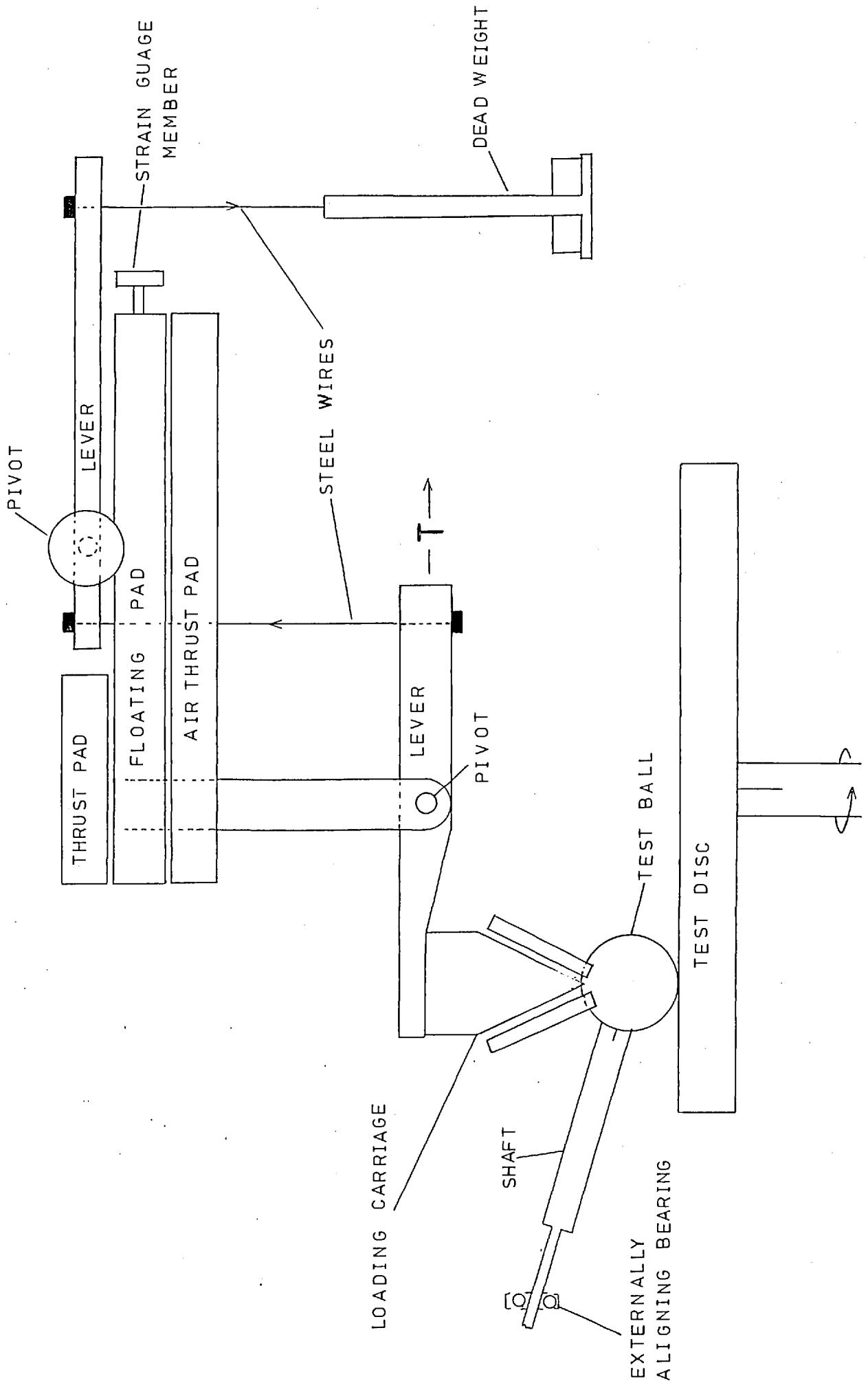

This design was preferred, since it was thought that a range of ball sizes could be accommodated by one carriage of this construction. The carriage was attached via two pivoted beams and two steel wires to a dead weight holder. The whole of this part of the apparatus was supported by an aerostatic floating pad bearing. This pad consisted of a polished steel block floating on a flat epoxy resin bed into which air jets had been implanted. Dried and filtered air was passed through the jets from a 5.6×10^5 Pa (80 p.s.i.) air supply to create an air cushion. Three other air cushions were used to contain the floating pad in the vertical and sideways directions.

At one end of the floating pad a strain gauge member was attached to secure the pad and measure traction forces at right angles to the rolling direction of the test ball. At the other end of the pad, a thin steel strip was fixed in order to make the pad more rigid at right angles to the force measurement direction (see fig. 2.5).

The load on the test ball could be varied from 1→15 lbs. with no sticking of the floating pad and this was considered sufficient for the purposes of the experiments to be performed.

2.5 TRACTION FORCE MEASUREMENT

All of the static forces transmitted between the rollers and each test ball cancel one another out in the plane perpendicular to the loading direction. In this apparatus the aim was to measure the traction force transmitted through the EHD film at right angles to the rolling direction, resulting from shearing in that direction. This was measured by a strain gauge bridge with four strain gauges stuck to a

strip of steel with two on one side and two on the other. They were connected in a Wheatstone bridge configuration with a balance potentiometer inserted to compensate for any difference in resistance between the gauges at zero load (see fig. 2.5).

The driving voltage was supplied by a stabilized 10 volt D.C. supply. This arrangement of the strain gauges has the advantage that it is temperature self-compensating. The traction force which appeared as an out of balance voltage was measured with an electronic microvoltmeter of high input impedance.

2.6 THE TEST BALLS

One of the aims of the work was to cover as wide a range of Hertz pressure distributions between ball and plate as possible. It was also thought that experiments in which one could vary the EHD contact width while keeping the peak Hertz pressure constant would also be of interest. The fact that the thermal conductivities and diffusivities of the materials (steel, tungsten carbide, sapphire, glass) were different was hoped to permit more insight into thermal effects in EHD traction. For these reasons the following types of ball were used.

(a) 2.54×10^{-2} M (1") glass ball

(b) (i) 2.54×10^{-2} M (1") steel ball

(ii) 1.74×10^{-2} M (0.6875") steel ball

(c) 2.54×10^{-2} M (1") tungsten carbide ball

FIG. 2.5

TRACTION FORCE MEASUREMENT

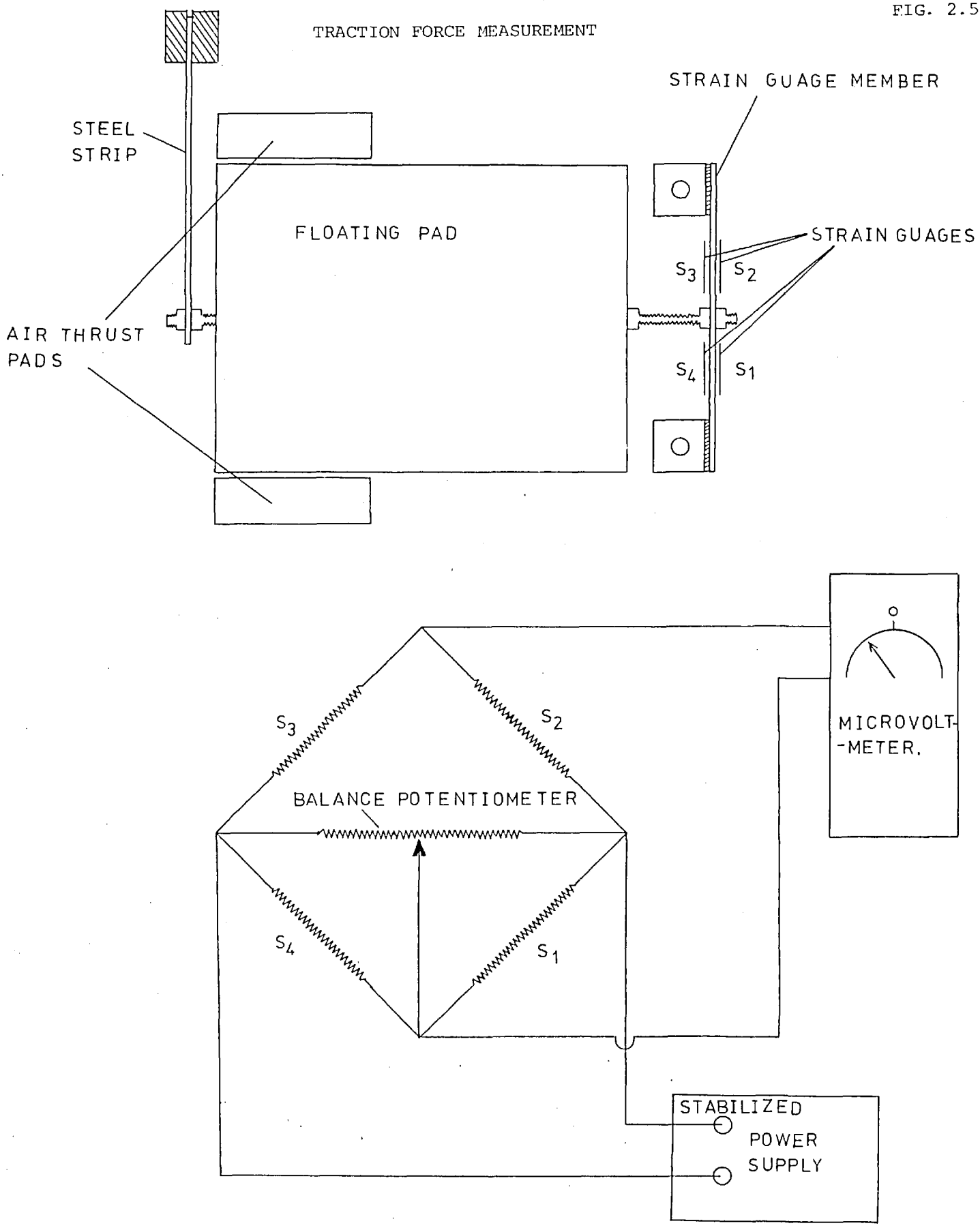

These different types of balls in conjunction with the sapphire disc permitted a range of Hertz contact widths ranging from 5.08×10^{-6} M (2×10^{-4} ins.) → 2.54×10^{-4} M (10^{-2} ins). and peak Hertz pressures ranging from 0.4 GPa (60 k.p.s.i.) → 1.75 GPa (250 k.p.s.i.). All the balls were surface finished to better than 2.54×10^{-8} M c.l.a. (1 μin.c.l.a.) so that the surface roughness was kept to an order of magnitude less than typical EHD film thicknesses to prevent asperity interaction contributions to the traction forces measured. A good surface finish was also necessary for the obtainment of good visibility of interference fringes in the film thickness measurements.

2.7 SKEWING AND TILTING OF THE BALLS

In order to control the axis of rotation of each ball, a shaft was attached to it. One end of the shaft was machined so that it could slide freely inside a double row externally aligning roller bearing which was held in a block of aluminium supported by an x,y,z, microscope movement (see fig. 2,4).

Each shaft was fixed to each ball by turning a cone shaped cup into which the ball was glued with an epoxy resin glue. The shaft would be inserted vertically into a block of wood. The glue was then applied to the cone shaped cup and the required ball allowed to settle into the cup. The whole combination was then placed in an oven at 100^{o}C for thirty minutes for the glue to cure. This was found to be a most accurate and efficient technique which gave eccentricities of balls with their shafts to better than 5×10^{-6} M (2×10^{-4} ins.).

The angles of the rotation of each ball had to be measured both in the horizontal and the vertical plane. The vertical component was easily measured by placing a piece of graph paper, stuck to a small sheet of steel, behind the ball shaft and sighting with one edge along the profile of the shaft over a known distance.

This method gave $\pm \frac{1}{2}^{o}$ accuracy which was more than sufficient considering that the vertical angular variation was over a range of 30^{o}. The horizontal component was measured with the aide of two 10^{-4} inch dial gauges, one to measure the displacement of one end of the ball shaft and the other to measure the lateral displacement of the ball due to some flexing of the ball loading system (see fig. 2.6).

Figure 7 shows the layout of the dial gauges and a schematic diagram to show the geometry in detail. The angle which will be referred to as the sideslip angle β is equal to $\psi_1 - \psi_2$.

$$\tan (\psi_1 - \psi_2) = \frac{\tan \psi_1 - \tan \psi_2}{1 + \tan \psi_1 \tan \psi_2}$$

since ψ_1 and ψ_2 are always very small ($<5^{o}$)

than $\tan (\psi_1 - \psi_2) = \tan \psi_1 - \tan \psi_2$

$$\text{or } \tan \beta = \frac{(D_2 - D_1)}{K_1} - \frac{(K_2 - D_2)}{M}$$

$$= \frac{1}{K_1} \left(D_2 \frac{(M+K_1)}{M} - D_1\right) - \frac{K_2}{M}$$

Since $\frac{K_2}{M}$ was a constant it could be eliminated by graphical plots of traction force versus tan β, which could be found from the dial gauge readings and the measured geometry of the rig.

FIG. 2.6

SKEW ANGLE MEASUREMENT

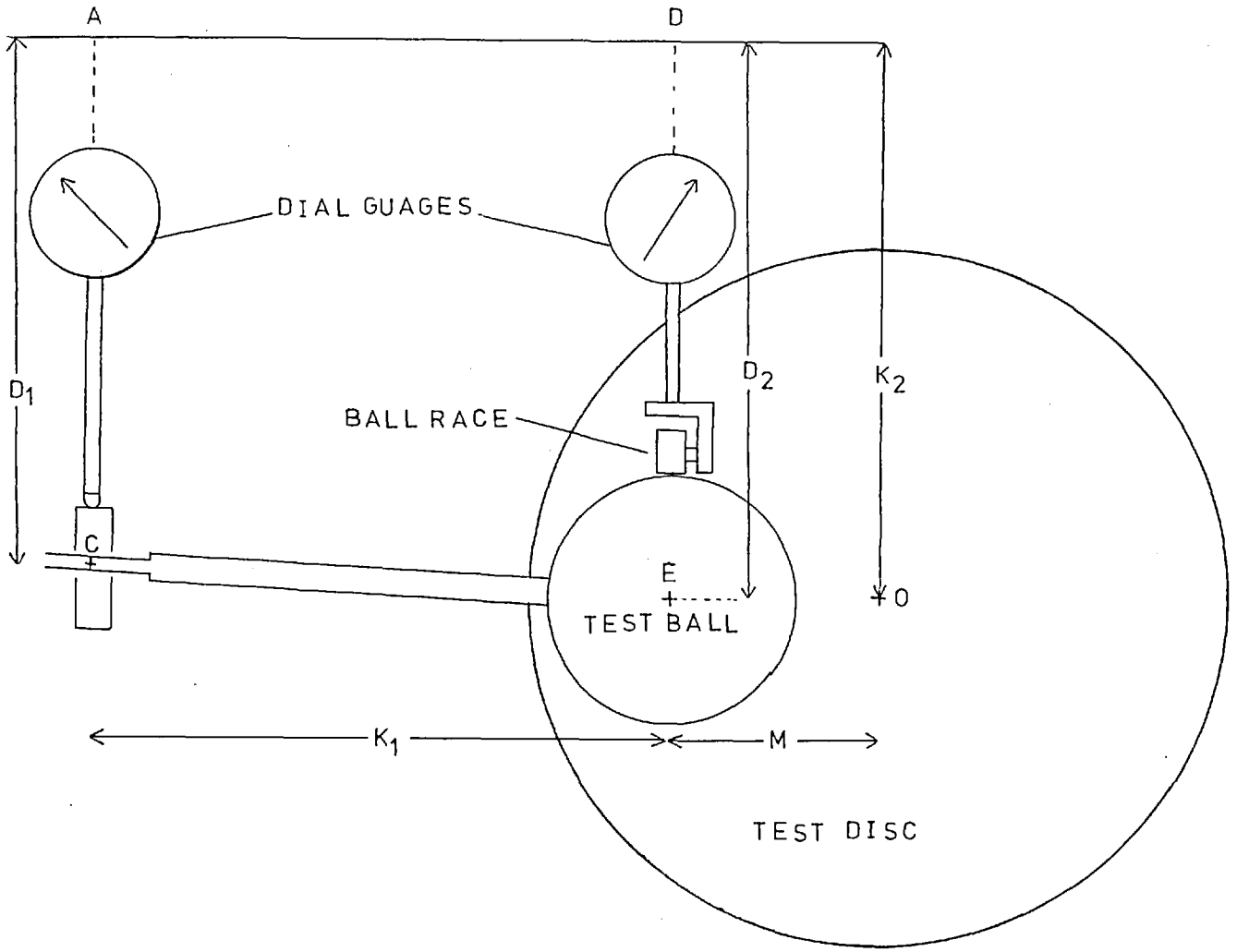

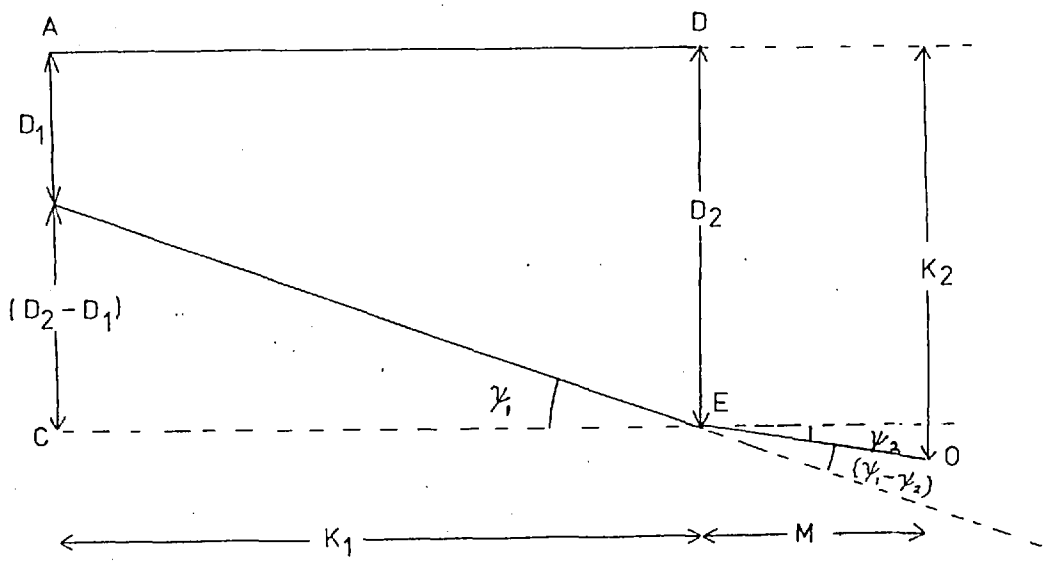

FIG. 2.7

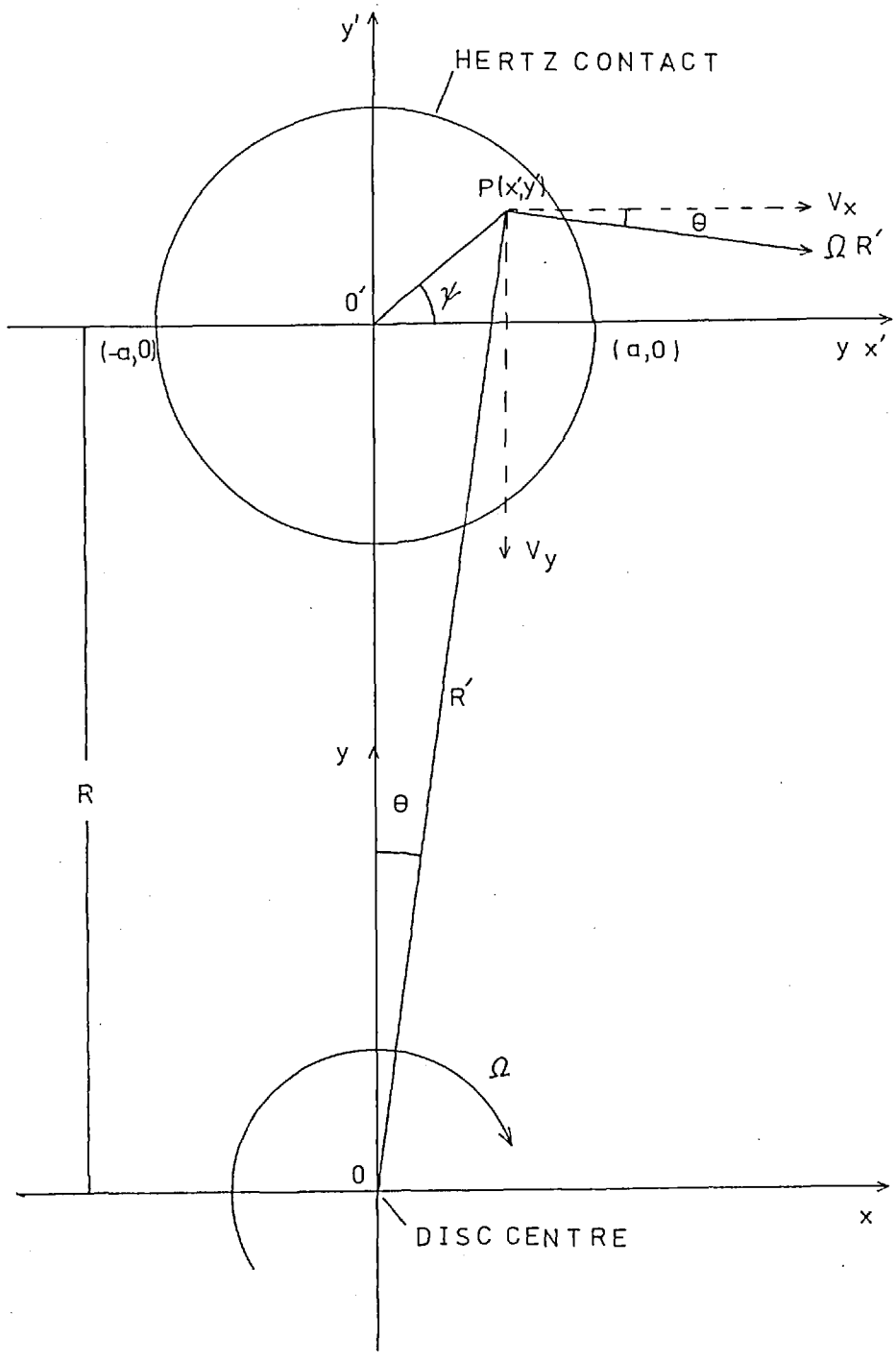

$$V_x = \Omega R' \cos\theta = \Omega(R + y') = U + \Omega y'$$

$$V_y = \Omega R' \sin\theta = \Omega x'$$

MOTION OF A POINT ON THE SURFACE OF A DISC

FIG. 2.8

(a) SIDESLIP MEASUREMENTS

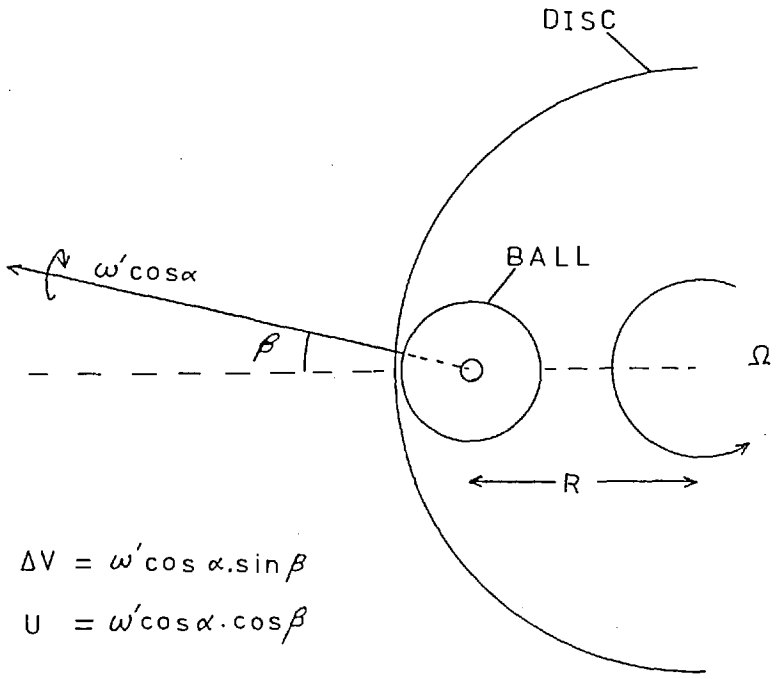

$$\Delta V = \omega' \cos\alpha . \sin\beta$$

$$U = \omega' \cos\alpha . \cos\beta$$

$$\frac{\Delta V}{U} = \tan\beta$$

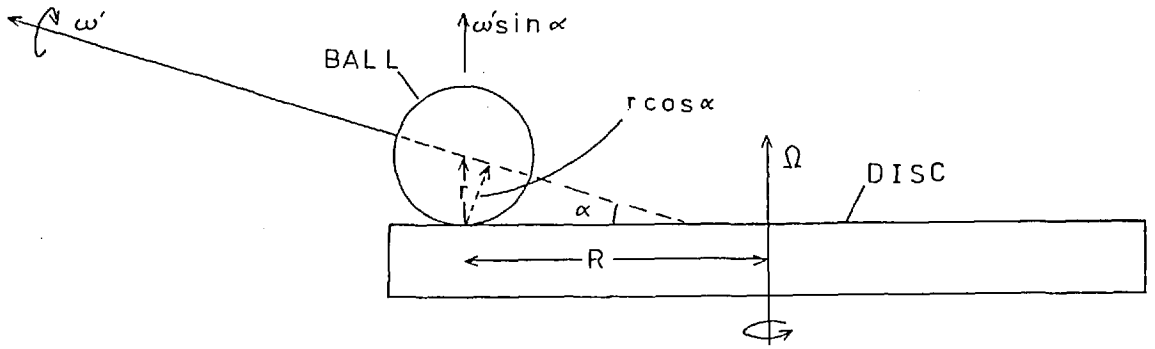

(b) SPIN MEASUREMENTS $(\frac{\Delta V}{U} = 0)$

NET SPIN $\omega_s = \omega' \sin\alpha - \Omega$

$$U = R\Omega = \omega' r \cos\alpha$$

$$\frac{\omega_s a}{U} = \frac{a \tan\alpha}{r} - \frac{a}{R}$$

CONTACT RADIUS a

ZERO SPIN FOR $\tan\alpha = \frac{r}{R}$

2.71 Kinematics of Ball Rolling against Disc

Fig. 2.7 shows how the motion of points on the surface of the disc within the Hertz contact area may be described in terms of a pure spin equal to the disc spin superimposed on the linear surface speed at the centre of a hertzian contact area.

Fig 2.8 shows how the sideslip/roll ratio may be calculated from the sideslip angle measured with the aid of the dial gauges.

Fig. 2.8 shows how the net spin in the contact may be found from consideration of the spin contribution of the ball motion and the disc surface motion. It also may be seen that the ball and disc surface motions conform when the axis of rotation of the ball possess through the centre of the disc which is the zero spin condition. The net spin is non-dimensionalised in the manner adopted by Johnson and Roberts (1).

2.8 MEASUREMENT OF DISC SPEED

It was thought to be of major importance that a fast, efficient and accurate method of speed measurement be used. The crudest method would have been to take the voltage output of the tachogenerator of the motor drive unit, but this was discarded as too inaccurate. It was decided that a high speed digital counter be used in combination with a photo diode, light source and an alternately mirrored and matt black tape, stuck to the side of the support disc would suffice (see fig.2.9). The photo diode was of the 6 volt variety and was connected in series with a 100 ohm load resistor and was powered by a 6 volt supply from the high speed counter. A high intensity focused 6 volt light source

was used. A piece of chrome tape was blanked off at half centimetre intervals with matt black tape. The voltage output from the photodiode circuit was amplified and shaped in the input circuits to drive the trigger circuit of the digital tachometer. It was possible to display the output of the photodiode to make sure that the driving conditions of the counter were satisfied. It was found that the variation in counts for constant motor speeds was better than 1 in 100 over the whole speed range encountered in the experiments. For some of the experiments the disc speed was very low (3 r.p.m.) and then a single mirror on the outside of the support disc was used to trigger an internal counter in the tachometer which would stop when the next pulse from the photodiode was received. This allowed the time for one or several revolutions to be measured very accurately.

The other method of disc speed measurement was to attach a perforated cup to the disc shaft and shine the light source through the holes. This obtained more intense and better shaped pulses of light to the photodiode (see fig. 2.9).

2.9 BALL SPEED MEASUREMENT

This was performed in either of two ways, depending upon the speed of rotation. One method was to measure time with a stopwatch for 100 revolutions of the ball shaft and this was accurate, providing a count was not lost. The other method was to stick a mirror on the side of the ball shaft and use the same method outlined in section 2.8.

FIG. 2.9

SPEED MEASUREMENTS

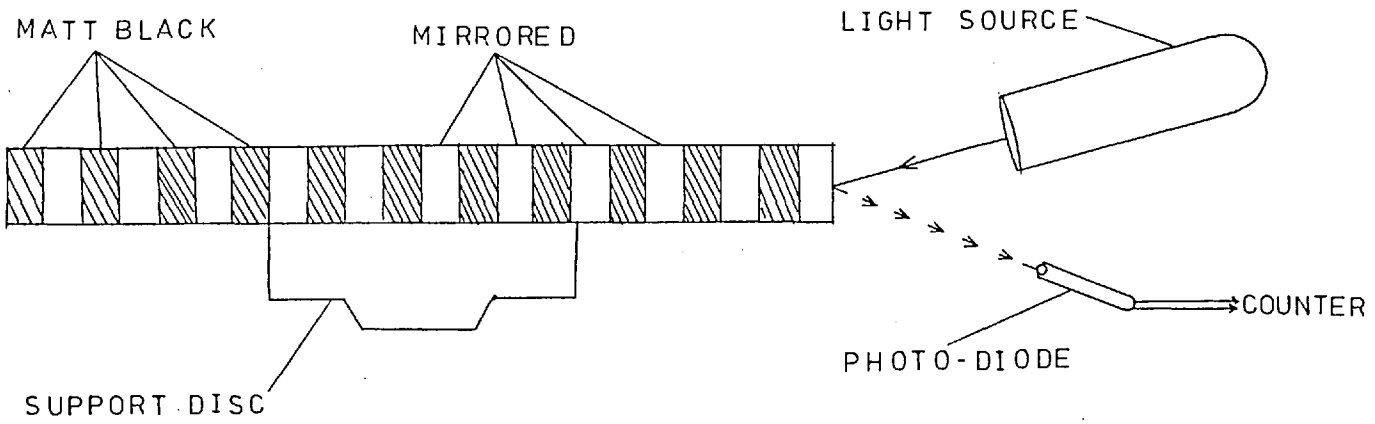

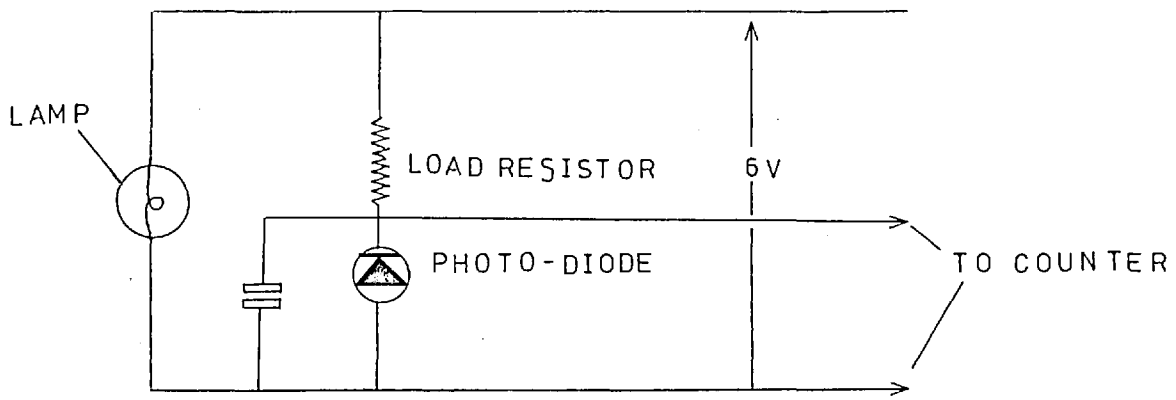

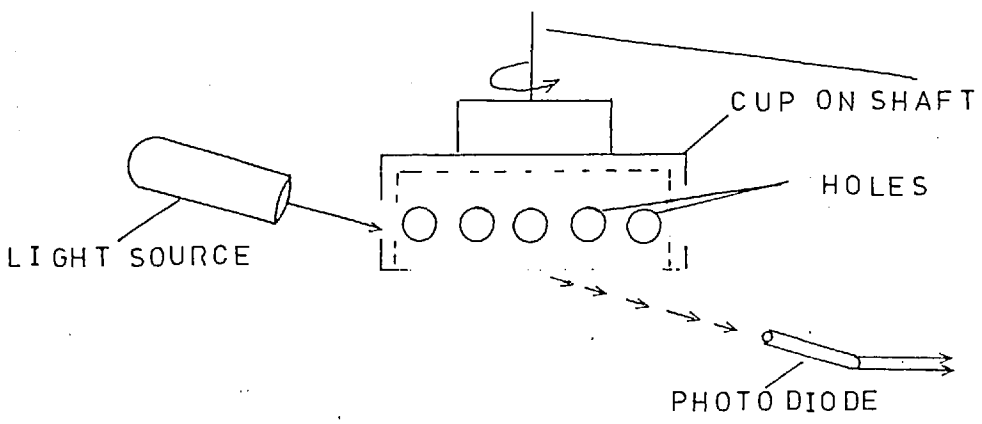

2.10 TEMPERATURE MEASUREMENT

Since it is the mean inlet temperature of oil to an EHD contact which determines the inlet viscosity and so to a major extent the film thickness, it was considered important that this be measured. This was less important in these experiments because the film thickness could be measured directly by optical interferometry, but it was thought to be particularly useful in showing up any unexpected behaviour in film formation with known non-Newtonian fluids.

The important temperatures in EHD traction are those occurring inside the EHD oil film. To date there have been various attempts at a direct measurement of EHD oil film temperature distributions (Kannel & Dow(2)),but there are considerable calibration problems associated with the work.

It was finally decided to use two chrome alumel thermocouples one at the inlet to the EHD contact and one at the outlet, so as to monitor any large temperature differences across the contact due to shear heating. Both of the thermocouples were cut from the same thermocouple wire and both were connected to the same electronic thermometer. The junctions of each thermocouple were about 10^{-2} ins. (2.54×10^{-4} M) diameter so that their thermal capacities would have a minimal influence on the temperature measurements. The thermocouples were mounted on a magnetic base which made positional adjustment of them easy.

The differences in temperature between the inlet and outlet surfaces was never found to be more than about $\frac{1}{2}^{o}$C during the experiments.

2.11 ATMOSPHERIC CONDITIONS

Gentle(3) carried out traction measurements in a similar traction rig with a 0.1% oxygen concentration and nitrogen atmosphere and found no noticeable difference in his results from those performed in air and so that procedure was not used.

2.12 TEMPERATURE CONTROL

Since this apparatus was designed to be used to test small samples (50 ml.) of fluids, a recirculatory fluid system with a temperature bath was ruled out from the start, and so the ball and disc had to be heated internally.

A 750 watt cylindrical heater was built to fit around the ball and disc. This consisted of a helical heater element fixed within a moulded asbestos composite cylinder, enclosed in a stainless steel jacket. The power to the heater was controlled by an electronic thermostat.

One problem encountered when traction tests were being performed was that the air thrust pad stuck, due to differential expansion. A heat shield was made from a plywood disc covered with aluminium foil to insulate the air thrust pad from the high temperature chamber.

This worked well for temperatures up to $80^{o}C$.

2.13 REFERENCES

1. JOHNSON, K.L. and ROBERTS, A.D., "Observations of an EHD film", Proc. Roy. Soc., London, A337, 217-242 (1972)

2. KANNEL, J.W. and DOW, T.A., "The evolution of surface pressure and temperature measurement techniques for use in the study of lubrication as metal rolling", Trans. ASME, 1974, paper no. 74, Lab S-7

3. GENTLE, C.R., Ph.D. Thesis, London University, 1971

C H A P T E R 3

THE INTERFEROMETRIC SYSTEM

The main reasons for adopting this technique were as follows:

(a) It is a well-developed technique with a wealth of previous experience of the use of it - (Cameron and Gohar(1), Wedeven(2), Foord(3), Gentle(8), Pemberton(5), etc.

(b) It is difficult to predict oil film thicknesses for point contact lubrication.

(c) The capacitance method is very cumbersome and relies on a knowledge of the dielectric constant under the conditions of EHD lubrication.

(d) Many of the interesting traction fluids are markedly non-Newtonian, thus rendering film thickness formulae doubtful.

(e) Optical interferometry permits a first-hand observation of starvation effects.

(f) The deformation profile of the surfaces may be seen, although a detailed knowledge of this relies upon a detailed knowledge of the variation of refractive index across a contact.

The principles of interferometry have been well understood since the time of Newton and are dealt with in detail by most books on optics. The technique of application of interferometry to EHD film thickness measurement is well described in Foord(3), Cameron and Gohar(1), Westlake(6) and Gentle(8).

Both chromatic and monochromatic two beam interferometry were used. The monochromatic interferometry was essential for the measurement of very thick films where many orders of fringes were possible due to the long coherence length of monochromatic light. This was also used for high speed microphotography, using a xenon flash tube.

The chromatic interferometry was used for measuring thinner films (2 to 15 x 10^{-7} M) where four shades of colour (yellow, red, blue, green) could lead to a more detailed measurement of film thickness.

Each of the discs was "sputtered" with a 200Å 18% reflectively 25% absorption layer of chromium. This method of deposition has been found to lead to much stronger coatings, particularly on sapphire. This is essential, considering the normal and shear stress conditions that any surface coating is subjected to in EHD traction

A magnesium fluoride anti-reflection coating was also deposited on the sapphire and quartz discs to eliminate unwanted reflections from the lower surface.

The optical arrangement is shown in fig.3.2. A long focal length lens (f = 2.54x10^{-2}M, N.A. = 0.15) had to be used to obtain a long working distance for the microscope. A beck side illuminator was used and this worked well and made the substitution of one light source for another an easy matter. The angled microscope tube was used to make observation not only more comfortable but also possible.

FIG. 3.1

TWO BEAM INTERFEROMETRY

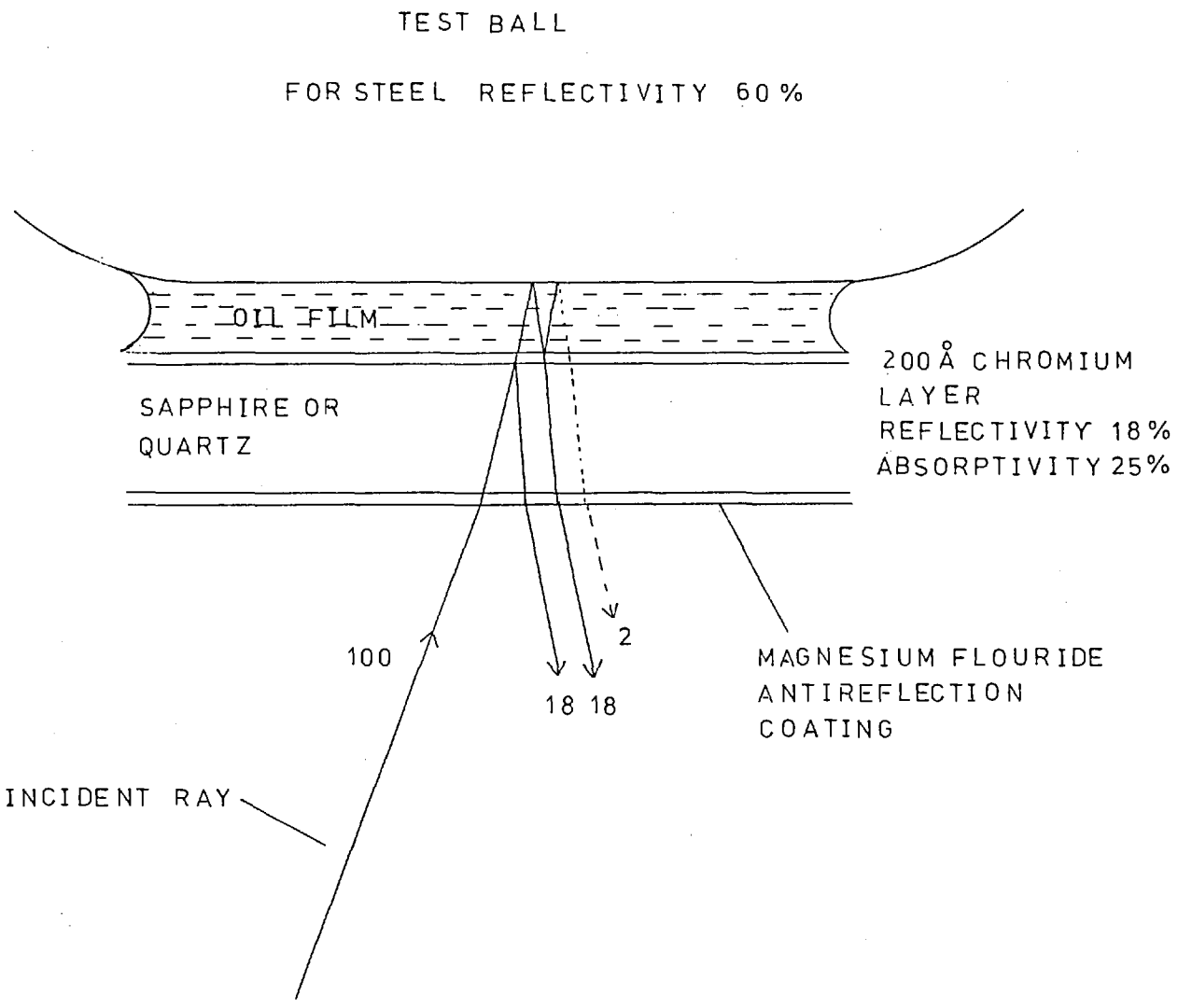

FIG. 3.2

THE OPTICAL SET UP

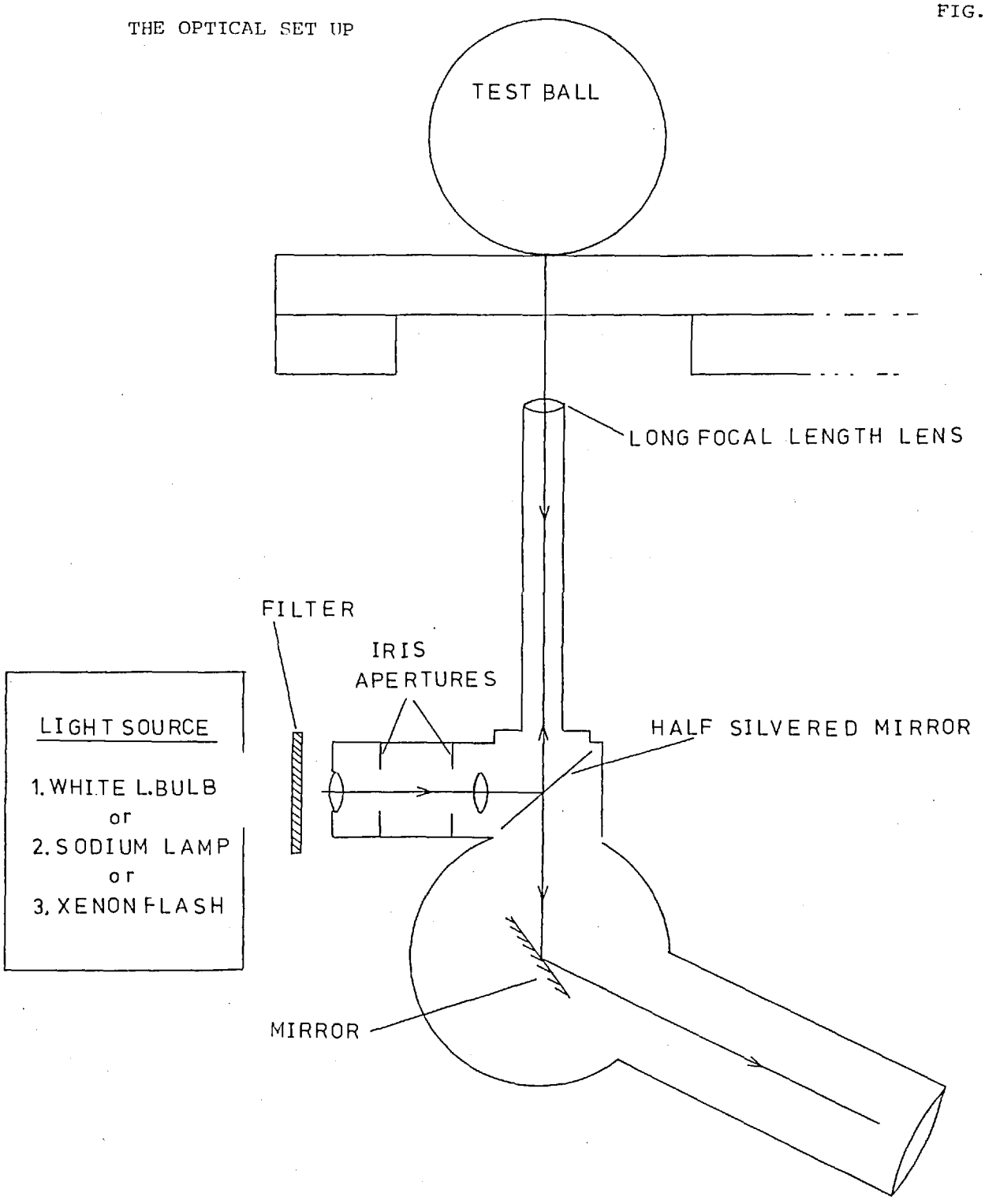

3.1 REFERENCES

1. CAMERON, A. and GOHAR, R. "Theoretical and experimental studies of the oil film in lubricated point contact", Proc. Roy. Soc. (A), 1966, 291, 520

2. WEDEVEN, L.D., Ph.D. Thesis, London University, 1970

3. FOORD, C.A., Ph.D. Thesis, London University, 1968

4. GENTLE, C.R., Ph.D. Thesis, London University, 1971

5. PEMBERTON, J., Ph.D. Thesis, London University, 1976

6. WESTLAKE, F.J., Ph.D. Thesis, London University, 1970

CHAPTER 4

EXPERIMENTAL PRELIMINARIES

Before it was possible to start an experiment, it was necessary to calibrate each instrument and make sure that the bearing surfaces were of a good finish.

4.1 BALL SURFACE FINISH

As mentioned in the previous chapter, it was most important that the ball surfaces be polished to better than 2.54×10^{-8} M c.l.a. (1 μinch c.l.a.). The tungsten carbide balls arrived with this finish and so were not touched. The steel balls, although superfinished, still required some polishing. This was done by placing the ball shaft in a collet chuck and spinning it at high speed (10,000 r.p.m.).

An electric drill, containing a small shaped cup, covered with polishing cloth and diamond paste, was then applied to the side of the spinning ball. It was found that by using 5 micron paste followed by 1 micron paste that a brilliant finish could be obtained for each ball.

4.2 THE DISC SURFACE FINISH

For optical reasons the discs were machined and polished to optical standards and so the surface roughness was not likely to interfere with traction measurements. The deposition of chromium on the surfaces also tended to fill in any of the valleys between the asperities. The use of such a thin film (200 Å) of chromium in no way masked the

bulk properties such as modulus of elasticity, thermal conductivity, and specific heat, but it did appear to affect dry traction tests which were performed with great reluctance although some success.

4.3 PREPARATION OF LUBRICANTS

It was not thought to be necessary to purify any of the fluids tested, since all were thought to be chemically stable at room temperature and pressure. They were, however, stored in a dark place since this would reduce oxidization. Tests made at different times, from a few minutes after opening each fluid sample bottle to several weeks, showed no significantly different traction and film thickness results, and so it was concluded that the parameters of the fluids were stable for the purposes of these experiments.

It was found, however, that it was better to complete each set of tests with fluid from the same original sample, because of the difficulty of manufacturers to duplicate the complex molecular compositions of the fluids.

4.4 CALIBRATION OF THE OPTICAL FILM THICKNESS

The condition for there to be a bright interference fringe is that:

$$\text{the optical thickness } h_{opt} = \tfrac{1}{2} \text{ path difference}$$

$$= \tfrac{1}{2} \left(N\lambda + \frac{B\lambda}{2\pi} \right)$$

where B is the phase change of the light on reflection from the polished surfaces, N is an integer known as the fringe order, λ is the wavelength of the component of the white light source which is interfering constructively in the conjunction.

Owing to the subjective nature of colours, it was necessary to make a calibration which would relate each observed colour to each film thickness. This was originally done by Cameron and Gohar(1) by allowing the ball to just touch the transparent disc in air and performing a "Newton's rings" experiment using a filar eyepiece or a travelling microscope. As shown by Gentle(2), this method ignores the small deformation of the two surfaces at the point of contact and so could lead to large inaccuracies in the calibration. The improved method, described by Gentle, was used in these experiments as is explained as follows.

The ball was loaded against the disc with a load of 1 lb. and the Hertz equation for the separation of the surfaces outside the contact area was used to calibrate the coloured fringes. This was done by measuring the radius of each colour and order of fringe with a filar eyepiece used with a travelling microscope. This was repeated for different loads for greater accuracy.

The Hertz equation for the gap between the surfaces outside the point of contact is given by:

$$h = \frac{a\ Pmax}{E'} \left[- \left(2 - \frac{r^2}{a^2}\right) \cos^{-1} \left(\frac{a}{r}\right) + \left(\frac{r^2}{a^2} - 1\right)^{\frac{1}{2}} \right]$$

where h is the separation of the surfaces

a is the Hertz contact radius

$Pmax = \frac{3N}{2\pi a^2}$ the maximum Hertz Pressure

r is the radial distance from the contact centre

In order to calculate the actual film thickness between the surfaces with oil between them, the refractive index of the fluid in in the contact had to be known.

$$\text{i.e. } h_{actual} = \frac{h_{opt}}{n(p,\theta)}$$

Until recently it was necessary to use an Abbé refractometer to measure the refractive index of each fluid as a function of temperature at atmospheric pressure. The refractive index at the contact centre pressure Pmax was calculated from the Lorentz-Lorentz equation

$$n_p = \left(\frac{1+2A}{1-A} \right)^{\frac{1}{2}}$$

$$\text{where } A = \frac{\rho_p}{\rho_o} \cdot \frac{(n_o^2 - 1)}{(n_o^2 - 2)}$$

where ρ_p is the density of fluid at pressure p

ρ_o is the density of atmospheric pressure

n_p is the refractive index of the fluid at pressure p

n_o is the refractive index of the atmospheric pressure

$\frac{\rho_p}{\rho_o}$ was obtained from bulk modulus data

This was thought to be inherently doubtful, since it assumed that the refractive index reaches an equilibrium value in the contact. It is clear from the work of Paul(3) that refractive index is a function, not only of temperature pressure and density, but also of shear rate and possibly of time because of relaxation processes following the virtual pressure step arising in e.h.d. lubrication.

It is important to note, however, that for low shear rates Paul(3) found fair agreement between his measurements and those predicted by the Lorentz-Lorentz formula and that since the equilibrium refractive index is only about 10% above normal, one would not expect it to be exceeded whatever the conditions prevailing in the e.h.d. contact.

It was decided that errors of less than $\pm$ 5% would be incurred if the room temperature refractive index were measured and

$n_p = 1.1\, n_o$ were used.

THE OPTICAL CALIBRATION OF FILM THICKNESS

Fringe		Optical Film Thickness
1st Order	Yellow	2.0×10^{-7} M
	Red	2.7
	Blue	3.4
	Green	4.3
2nd Order	Yellow	4.7
	Red	5.6
	Blue	6.1
	Green	6.7
3rd Order	Yellow	7.6
	Red	8.3
	Blue	8.9
	Green	9.6

4.5 CALIBRATION OF THE TRACTION FORCE MEASUREMENTS

The apparatus was set up with the ball rolling against the disc as was the case during actual experiments.

Forces were applied to the floating pad via a nylon string and a low friction pulley, and the strain gauge bridge output measured for each condition. This was performed in both directions so as to check that there was no sticking of the pad bearing or hysteresis of the strain gauge support member.

This calibration was checked before each experimental run, particularly if the temperature had been varied, as this led to a drift in the calibration due to slight changes in the differences of resistance of the four strain gauges.

It was found that measurements were very linear and that the graph for unloading was the same as that for loading. This calibration method had the advantage that it was simple and easy to repeat at any time.

4.6 THE NORMAL LOAD N CALIBRATION

It was found by simply measuring the weights and lengths of the various parts of the loading system to calculate the normal load/dead weight calibration constant.

4.7 PRELIMINARY COMPLIANCE TESTS

From the outset of this work it was realised that, under the conditions of shearing of very thin (1μM) e.h.d. films, the compliances of the ball and disc could well influence the results obtained from the

apparatus. It was pointed out by Johnson and Roberts(4) that results from this type of apparatus could be mistakenly interpreted as evidence of "elastic" behaviour of e.h.d. films when in fact they would arise from the elastic deformation of the bearing surfaces, either side of a very thin, highly viscous film (see Section 6.61).

It was therefore decided to conduct some dry contact traction tests to see what agreement could be found between the ball on plate dry contact traction and crowned disc on disc dry traction results obtained by Johnson and Roberts(4). They found experimentally that for dry traction:

$$T'_{\beta} = 1.78 \frac{G_s}{Pmax} \cdot \frac{N.U}{\Delta V}$$

where T'_{β} is the dry traction force

G_s is the elastic shear modulus of the discs

N is the normal load

U is the mean rolling velocity

ΔV is the sideslip velocity

There were three basic differences between the ball on plate and the two disc system.

(a) The ball and plate materials were of different elastic compressive shear moduli and poisson ratios.

(b) The ball and plate had different geometries.

(c) The surface finish on the ball (2.5×10^{-8} M c.l.a.) was quite different from that of the plate (2×10^{-9} M c.l.a.).

Bearing these facts in mind, it was still thought to be appropriate to perform some dry traction tests, although the above differences could lead to lower gradient traction curves than expected.

4.8 EXPERIMENTAL METHOD (DRY TRACTION)

The ball and plate were first thoroughly cleaned in toluene and acetone in an ultrasonic cleaner. These parts were then assembled with $\tan \alpha = \frac{r}{R}$ for zero relative spin between the surfaces. The plate was then rotated very slowly and the traction force measured for different sideslip angles. This was performed for each material combination. These results were plotted in the form T/N versus $\Delta V/U$ which has been adopted for all sideslip traction curves in this work (see fig. 5.1).

The shear moduli of the materials was calculated from the conventional elasticity equation

$$G = \frac{E}{2(1 + \sigma)}$$

where σ is the poisson ratio

E is the compressive modulus

The effective shear modulus of each material combination was approximated by

$$\frac{1}{G_s} = \frac{1}{2} \left(\frac{1}{G_1} + \frac{1}{G_2}\right)$$

$$\text{if} \quad m'_\beta = \frac{T_\beta'/N}{\Delta V/U}$$

$$\text{then} \quad m'_\beta = 1.78 \frac{G_s}{Pmax}$$

The gradients of the traction curves were plotted versus $\frac{1}{Pmax}$ and showed lower values than expected. The tungsten carbide ball on sapphire results were about 12% lower than predicted except a high pressure where they were found to be 30% lower (see fig. 4.1).

These experiments were quite easy to perform but did lead to a lot of scatter. All the runs were repeated and an attempt was made to clean away debris from the surfaces between runs, but it was very difficult to be absolutely sure and it was thought that debris could reduce the traction gradients through increased slip. It is also well known that EN31 balls have a very thin oxide layer which has a lower coefficient of friction than the bare metal and this might aid microslip.

All in all, there was fair agreement between the results and the formula, and so it was decided to adopt this for lack of solid evidence to the contrary.

The main point was to obtain results for the films with compliances significantly more than the joint surface compliances.

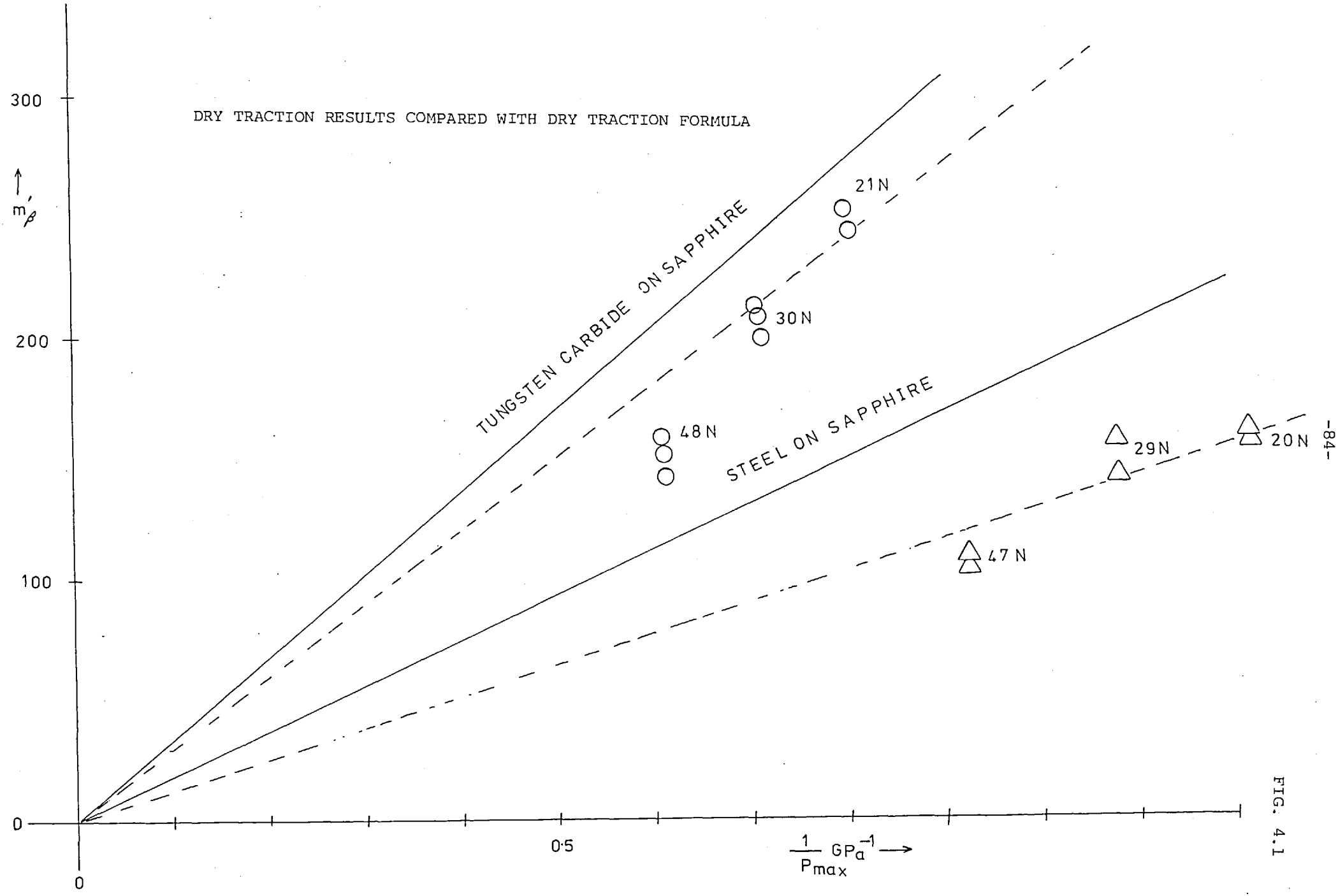
DRY TRACTION RESULTS COMPARED WITH DRY TRACTION FORMULA
300
200
100
0
0
0·5
m'_β
$\frac{1}{P_{max}}$ GPa^{-1} →
TUNGSTEN CARBIDE ON SAPPHIRE
STEEL ON SAPPHIRE
21N
30N
48N
29N
20N
47N

FIG. 4.1

4.9 REFERENCES

1. CAMERON, A. and GOHAR, R., "Theoretical and experimental studies of the oil film in lubricated point contact", Proc. Roy. Soc., (A) 291, 520

2. GENTLE, C.R., Ph.D. Thesis, London University, 1971

3. PAUL, G.R., Private communication

4. JOHNSON, K.L. and ROBERTS, A.D. "Observations of viscoelastic behaviour of an EHL film", Proc. Roy. Soc. London, (A) 337, 212-242, (1972)

CHAPTER 5

EXPERIMENTAL METHOD

Each test run was split into three main parts; film thickness/speed measurement, traction with sideslip, and traction with spin. Before each test run with a new fluid, the ball, disc, and the ball loading nest of rollers were cleaned thoroughly, first with toluene and then with acetone to remove any traces of toluene. It was easy to see when the disc was clean by the thin film interference patterns on the surface which disappeared as the acetone evaporated from the surface.

5.1 FILM THICKNESS MEASUREMENT

About 10 m.l. of fluid was poured onto the ball and disc with a light load on the ball. The speed of the disc was then steadily increased still with a light load on the ball to prevent surface damage from asperity interaction. The load was then increased to that required and the test proceeded with.

As some of the fluids were of very high viscosity at room temperature (5P4E has a viscosity of about 3.0 Pa secs. at $20^{o}C$), a few rotations of the disc were made before a track in the pool of fluid was formed to provide stable inlet conditions for elastohydrodynamic film formation. Initially small droplets of fluid would cause the film thickness to vary by up to 3×10^{-7} M during each rotation of the disc.

The film thickness was measured by speeding the disc up gradually from stationary to the speed at which the central region of the contact

became yellow. At this point the reading of the digital counter, which could be set for a long or a short time count according to the disc speed, was noted. The motor speed was then increased until the next fringe colour was most distinct and so the process was repeated to three or four orders of fringe.

For those experiments where very thick films were studied, white light interferometry was not suitable and the light source was changed for a sodium lamp (D_1 = 5896Å, D_2 = 5890Å) which permitted many orders of fringe to be seen clearly.

Throughout all the tests the temperature was monitored by thermocouples so that any increase in bulk fluid temperature could be observed. This was important with high viscosity fluids (e.g. 5P4E) because small changes in temperature at room temperature lead to large changes in viscosity and so film thickness. At high temperature the variation of viscosity with temperature becomes progressively less, thus allowing greater tolerances in temperature.

One of the advantages of the inteferometric method of film thickness measurement is that it enables the experimenter to observe the immediate onset of starvation as a non-uniformity of fringe pattern coupled with the approach of the inlet wake of fluid to less than about 1.5 Hertz contact width from the inlet zone of the contact. Checks were made during traction tests that the contact was fully flooded.

5.2 TRACTION MEASUREMENTS (SIDESLIP) (see fig. 5.1)

For each test run a routine calibration check was made on the strain gauge bridge to see if any sticking of the floating pad was occurring. This had happened on occasion through differential expansion

of the pad bearing in high temperature experiments. The disc was then set in motion to create a thick enough e.h.d. film to prevent scuffing and the tilt angle adjusted for the condition

$$\tan \alpha = \frac{r}{R} \quad \text{(see Section 2.71)}$$

where there would be zero relative spin between the ball and disc. The load on the ball was then set by placing an appropriate dead weight on the scale pan.

The rolling speed was then set to obtain a film thickness greater than the surface roughness and the reading on the microvoltmeter noted for each pair of dial gauge readings. An attempt was made to vary the ball axis in such a way that the traction force varied by similar amounts for each change of sideslip β angle so as to ensure a sufficient supply of data points where the variation of traction force was greatest.

5.3 TRACTION MEASUREMENTS (SPIN VARIED) (see fig. 5.1)

The tilt angle was set and "forward and reverse" sideslip traction tests were performed. These were then plotted and the intersection of the traction curves taken as a measure of the force T_α arising purely from spin in the contact. This was done for different tilt angles so that a plot of $\frac{T_\alpha}{N}$ versus $\frac{\omega_s a}{U}$ could be made after correcting for the component of the ball shaft weight in the traction force direction.

The correction for the component of the weight is

$$F_2(\alpha) = \frac{W \sin 2\alpha}{4}$$

where W is the weight of the shaft (0.1 kg). This was not found to be significant except for low values of $T\alpha$.

5.4 BALL SHAFT CORRECTION

Correction for the component of the weight of the ball shaft acting at right angles to the rolling direction of the ball.

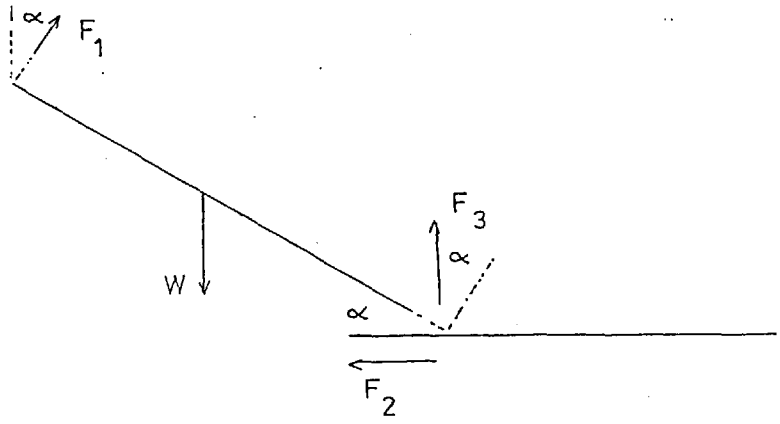

$$F_1 \sin \alpha = F_2 \qquad (1)$$

$$F_1 \cos \alpha + F_3 = W \qquad (2)$$

$$F_3 \cos \alpha = F_2 \sin \alpha + F_1 \qquad (3)$$

$$F_1 \cos^2 \alpha + F_2 \sin \alpha + F_1 = W \cos \alpha$$

$$F_2 \cos^2 \alpha + F_2 \sin^2 \alpha + F_2 = W \cos \alpha \sin \alpha$$

$$\therefore \quad F_2 = \frac{W \cos \alpha \sin \alpha}{2}$$

$$= \frac{W \sin 2\alpha}{4}$$

This force had to be subtracted from the results and was particularly significant when low traction fluids were tested.

FIG. 5.1

GRAPHICAL ANALYSIS
OF RESULTS

$$\bar{\tau}_{\frac{1}{2}} = \frac{T_{\frac{1}{2}}}{\pi a^2}$$

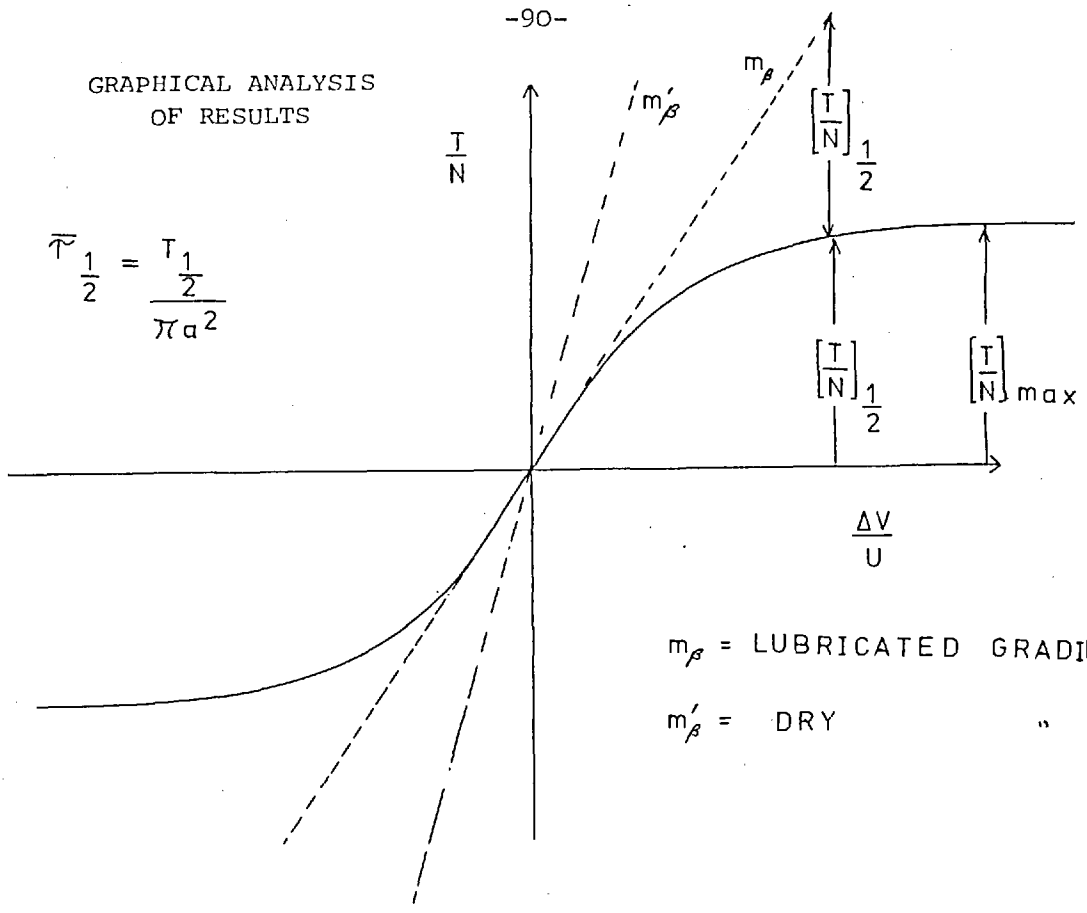

m_β = LUBRICATED GRADIENT

m'_β = DRY "

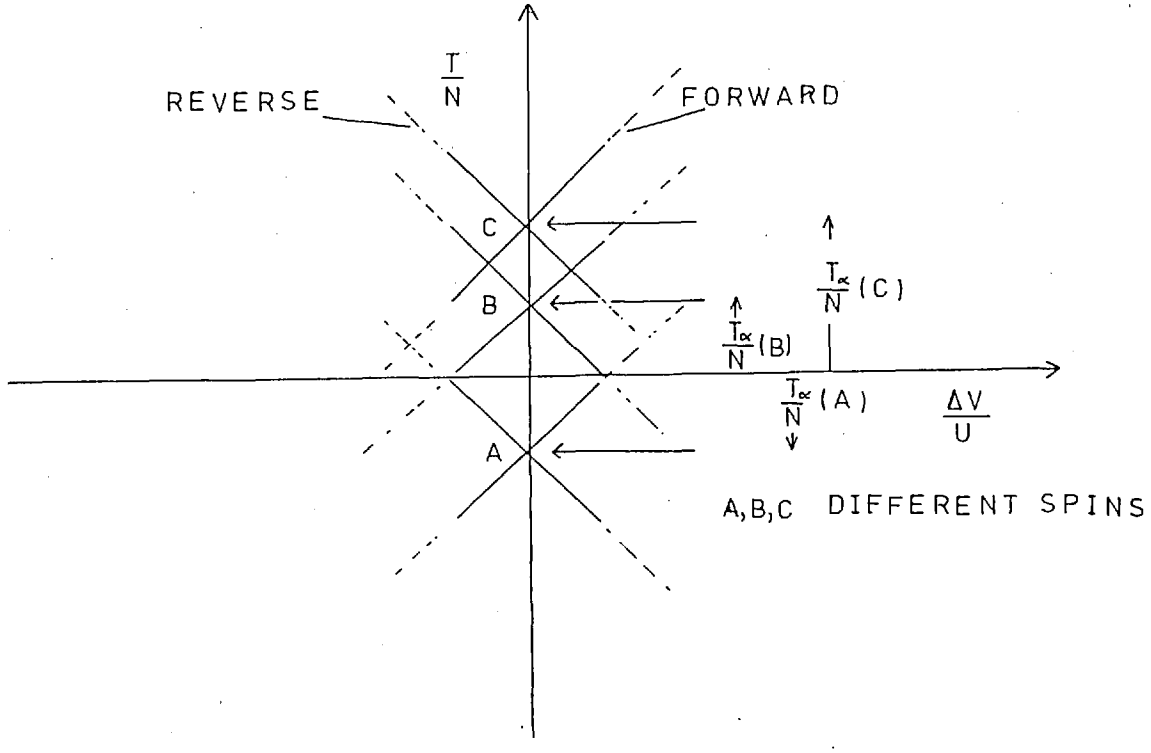

A,B,C DIFFERENT SPINS

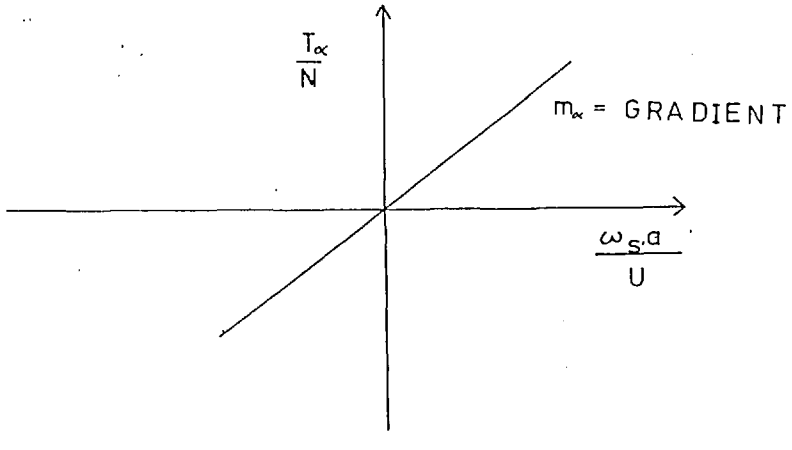

CHAPTER 6

THEORY OF THE ANALYSIS OF THE RESULTS

In this chapter the theory and methods of analysis of the film thickness and traction with spin and sideslip are discussed.

6.1 DERIVATION OF APPROXIMATE PRESSURE VISCOSITY VALUES FROM FILM THICKNESS RESULTS

These were mostly used for interpretation of traction data but this method of film thickness measurement facilitated an approximate comparison of the pressure viscosity coefficients of the various fluids.

The film thickness for a rolling point contact may be described as

$$\frac{h}{R} = K \left(\frac{\eta_o U}{E'R}\right)^a \left(\frac{N}{E'R^2}\right)^b (\alpha' E')^c \qquad (1)$$

where a is about 0.7, b is about -0.15, and c is about 0.6 and K is a constant. A film thickness/rolling speed experimental run was performed for each fluid and a reference fluid for the same values of E', R and N. These results were then plotted in the form of log h versus log $(\eta_o U)$ thus yielding a set of nearly parallel straight lines of gradient 0.7. The displacements between these lines provided a simple approximate method of comparing the pressure/viscosity coefficient (α' value) of each fluid. Implicit in the above equation is that for the purposes of elastohydrodynamic film thickness formulation the viscosity is an exponential function of pressure, i.e.

$$\eta(P) = \eta_o \exp(\alpha' P) \qquad (2)$$

when η_o is the viscosity at atmospheric pressure, and α' is the pressure viscosity coefficient and P is the pressure. Under the above conditions for a constant value of $\eta_o U$

$$h = K'(\alpha')^{0.6} \tag{3}$$

where K' is a constant

$$\frac{hTest}{hREF} = \frac{\alpha TEST}{\alpha REF}^{0.6} \tag{4}$$

when hTEST is the film thickness of the test fluid

hREF is the film thickness of the reference fluid

α'TEST is the α' value of the test fluid

α'REF is the α' value of the reference fluid

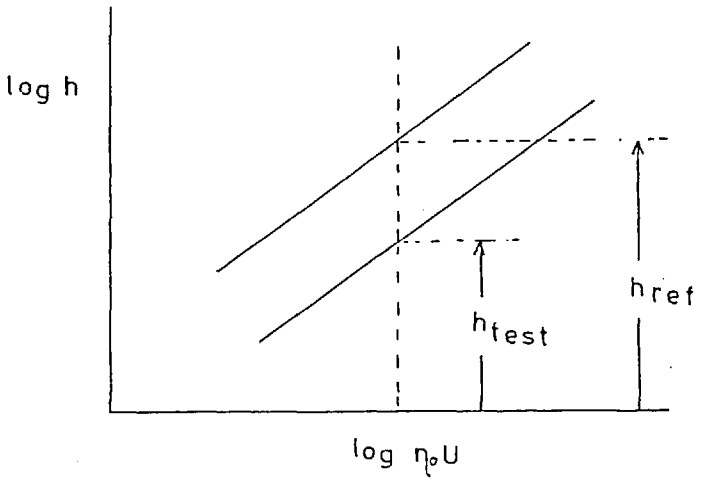

$$\alpha'TEST = \alpha'REF \left[\frac{hTEST}{hREF}\right]^{\frac{1}{0.6}}$$

$$= \alpha'REF \left[\frac{hTEST}{hREF}\right]^{1.666} \tag{5}$$

For some oils, such as silicone fluids, the viscosity is both time dependent and shear rate dependent and so the viscosity is not as high in the contact as expected, and this means that a very low value of α' is found by this method, and it cannot be used to give the true pressure/viscosity behaviour.

6.2 THEORY OF THE TRACTION EXPERIMENTS

As described in Sections 5.2 and 5.3, two basic types of traction experiment were performed with the apparatus.

(a) Rolling with 'spin'

In this case the oil film was subjected to small amounts of differential spin in its passage through the contact for zero sideslip (i.e. $\frac{\Delta V}{U} = 0$) and the resultant traction force measured.

(b) Rolling with 'sideslip'

In this case the ball axis was tilted in such a way that $\tan \alpha = \frac{r}{R}$ (ZERO NET SPIN) in the plane of the disc and the spin component of the ball's motion conformed with the motion of points on the surface of the disc. Sideslip was introduced by varying the 'shear' angle β of the ball axis.

Both of the above arrangements lead to the formation of a thin elastohydrodynamic film of nearly uniform thickness and radius a.

For the purposes of analysis, the contact area is assumed to be circular of radius a and of uniform film thickness h and either of (1) uniform viscosity η or (2) uniform elastic modulus G.

6.3 ROLLING WITH 'SPIN' (UNIFORM NEWTONIAN VISCOSITY η)

It is clear that the y component of the shear rate through the contact is given by

$$\dot{\gamma}_y = \frac{\omega_s x}{h} \qquad (6)$$

which is antisymmetric with respect to the centre of the contact area. No net traction force Tα would be expected for a Newtonian viscous film, i.e.

$$T\alpha = \int_{\text{CONTACT AREA}} \eta \frac{\omega_s x}{h} \, dydx$$

$$= \int_{-a}^{+a} 2\eta \frac{\omega_s x\sqrt{a^2-x^2}}{h} \, dx$$

$$= 0 \qquad (7)$$

6.4 ROLLING WITH 'SIDESLIP' (UNIFORM NEWTONIAN VISCOSITY)

The traction force would simply be that due to viscous drag, i.e.

$$T_\beta = \pi a^2 \eta \frac{\Delta V}{h} \qquad (8)$$

6.5 ROLLING WITH 'SPIN' (UNIFORM SOLID FILM OF ELASTIC MODULUS G)

If we consider the y component of the shear rate through the film at some point P (x,y)

$$\dot{\gamma}_y = \frac{\omega_s x}{h} \qquad (9)$$

and if the contact area is taken to bounded by the circle $x_o^2 + y_o^2 = a^2$ then by integrating along a flowline parallel to the x axis

$$\gamma_y = \int_0^t \frac{\omega_s x}{h}\,dt = \int_{-x_o}^{x} \frac{\omega_s x}{h}\,dx$$

$$= \frac{\omega_s}{2hU}\,(x^2 - x_o^2)$$

Then for an elastic solid film

$$T_\alpha = G \int_{\text{CONTACT AREA}} \gamma_y\,dydx$$

$$= \frac{\pi\omega_s a^4}{4hU}\,G \qquad (10)$$

6.6 ROLLING WITH 'SIDESLIP' (ELASTIC SOLID FILM OF ELASTIC SHEAR MODULUS G)

The sideslip velocity ΔV is constant through the contact and so the shear rate through the contact in the y direction is

$$\dot{\gamma}_y = \frac{\Delta V}{h}$$

by integrating with respect to time along a flowline

$$\gamma_y = \frac{2\Delta V x_o^2}{hU}$$

and so

$$T_\beta = \int_{\text{CONTACT AREA}} G\gamma_y\,dydx$$

$$= \frac{8a^3}{3h}\,\frac{\Delta V}{U}\,G \qquad (11)$$

Equations (8), (10) and (11) may be rewritten in terms of the gradients of traction curves m_α and m_β as (15), (16), (17)

$$\text{when } m_\alpha = \frac{T_\alpha/N}{\omega_s a/U} \qquad (12)$$

$$m_\beta = \frac{T_\beta/N}{\Delta V/U} \qquad (13)$$

$$P_{max} = \frac{3}{2}\frac{N}{\pi a^2} \tag{14}$$

$$m_\beta = \frac{3\eta U}{2P_{max}h} \tag{15}$$

$$m_\alpha = \frac{3aG}{8hP_{max}} \tag{16}$$

$$m_\beta = \frac{4aG}{\pi hP_{max}} \tag{17}$$

For viscous case

$$\frac{m_\alpha}{m_\beta} = 0 \tag{18}$$

For elastic case

$$\frac{m_\alpha}{m_\beta} = \frac{3\pi}{32} = 0.294 \tag{19}$$

The gradients of experimental traction curves may now be compared directly with the predictions of (18) and (19) except for the fact that the ball and plate surfaces are not rigid and so apparent elastic behaviour of the fluid film could be solely a result of the elastic deformation of the surfaces with a thin highly viscous film interspersed between them.

6.7 THE ELASTIC COMPLIANCES OF THE BALL AND DISC

Johnson and Roberts(1) considered this difficulty with two discs and a circular contact area and so for completeness their analysis will be quoted.

6.71 (1) Viscous film

The surface tractions which arise when a thin viscous film of uniform viscosity η and thickness h separates two elastic rollers throughout a circular area of radius a have been analysed

by A. Kalker (private communication from K.L. Johnson) by means of a 'strip theory'. This approach simplifies the three-dimensional problem by dividing it into a series of thin strips parallel to the rolling direction; two-dimensional theory is applied to each strip and the surface stresses summed, neglecting any interaction between the strips. He obtained the following results for rolling with spin.

$$T\alpha = \frac{1}{3}\pi G_s a^2 \phi^2 \left(\frac{\omega_s a}{U}\right) \tag{20}$$

and for rolling with sideslip

$$T_\beta = \frac{1}{4}\pi^2 G_s a^2 \phi \left(\frac{\Delta V}{U}\right) \tag{21}$$

where $\phi = \frac{2}{\pi} \arctan\left(\frac{2\eta U}{G_s h}\right)$ and when G_s denotes the elastic shear modulus of the discs.

For low viscosities the compliance of the discs is low in comparison with the film and $\phi \approx \frac{4\eta U}{G_s h}$. Equations (20) and (21) then reduce to equations (7) and (8) in which disc compliance has been ignored.

Equations (20) and (21) may be expressed in terms of the gradients of the traction curves.

$$m_\alpha = \frac{1}{2} \frac{G_s}{Pmax} \phi^2 \tag{22}$$

$$m_\beta = \frac{3\pi}{8} \frac{G_s}{Pmax} \phi \tag{23}$$

If the film is very thin and viscous then $\frac{2\eta U}{Gh} \to \infty$ and so $\phi \to 1.0$.

In those circumstances equations (22) and (23) should correspond to equations (24) and (25) for dry contact.

$$m'_\alpha = 0.72 \frac{G_s}{Pmax} \tag{24}$$

$$m'_\beta = 1.78 \frac{G_s}{Pmax} \tag{25}$$

The discrepancies (0.5 compared with 0.72 and 1.18 compared to 1.78) are due to the approximation involved in the strip theory. Kalker (1966) has commented that strip theories of elastic rolling contact give coefficients which are 30-40% low and recommended (1968) making a correction to bring them into line with experiment. Accordingly, we shall retain the form of the equations (22) and (23) but will change the coefficients

$$m_\alpha = 0.72 \frac{G_s}{P_{max}} \phi^2 = m'_\alpha \phi^2 \qquad (26)$$

and

$$m_\beta = 1.78 \frac{G_s}{P_{max}} \phi = m'_\beta \phi \qquad (27)$$

where the prime denotes dry contact. Equation (27) may be used to find the viscosity from the traction curves

$$\eta = \frac{G_s h}{2U} \tan \left(\frac{\pi}{2} \cdot \frac{m_\beta}{m'_\beta}\right) \qquad (28)$$

We also obtain the influence of disc compliance on the ratio of the traction gradients

$$\frac{m_\alpha}{m_\beta} = 0.404 \frac{m_\beta}{m'_\beta} \qquad (29)$$

The effect is small, provided $m_\beta \ll m'_\beta$.

6.72 Elastic film

A strip theory for an elastic film has not been found, but a simple analysis is possible on the basis of representing the two discs and the intervening film as three elastic springs connected in series.

We begin by writing

$$m_\alpha = \frac{T_\alpha/N}{w_s a/U} = \frac{3a}{8Pmax}\left(\frac{1}{C_\alpha}\right) \qquad (30)$$

$$m_\beta = \frac{T_\beta/N}{\Delta V/N} = \frac{4a}{\pi Pmax}\left(\frac{1}{C_\beta}\right) \qquad (31)$$

where C_α and C_β are the total compliances of the film and rollers for rolling with spin and sideslip respectively. We now assume that the total compliances can be found from the simple addition of the compliance of the rollers in dry contact C' and the compliance of a uniform film with rigid rollers C", i.e.

$$C_\alpha = C_\alpha' + C_\alpha'' \quad \text{and} \quad C_\beta = C_\beta' + C_\beta''$$

From equations (8) and (10)

$$C_\alpha'' = C_\beta'' = \frac{h}{G}$$

$$C_\alpha' = \frac{3a}{8Pmax\ m_\alpha'} \quad \text{and} \quad C_\beta' = \frac{4a}{\pi Pmax\ m_\beta'}$$

where m_α' and m_β' are given by equations (24) and (25).

Substituting the above expressions for compliances into the equation (31) gives

$$\frac{C_\beta''}{C_\beta'} = \frac{h\pi Pmax\ m_\beta'}{G.4a} = \frac{m_\beta'}{m_\beta} - 1$$

whence $$\frac{4aG}{\pi hPmax} = \frac{m_\beta' m_\beta}{m_\beta' - m_\beta}$$

$$\therefore\ G = \frac{\pi hPmax}{4a}\left(\frac{m_\beta' m_\beta}{m_\beta' - m_\beta}\right) \qquad (32)$$

Thus G may be found from the measured gradient m_β of the traction curve. Dividing equations (30) and (31) gives

$$\frac{m_\alpha}{m_\beta} = \frac{3\pi}{32}\frac{C_\beta''}{C_\alpha''}\frac{(1 + C_\beta'/C_\beta'')}{(1 + C_\alpha'/C_\alpha'')}$$

$$\frac{C_\alpha'}{C_\alpha''} = \frac{C_\alpha'}{C_\beta'} \cdot \frac{C_\beta'}{C_\alpha''} = 0.72\,\frac{C_\beta'}{C_\beta''}$$

Substitution gives:

$$\frac{m_\alpha}{m_\beta} = \frac{1}{1 - 0.28\, m_\beta/m_\beta'} \qquad (33)$$

From the above analysis it may be seen that viscous behaviour may be distinguished from elastic behaviour by a plot of $\frac{m_\alpha}{m_\beta}$ versus $\frac{m_\beta}{m_\beta'}$ where points, arising from viscous behaviour, would appear close to the curve described by:

$$\frac{m_\alpha}{m_\beta} = 0.404\,\frac{m_\beta}{m_\beta'} \ ,$$

and points, arising from elastic behaviour would appear close to the curve

$$\frac{m_\alpha}{m_\beta} = \frac{1}{1 - 0.28\, m_\beta/m_\beta'}$$

6.8 CALCULATION OF CONTACT RADIUS AND MAXIMUM HERTZ PRESSURE

For a point contact between a sphere and flat surface

$$a^3 = \left(\frac{1 - \sigma_1^2}{E_1} + \frac{1 - \sigma_2^2}{E_2}\right)\frac{3RN}{4}$$

where:

σ_1 is the Poisson's ratio for the ball

σ_2 is the Poisson's ratio for the plate

E_1 is the elastic compression modulus of ball and

E_2 is the elastic compression modulus of plate and

R is the radius of the ball

N is the normal load between surfaces

The Hertz pressure distribution is given by

$$P = Pmax \left(1 - \frac{r^2}{a^2}\right)^{\frac{1}{2}}$$

$$Pmax = \frac{3N}{2\pi a^2}$$

6.9 REFERENCE

1. JOHNSON, K.L. and ROBERTS, A.D., "Observations of viscoelastic behaviour of an EHD film", Proc. Roy Soc., London, (A) 337, 217-242, (1972)

CHAPTER 7

RESULTS AND DERIVED PARAMETERS

7.1 In this chapter are presented a representative set of experimental data for film thickness and traction results from the apparatus described in Chapters 2, 3, 4 and 5.

Also included in this chapter are plots of derived parameters and their variation with rolling speed, pressure and temperature, together with some plots of their inter-correlation.

This experimental information is analysed and discussed in Chapter 8.

FIG. 7.1

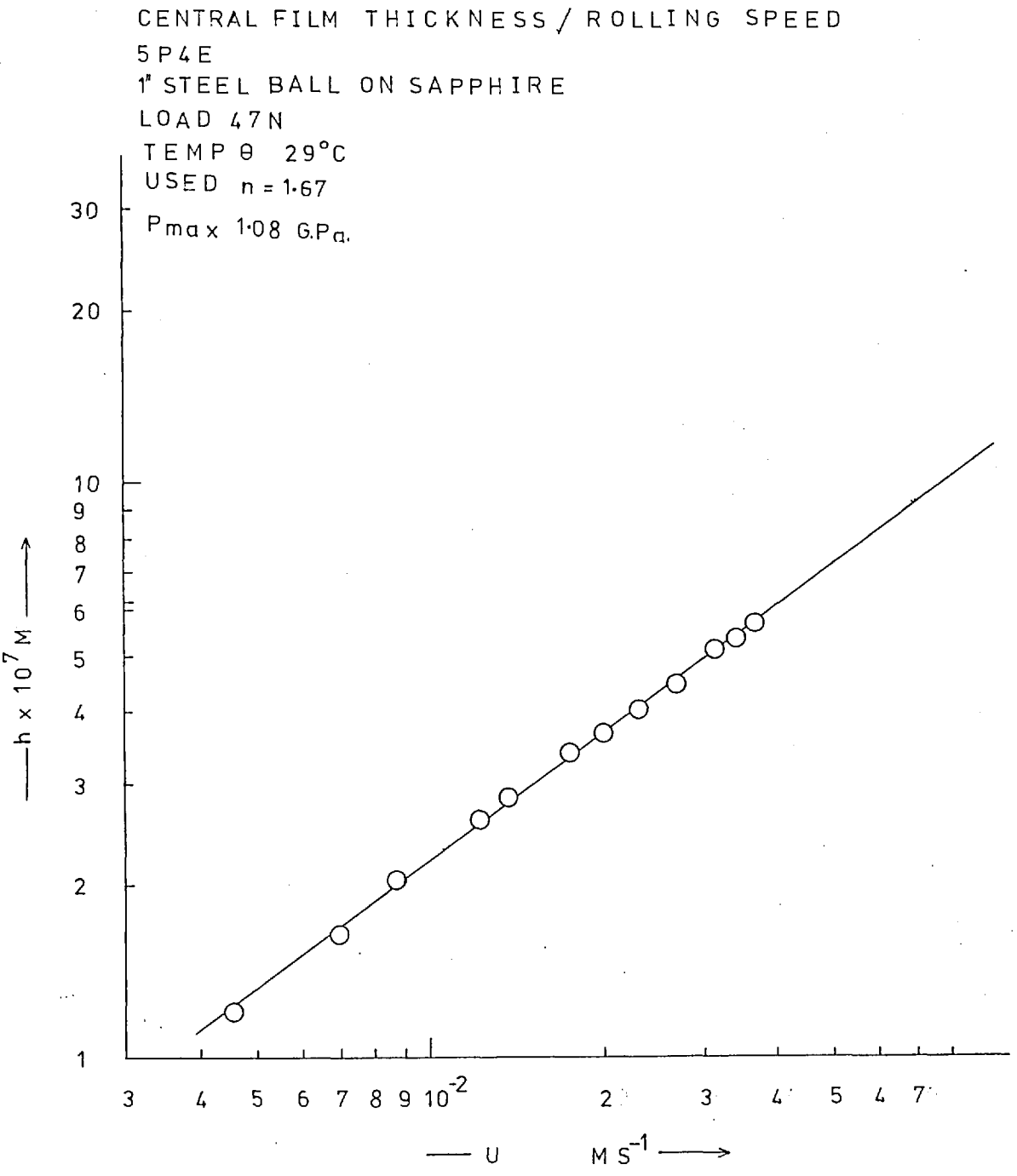
CENTRAL FILM THICKNESS / ROLLING SPEED
5P4E
1" STEEL BALL ON SAPPHIRE
LOAD 47N
TEMP θ 29°C
USED n = 1·67
Pmax 1·08 G.Pa.
30
20
10
9
8
7
6
5
4
3
2
1
h x 10^7 M
3 4 5 6 7 8 9 10^-2 2 3 4 5 4 7
U M S^-1

FIG. 7.2

CENTRAL FILM THICKNESS / ROLLING SPEED FOR XRM 109 F

1 STEEL BALL ON SAPPHIRE
LOAD 47 N
TEMP θ 25°C
USED REFRACTIVE INDEX n = 1·62
Pmax 1·08 G.Pa.

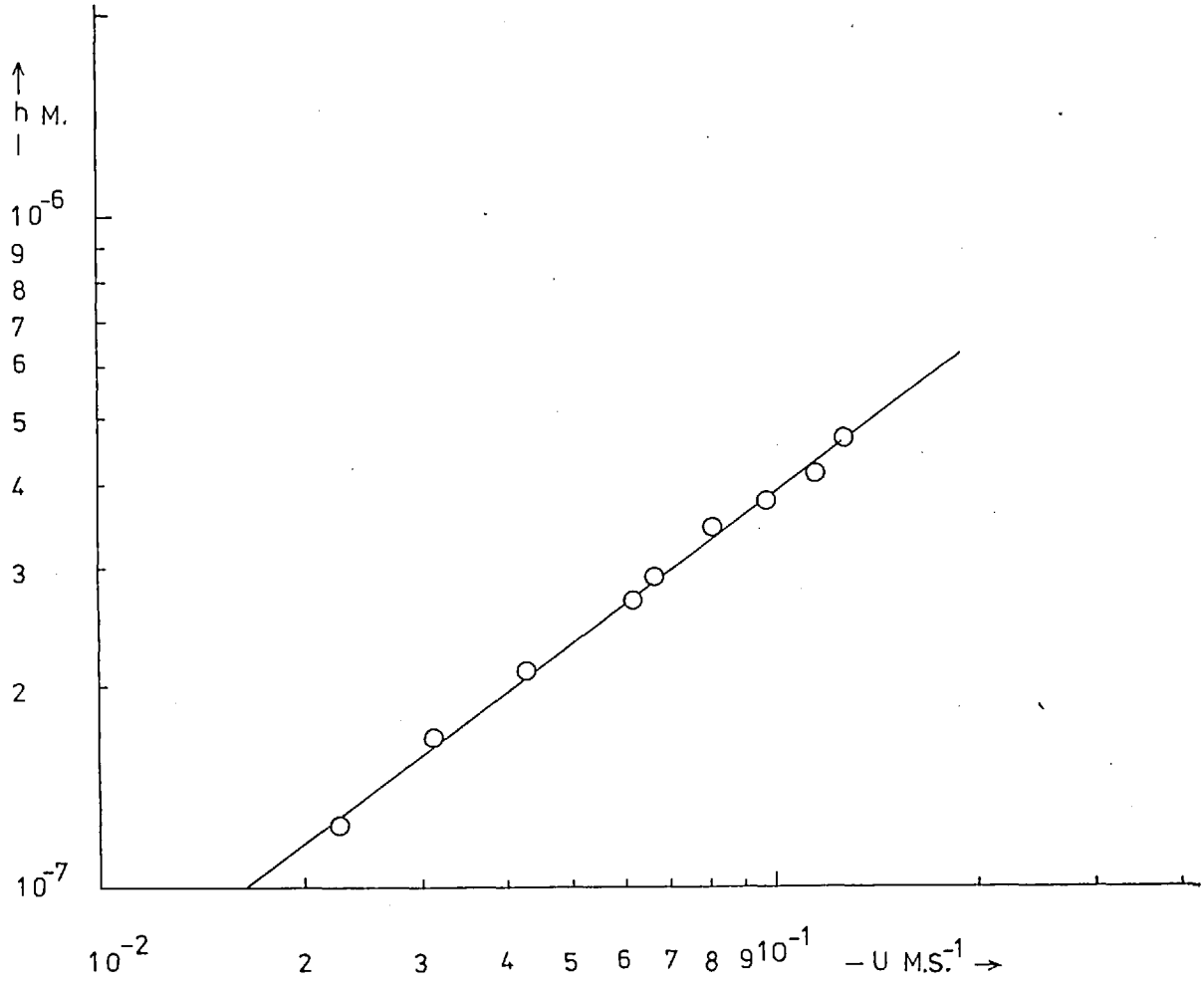

FIG. 7.3

CENTRAL FILM THICKNESS/ROLLING SPEED
BP BRIGHT STOCK

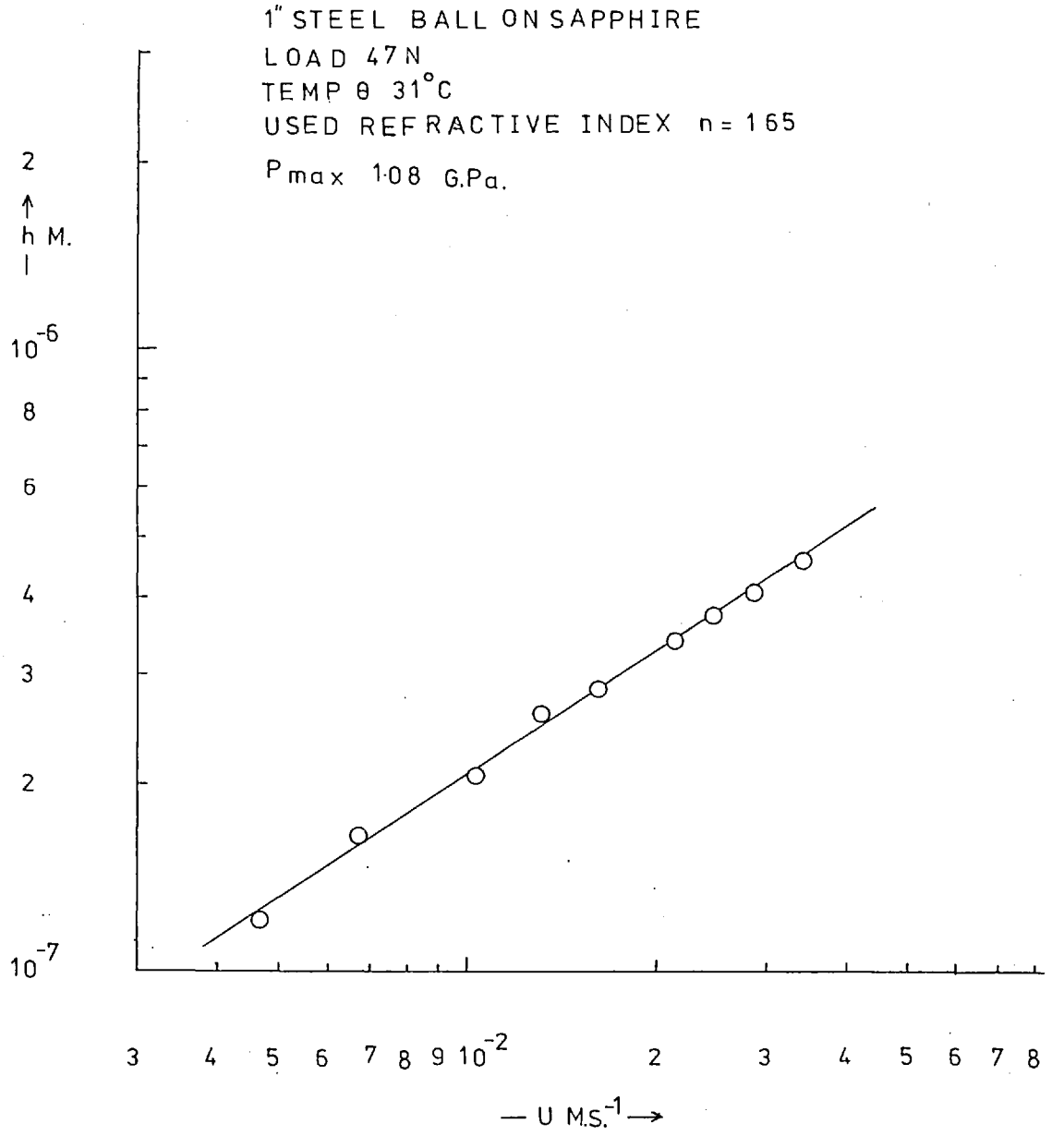

FIG. 7.4

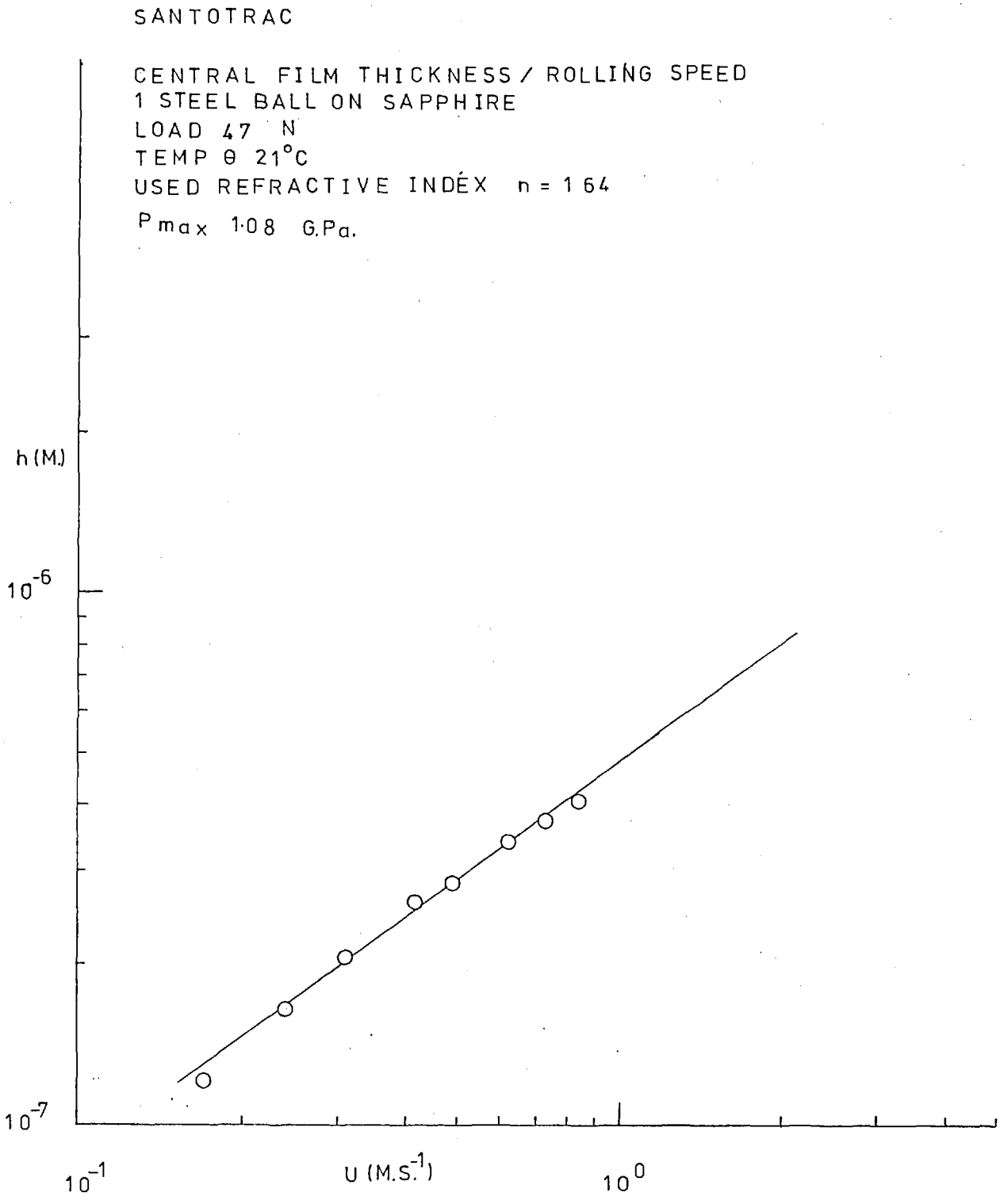
SANTOTRAC
CENTRAL FILM THICKNESS / ROLLING SPEED
1 STEEL BALL ON SAPPHIRE
LOAD 47 N
TEMP θ 21°C
USED REFRACTIVE INDEX n = 1 64
Pmax 1·08 G.Pa.
h (M.)
10-6
10-7
10-1
U (M.S.-1)
10 0

FILM THICKNESS
1" STEEL BALL ON SAPPHIRE
LOAD 47N
Pmax 1·08 G.Pa.

FIG. 7.5

		TEMP θ	α' VALUE
○	REFERENCE FLUID	21·5°C	21·5 GPa.$^{-1}$
△	5P4E	29·0°C	43·4 "
□	XRM 109F	27·0°C	11·0 "
◇	BP BRIGHT STOCK	31·0°C	28·3 "
✕	SANTOTRAC	26·3°C	21·5 "

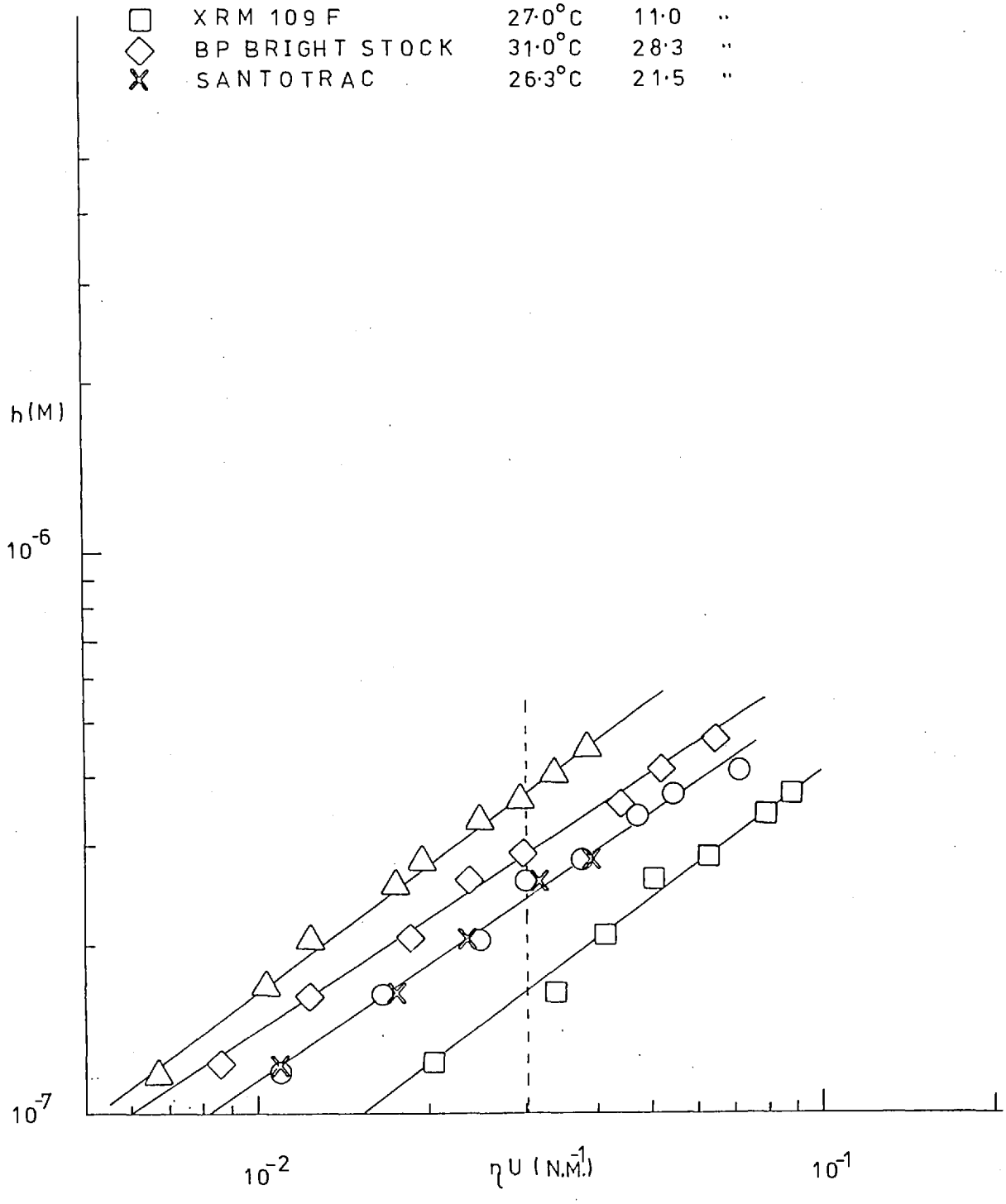

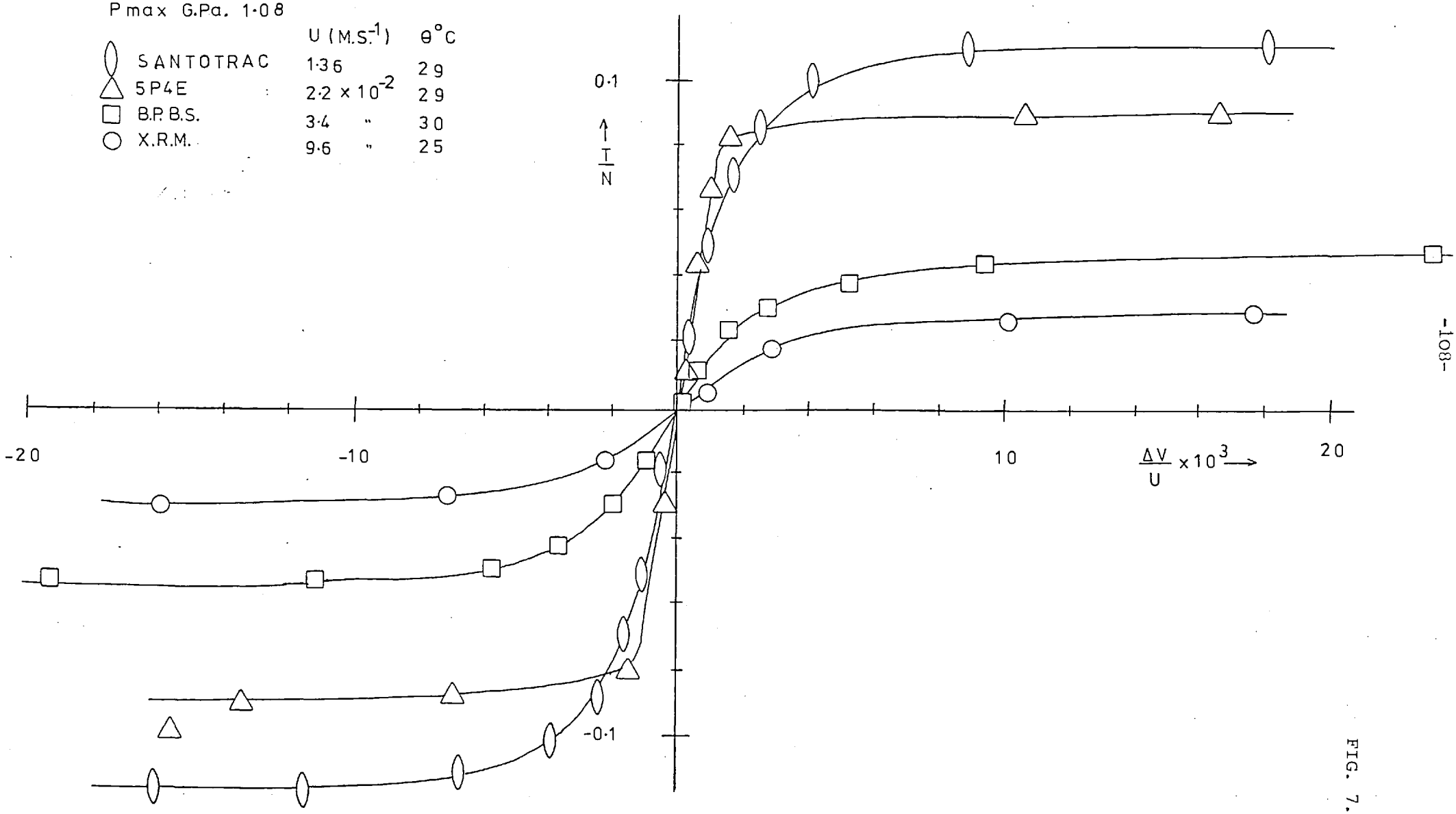
LOAD 47 N
1"STEEL BALL ON SAPPHIRE
Pmax G.Pa. 1·08
U (M.S.-1) θ°C
SANTOTRAC 1·36 29
5P4E 2·2 x 10-2 29
B.P.B.S. 3·4 " 30
X.R.M. 9·6 " 25
0·1
T/N
-20
-10
10
20
ΔV/U x 10^3
-0·1

FIG. 7.6

BP BRIGHT STOCK

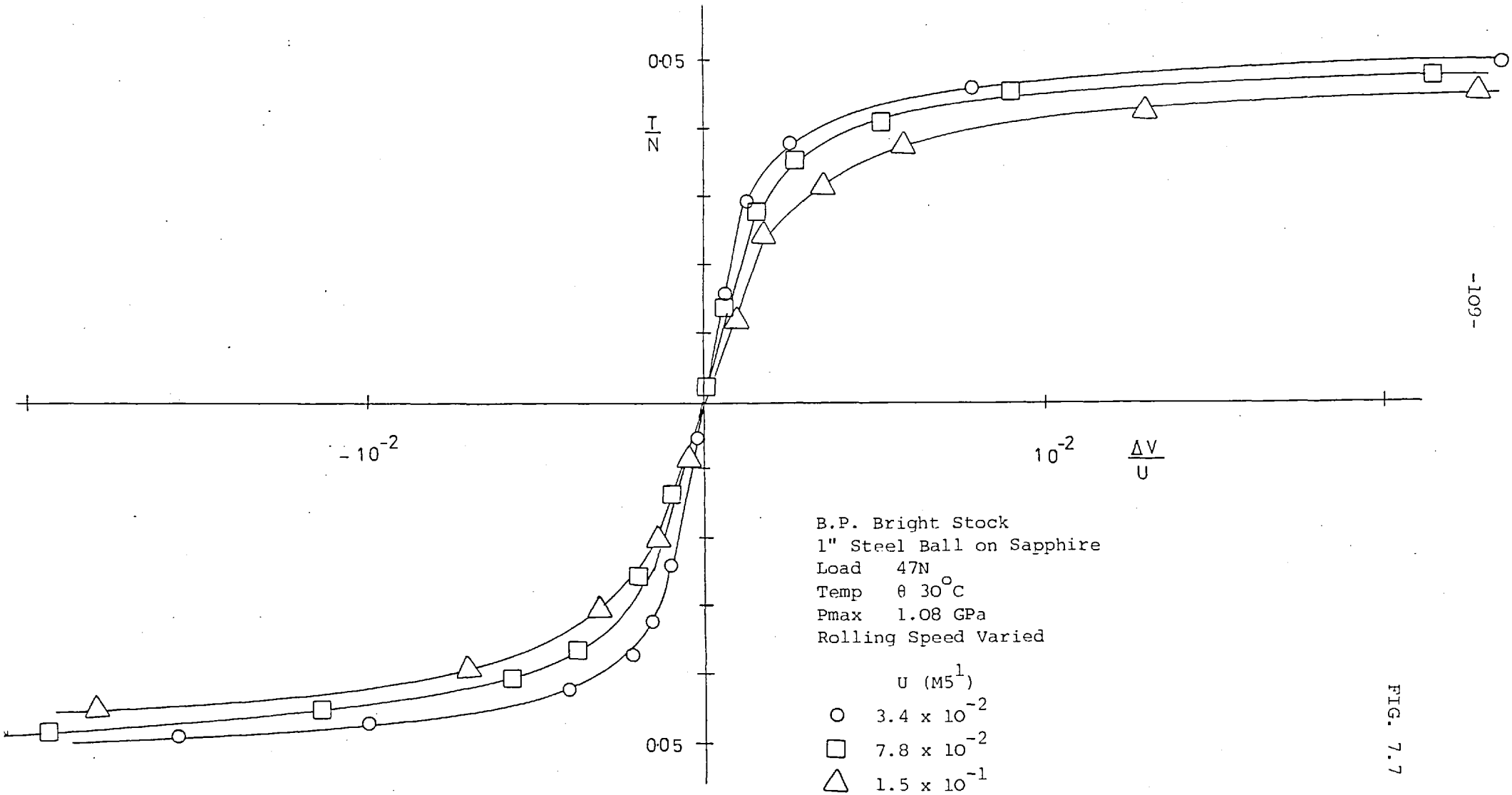

FIG. 7.7

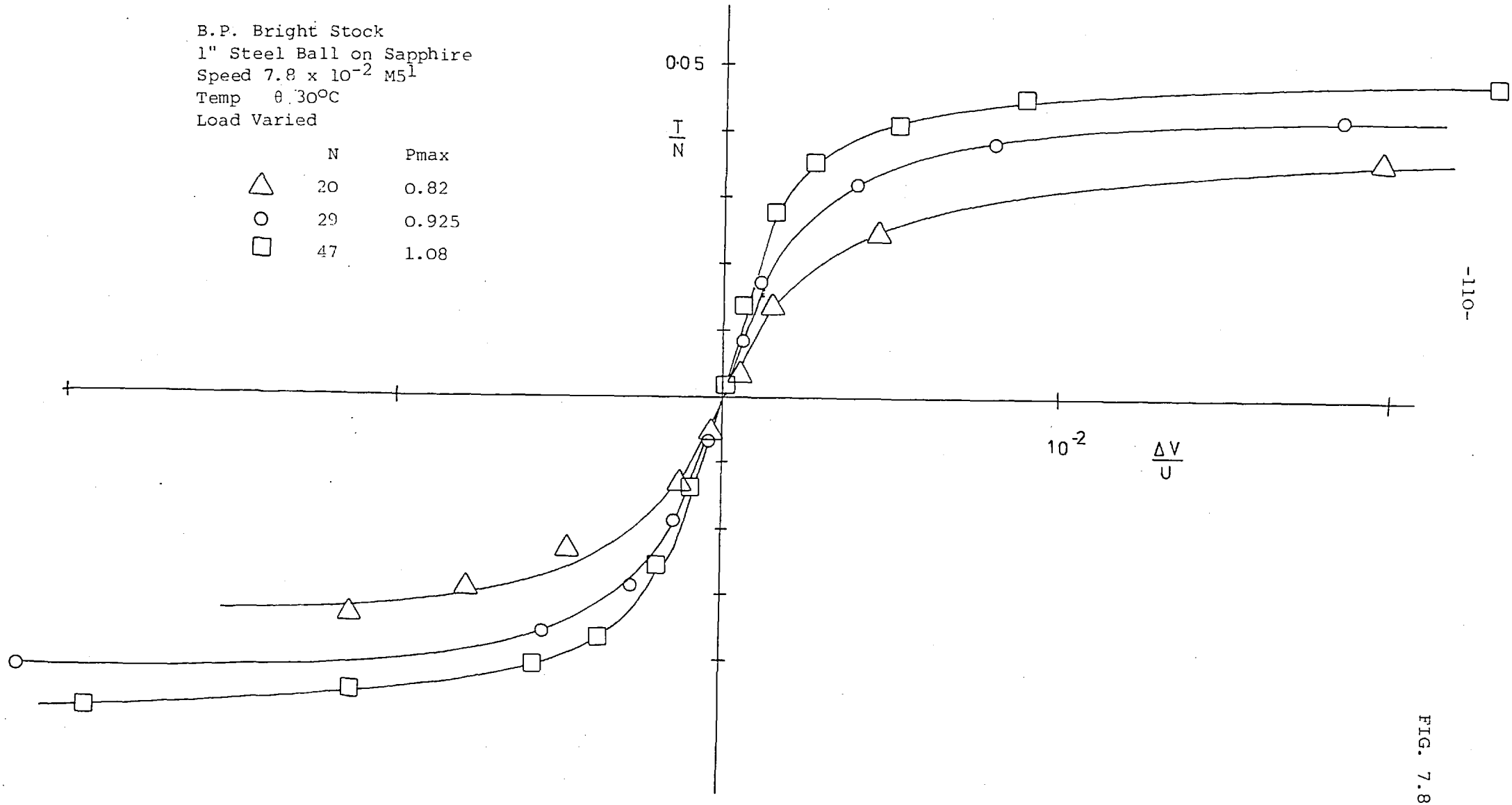
B.P. Bright Stock
1" Steel Ball on Sapphire
Speed 7.8 x 10^{-2} MS^{-1}
Temp θ 30°C
Load Varied
N
Pmax
20
0.82
29
0.925
47
1.08
0·05
$\frac{T}{N}$
10^{-2}
$\frac{\Delta V}{U}$

FIG. 7.8

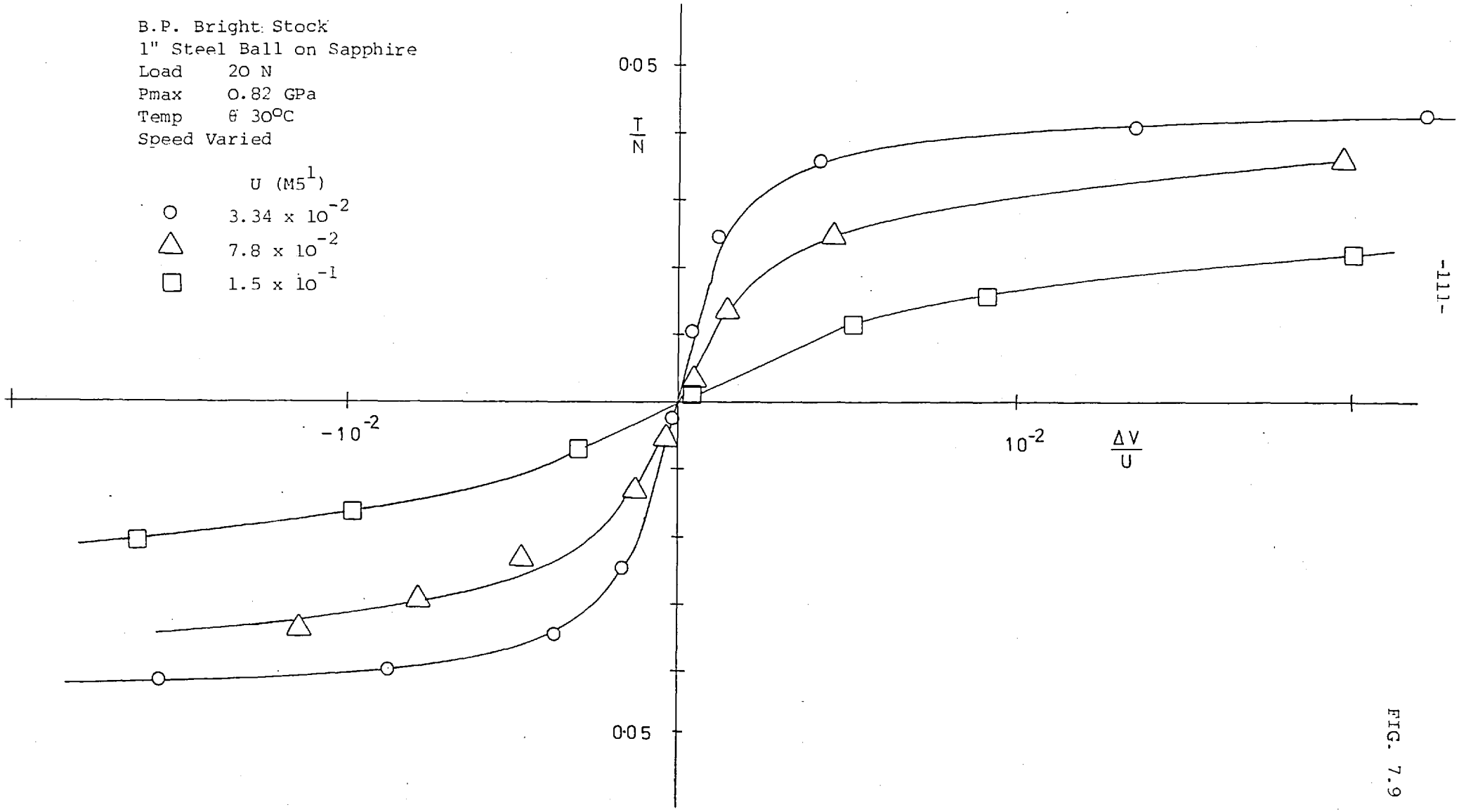
B.P. Bright Stock
1" Steel Ball on Sapphire
Load 20 N
Pmax 0.82 GPa
Temp @ 30°C
Speed Varied
U (M5^1)
3.34 x 10^-2
7.8 x 10^-2
1.5 x 10^-1
0·05
T/N
-10^-2
10^-2
ΔV/U
0·05

FIG. 7.9

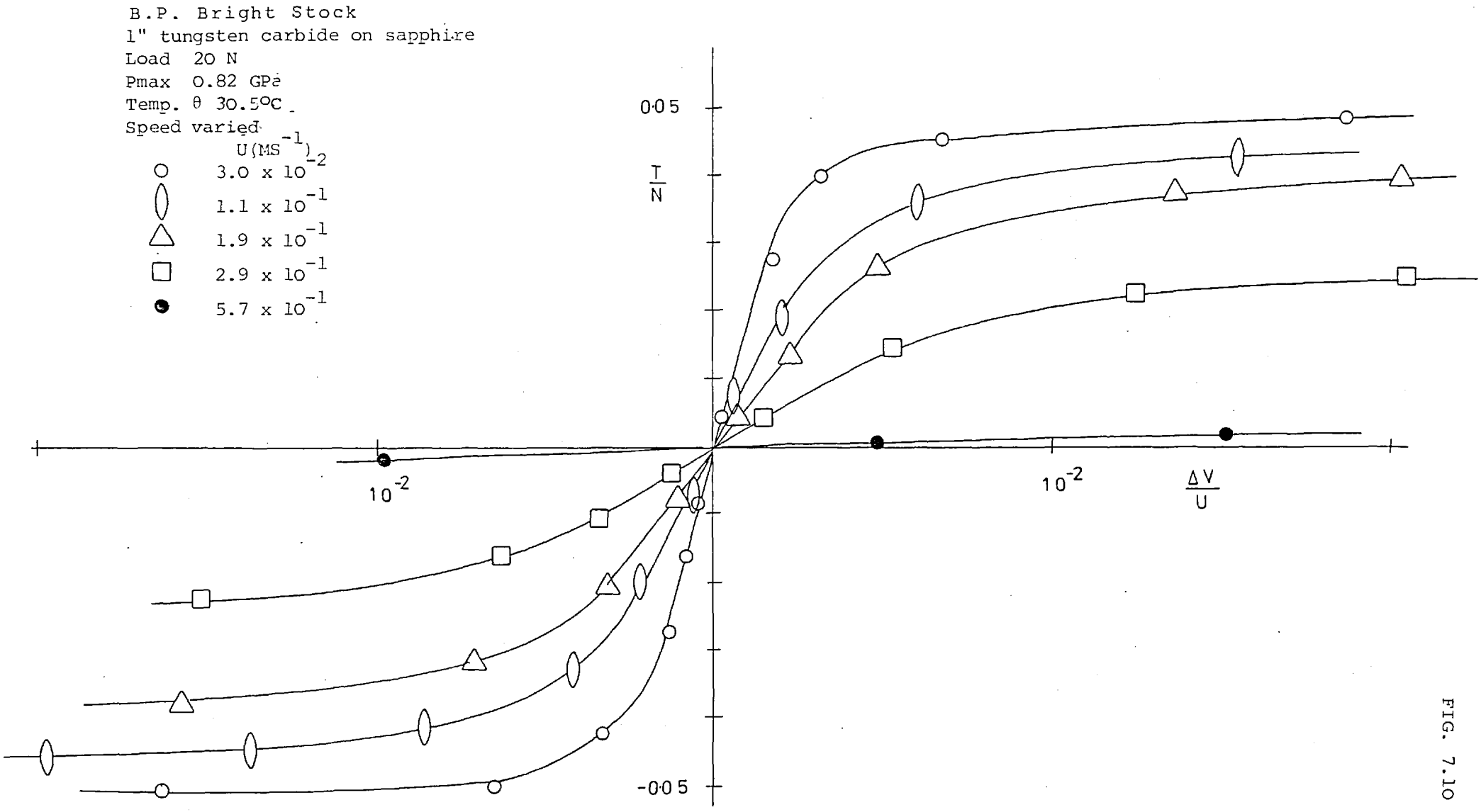
B.P. Bright Stock
1" tungsten carbide on sapphire
Load 20 N
Pmax 0.82 GPa
Temp. θ 30.5°C
Speed varied
U(MS^{-1})$_{-2}$
3.0 x 10^{-1}
1.1 x 10^{-1}
1.9 x 10^{-1}
2.9 x 10^{-1}
5.7 x 10^{-1}
0·05
T/N
-0·05
10^{-2}
10^{-2}
ΔV/U

FIG. 7.10

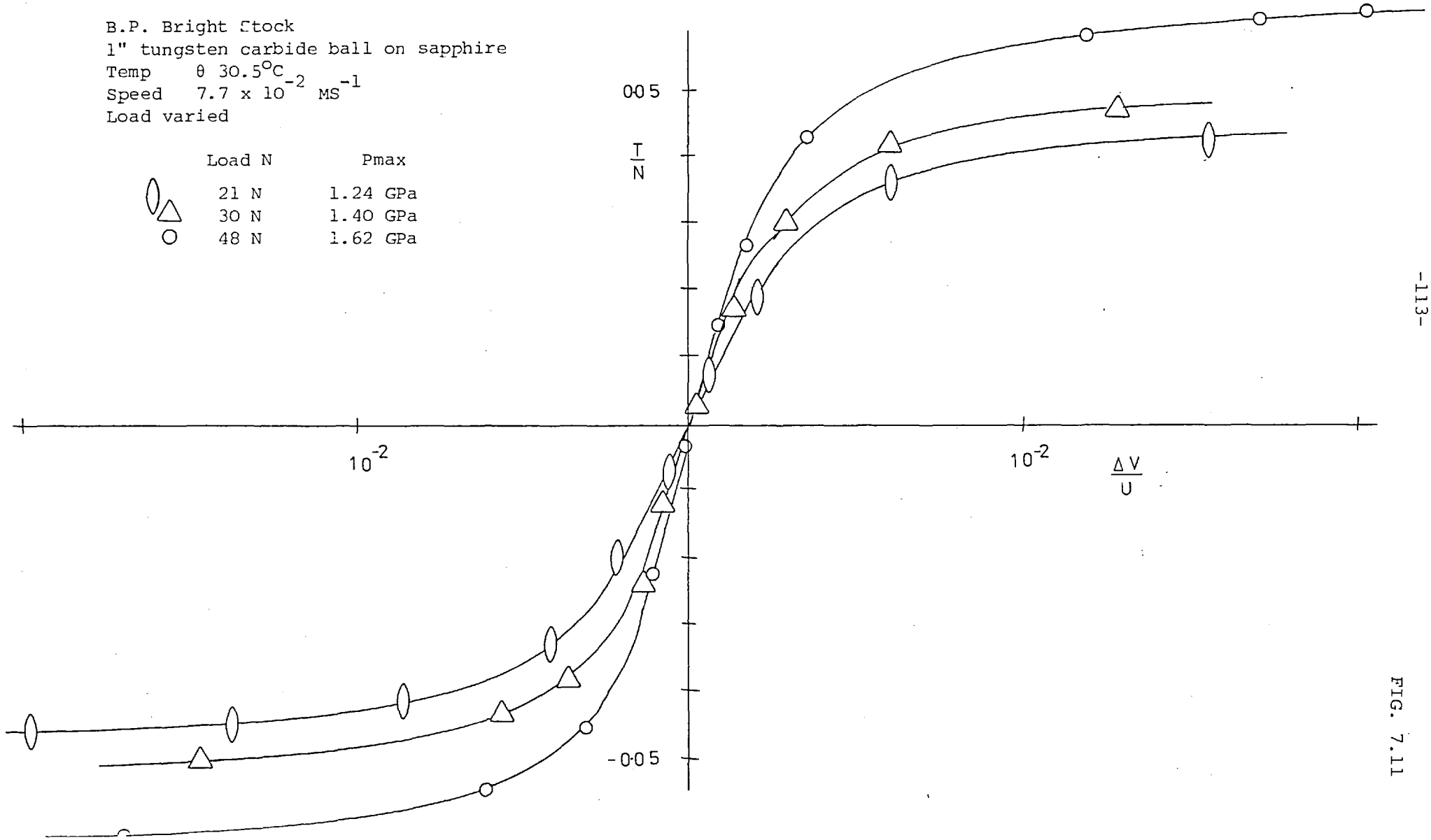
B.P. Bright Stock
1" tungsten carbide ball on sapphire
Temp θ 30.5°C
Speed 7.7 x 10^-2 MS^-1
Load varied
Load N
Pmax
21 N
1.24 GPa
30 N
1.40 GPa
48 N
1.62 GPa
0·05
T/N
-0·05
10^-2
10^-2
ΔV/U

FIG. 7.11

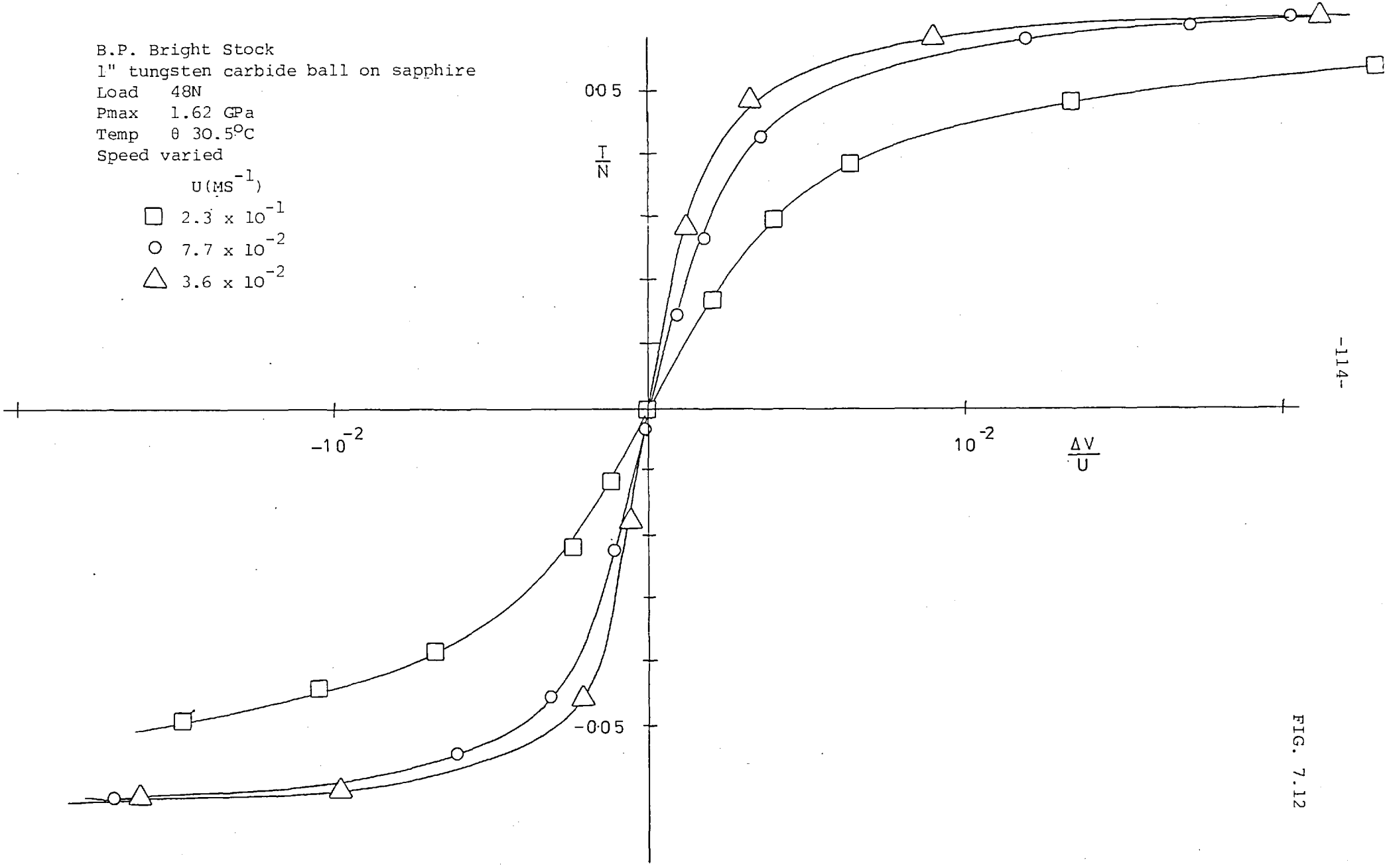
B.P. Bright Stock
1" tungsten carbide ball on sapphire
Load 48N
Pmax 1.62 GPa
Temp θ 30.5°C
Speed varied
U(MS⁻¹)
2.3 x 10⁻¹
7.7 x 10⁻²
3.6 x 10⁻²
0·05
I/N
-10⁻²
10⁻²
ΔV/U
-0·05

FIG. 7.12

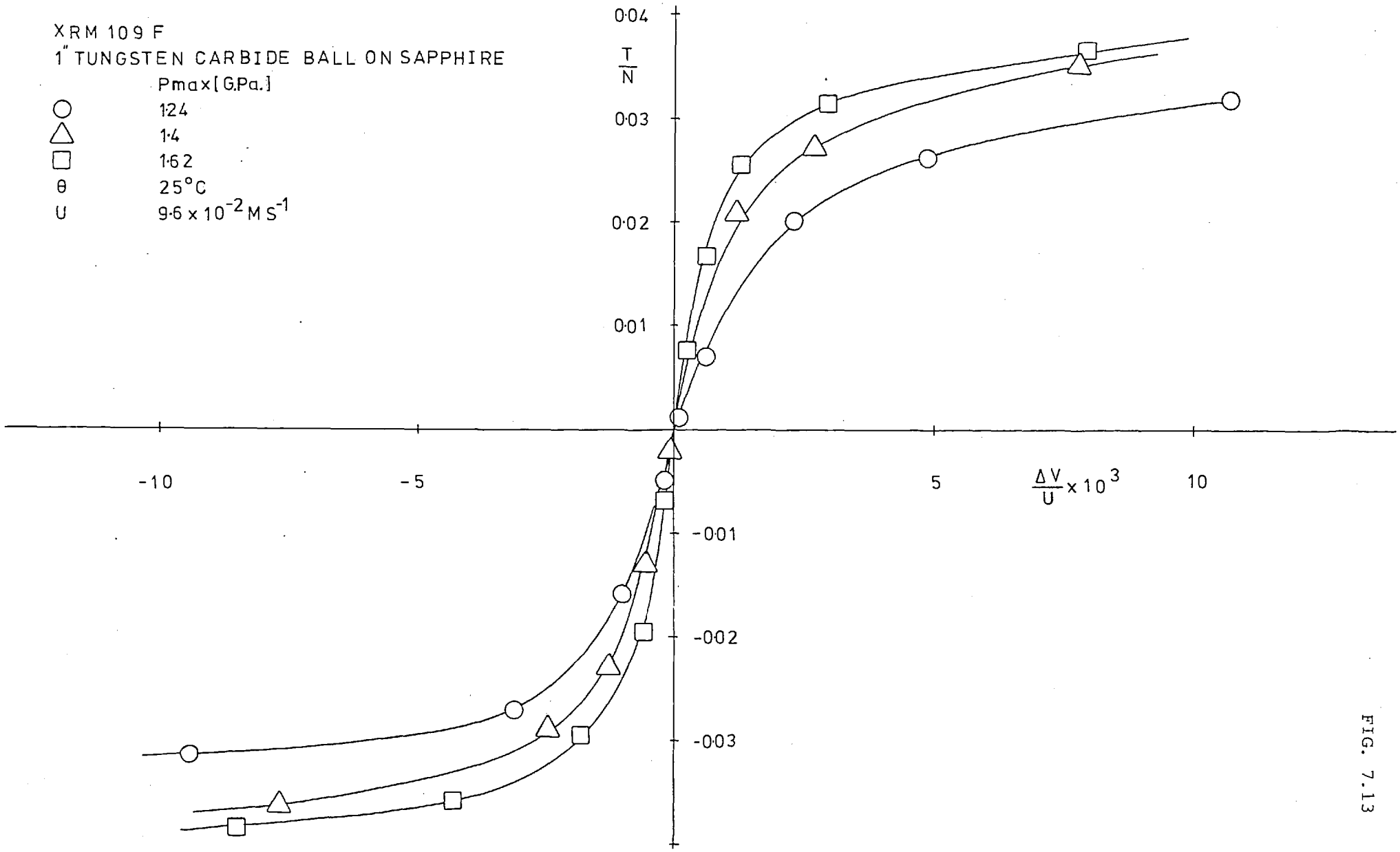
XRM 109 F
1" TUNGSTEN CARBIDE BALL ON SAPPHIRE
Pmax[G.Pa.]
1·24
1·4
1·62
θ 25°C
U 9·6 x 10⁻² M S⁻¹
0·04
T/N
0·03
0·02
0·01
-10
-5
5
ΔV/U x 10³
10
-·001
-·002
-·003

FIG. 7.13

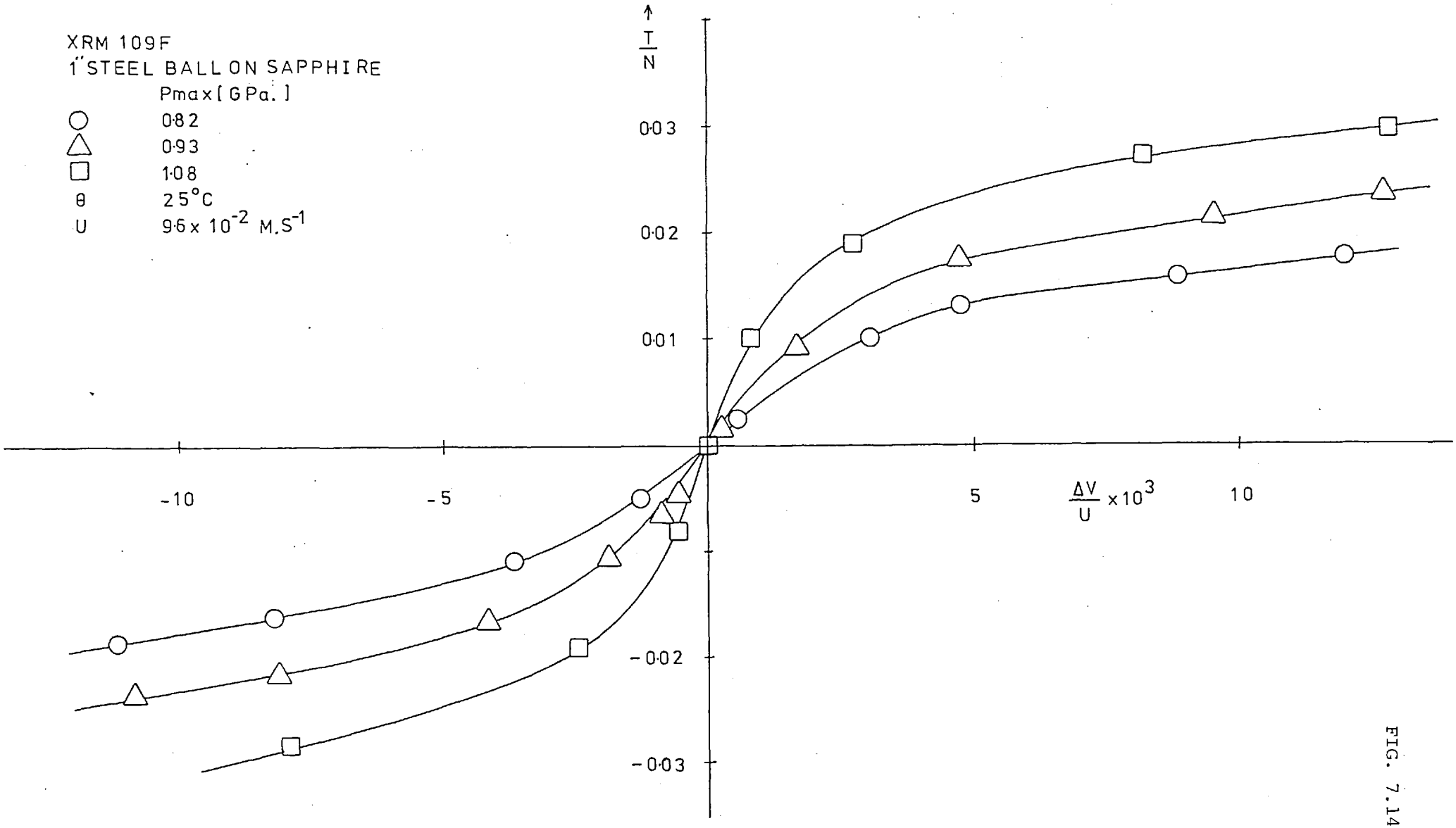
XRM 109F
1" STEEL BALL ON SAPPHIRE
Pmax [GPa.]
○ 0·82
△ 0·93
□ 1·08
θ 25°C
U 9·6 x 10⁻² M.S⁻¹
↑ T/N
0·03
0·02
0·01
-0·02
-0·03
-10
-5
5
10
ΔV/U x10³

FIG. 7.14

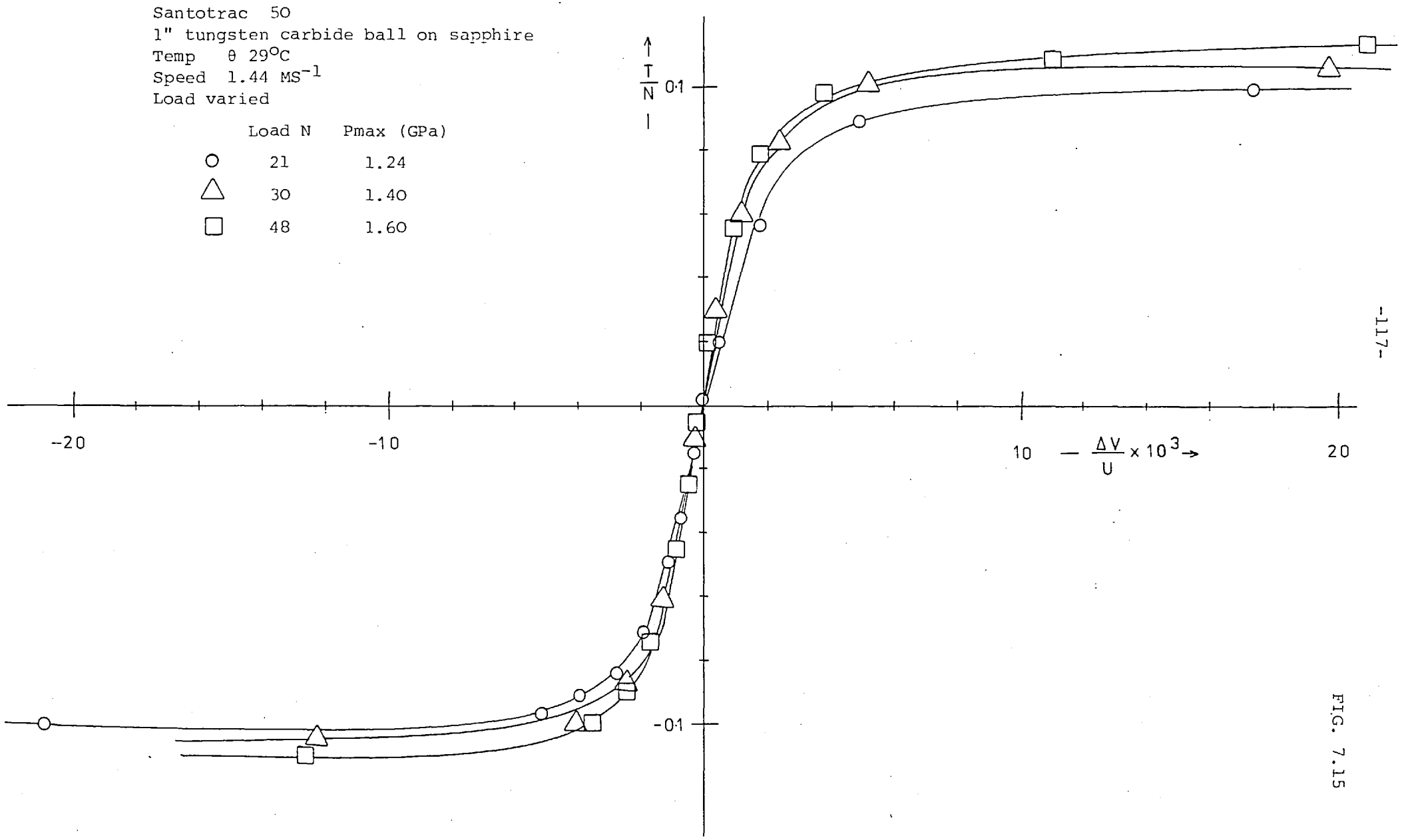
Santotrac 50
1" tungsten carbide ball on sapphire
Temp θ 29°C
Speed 1.44 MS⁻¹
Load varied
Load N Pmax (GPa)
21 1.24
30 1.40
48 1.60
T/N
0·1
-0·1
-20
-10
10
20
ΔV/U x 10³

FIG. 7.15

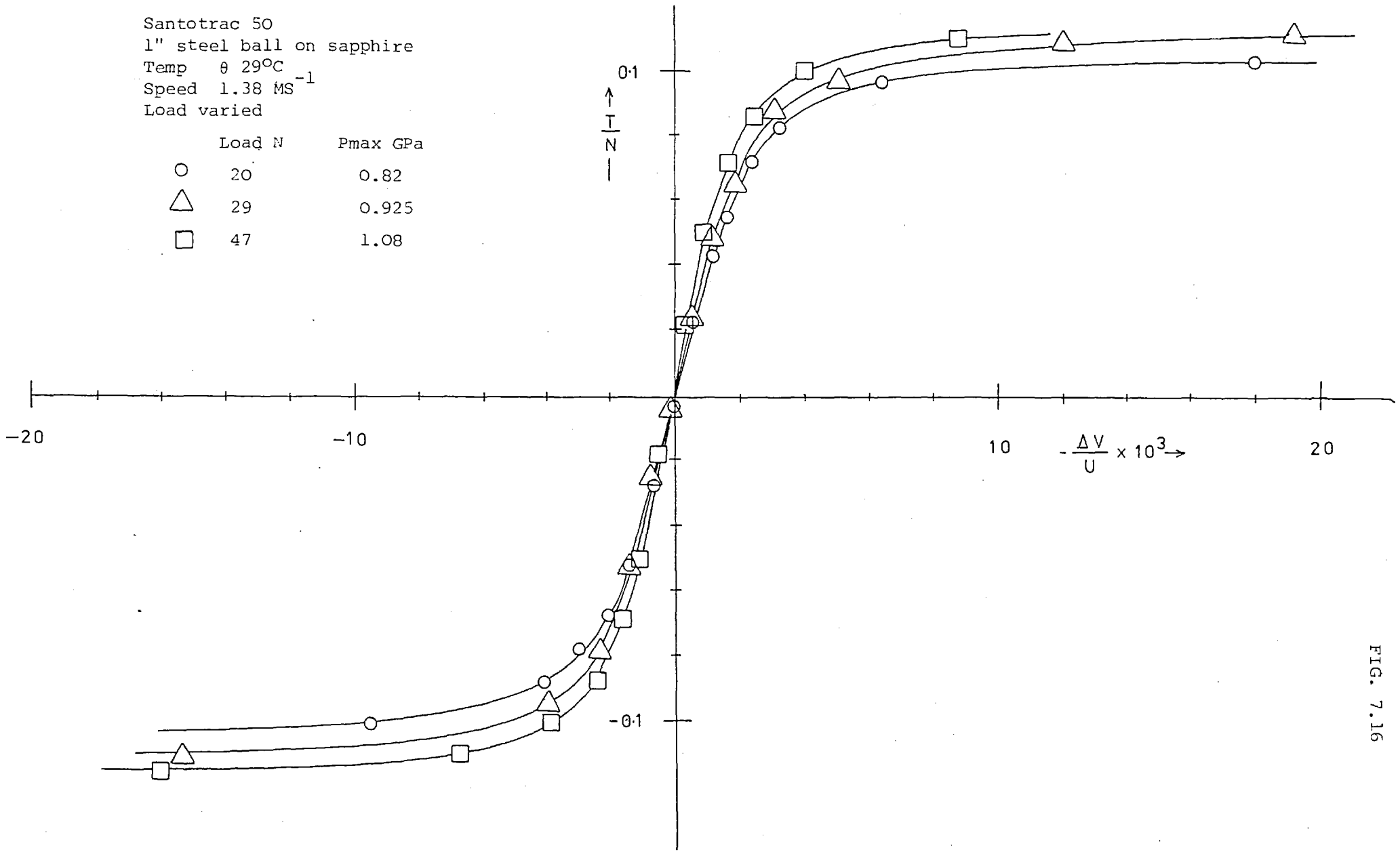
Santotrac 50
1" steel ball on sapphire
Temp θ 29°C
Speed 1.38 MS-1
Load varied
Load N
Pmax GPa
20
0.82
29
0.925
47
1.08
0·1
-0·1
I/N
-20
-10
10
20
-ΔV/U x 10³

FIG. 7.16

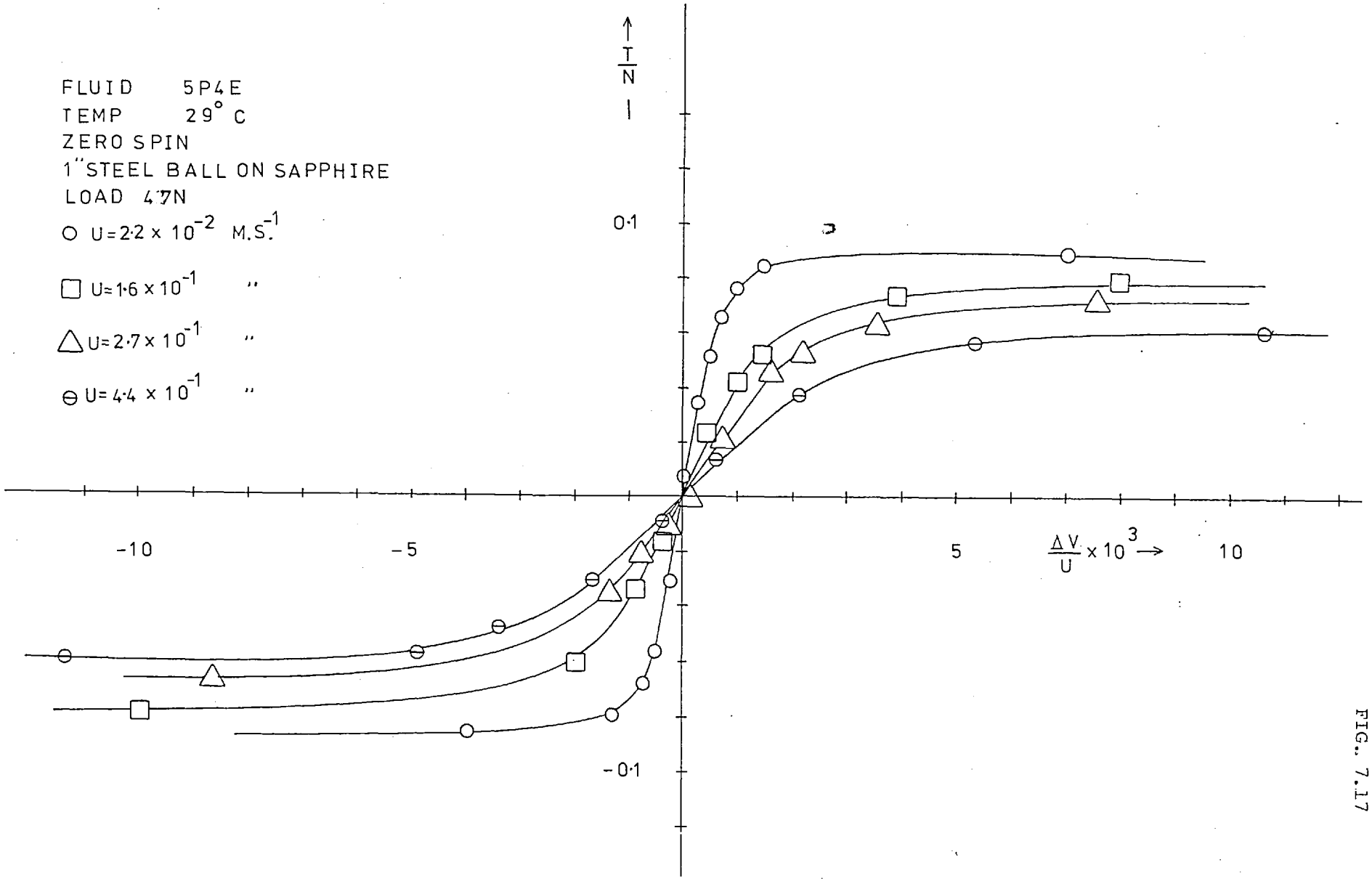
FLUID 5P4E
TEMP 29° C
ZERO SPIN
1" STEEL BALL ON SAPPHIRE
LOAD 4·7N
○ U=2·2 x 10⁻² M.S.⁻¹
□ U=1·6 x 10⁻¹ "
△ U=2·7 x 10⁻¹ "
⊖ U=4·4 x 10⁻¹ "
T/N
0·1
-0·1
-10
-5
5
10
ΔV/U x 10³ →

FIG. 7.17

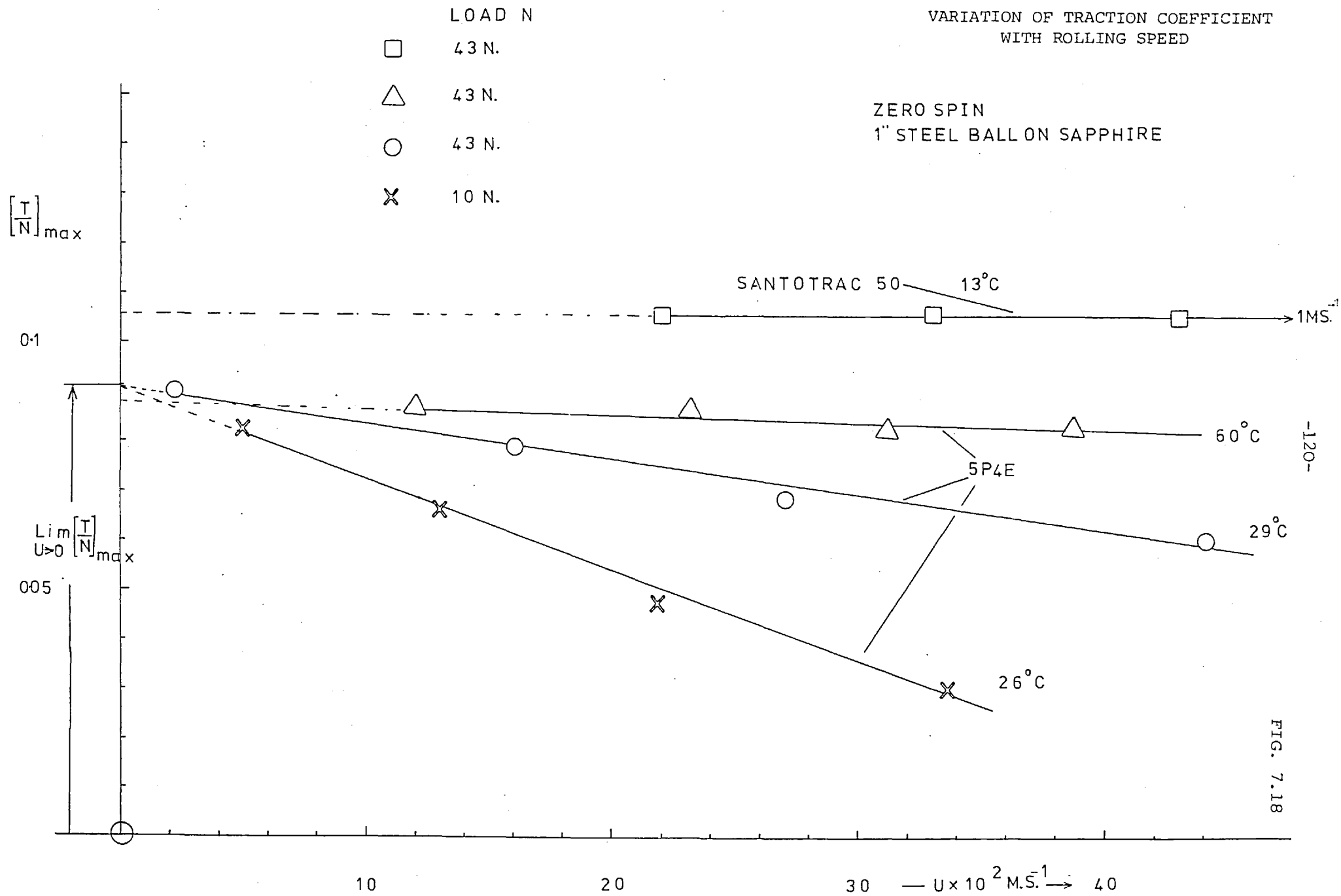
LOAD N
43 N.
43 N.
43 N.
10 N.
VARIATION OF TRACTION COEFFICIENT WITH ROLLING SPEED
ZERO SPIN
1" STEEL BALL ON SAPPHIRE
$\left[\frac{T}{N}\right]_{max}$
SANTOTRAC 50
13°C
1MS.
0·1
60°C
5P4E
29°C
$\lim_{U>0}\left[\frac{T}{N}\right]_{max}$
005
26°C
10
20
30
— U x 10 2 M.S. -1 →
40

FIG. 7.18

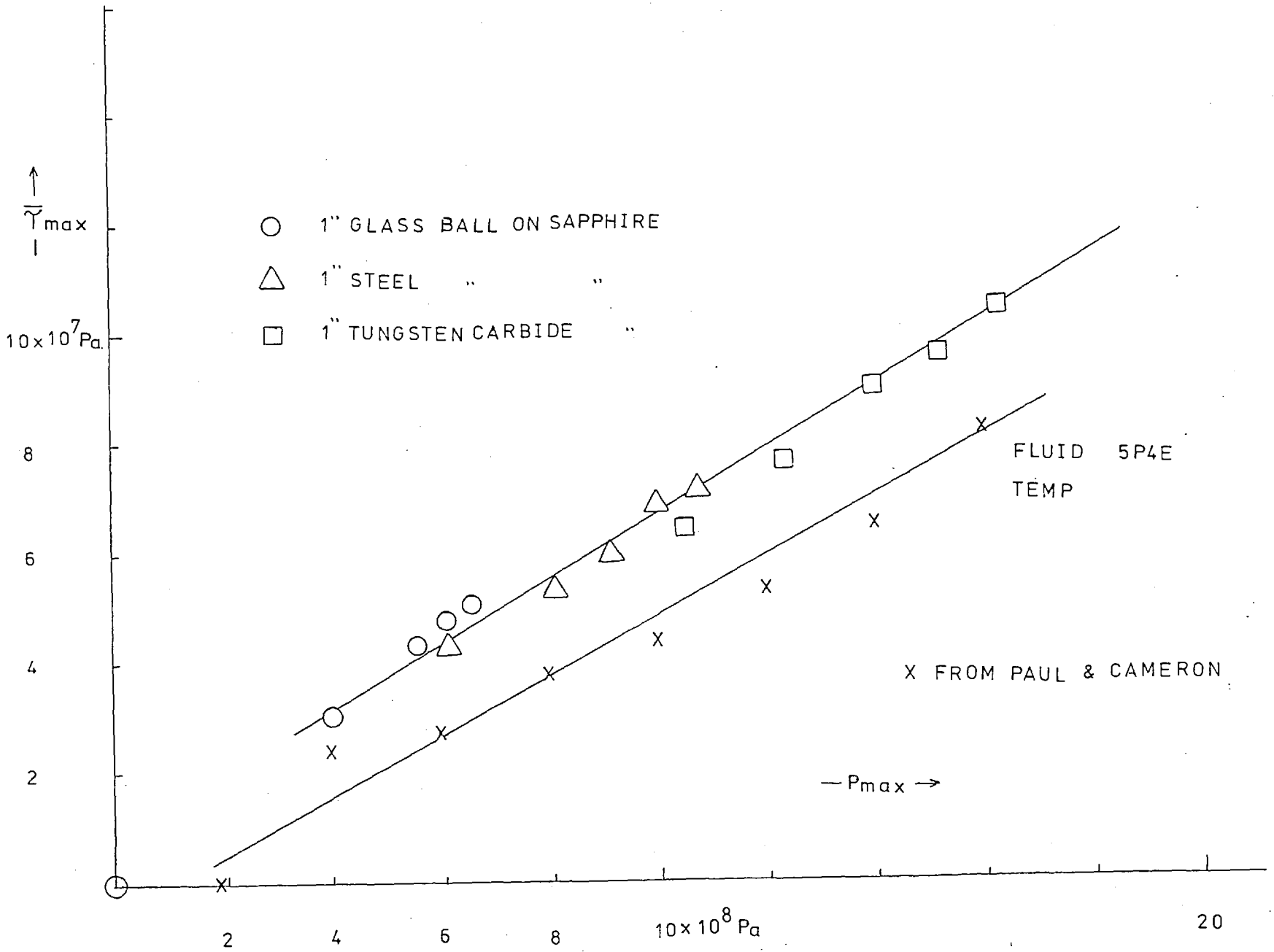
$\tilde{\tau}_{max}$
10×10^7 Pa.
8
6
4
2
1" GLASS BALL ON SAPPHIRE
1" STEEL " "
1" TUNGSTEN CARBIDE "
FLUID 5P4E
TEMP
X FROM PAUL & CAMERON
— Pmax →
2
4
6
8
10×10^8 Pa
20

FIG. 7.19

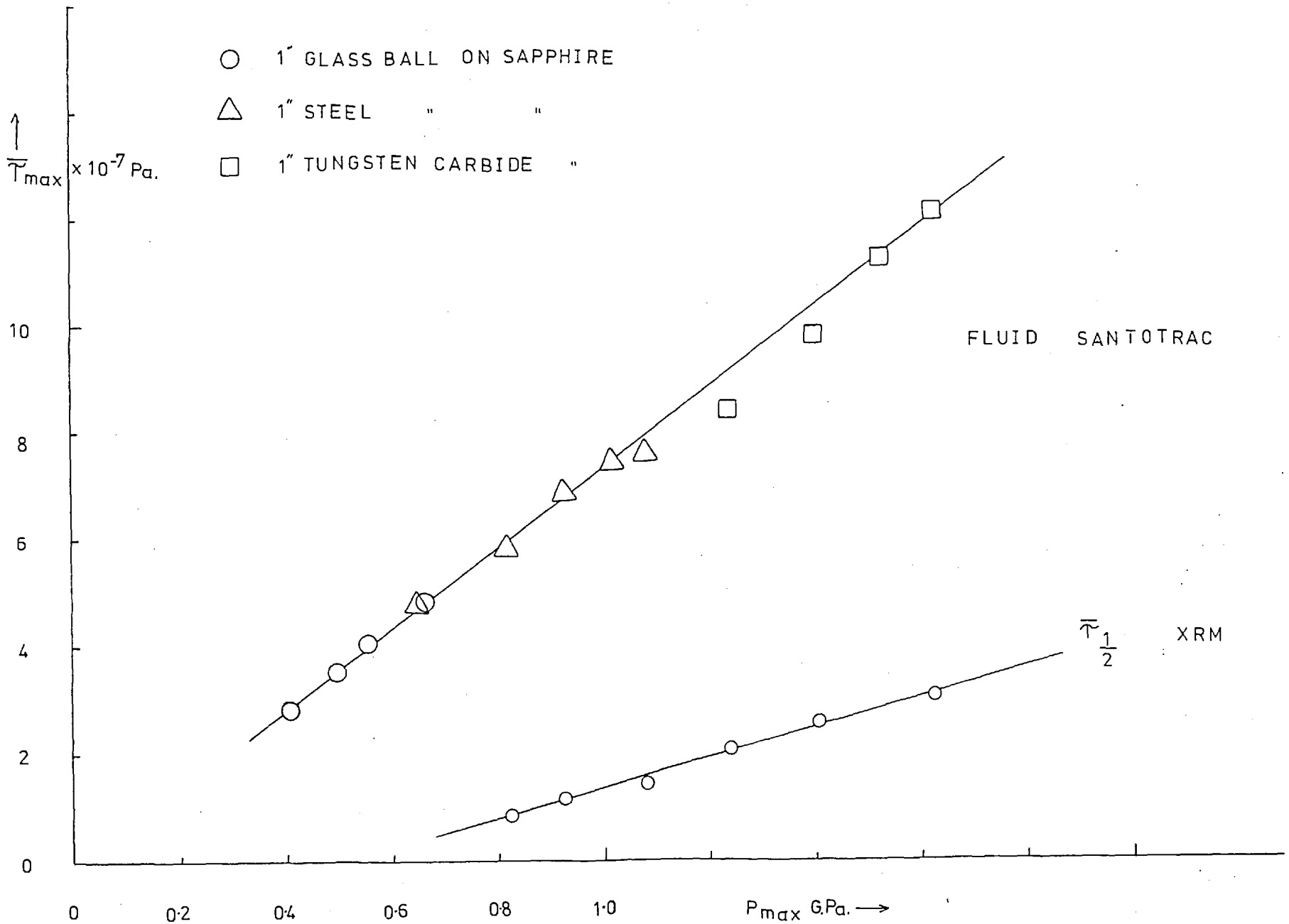
1" GLASS BALL ON SAPPHIRE
1" STEEL " "
1" TUNGSTEN CARBIDE "
τ_{max} x 10^{-7} Pa.
FLUID SANTOTRAC
$\tau_{\frac{1}{2}}$ XRM
0
2
4
6
8
10
0
0·2
0·4
0·6
0·8
1·0
P_{max} G.Pa. ⟶

FIG. 7.20

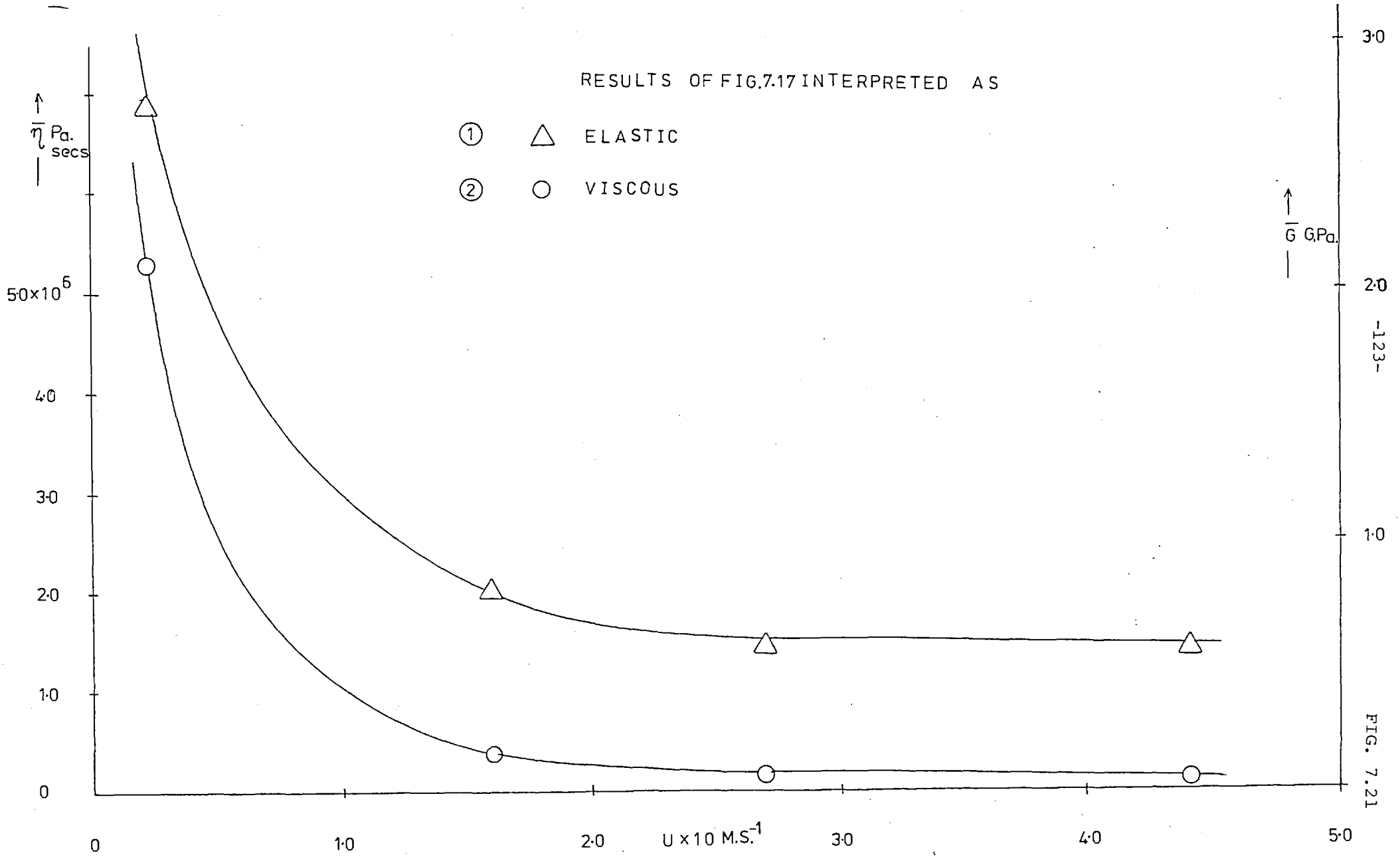
RESULTS OF FIG.7.17 INTERPRETED AS
① △ ELASTIC
② ○ VISCOUS
η Pa. secs
5·0×10^6
4·0
3·0
2·0
1·0
0
0
1·0
2·0
U x 10 M.S.^-1
3·0
4·0
5·0
G G.Pa.
3·0
2·0
1·0

FIG. 7.21

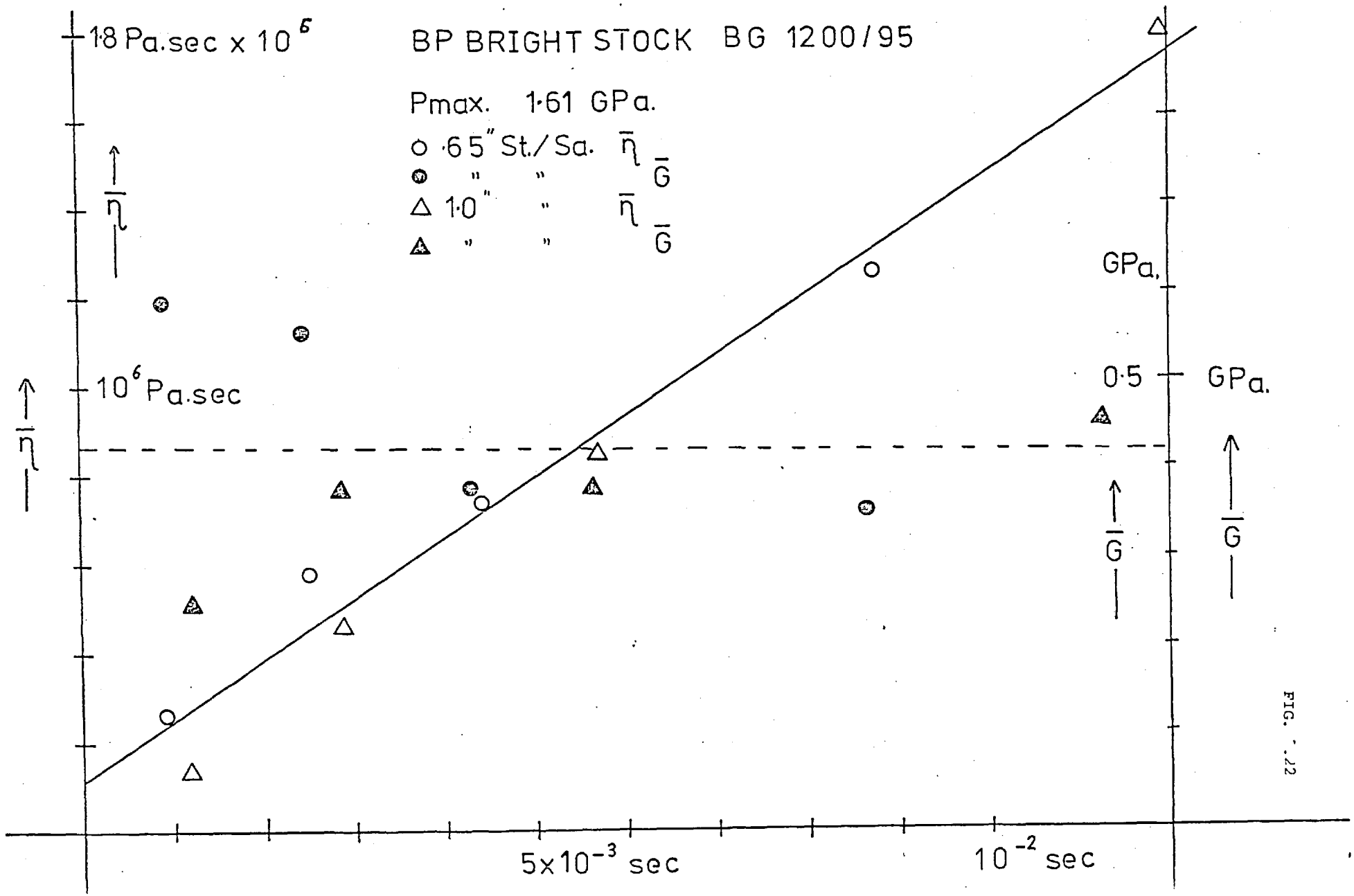
1·8 Pa.sec x 10^6
BP BRIGHT STOCK BG 1200/95
Pmax. 1·61 GPa.
○ ·65" St./Sa. η̄
◉ " " Ḡ
△ 1·0" " η̄
▲ " " Ḡ
η̄
10^6 Pa.sec
GPa.
0·5 GPa.
Ḡ
Ḡ
5x10^-3 sec
10^-2 sec

FIG. 7.22

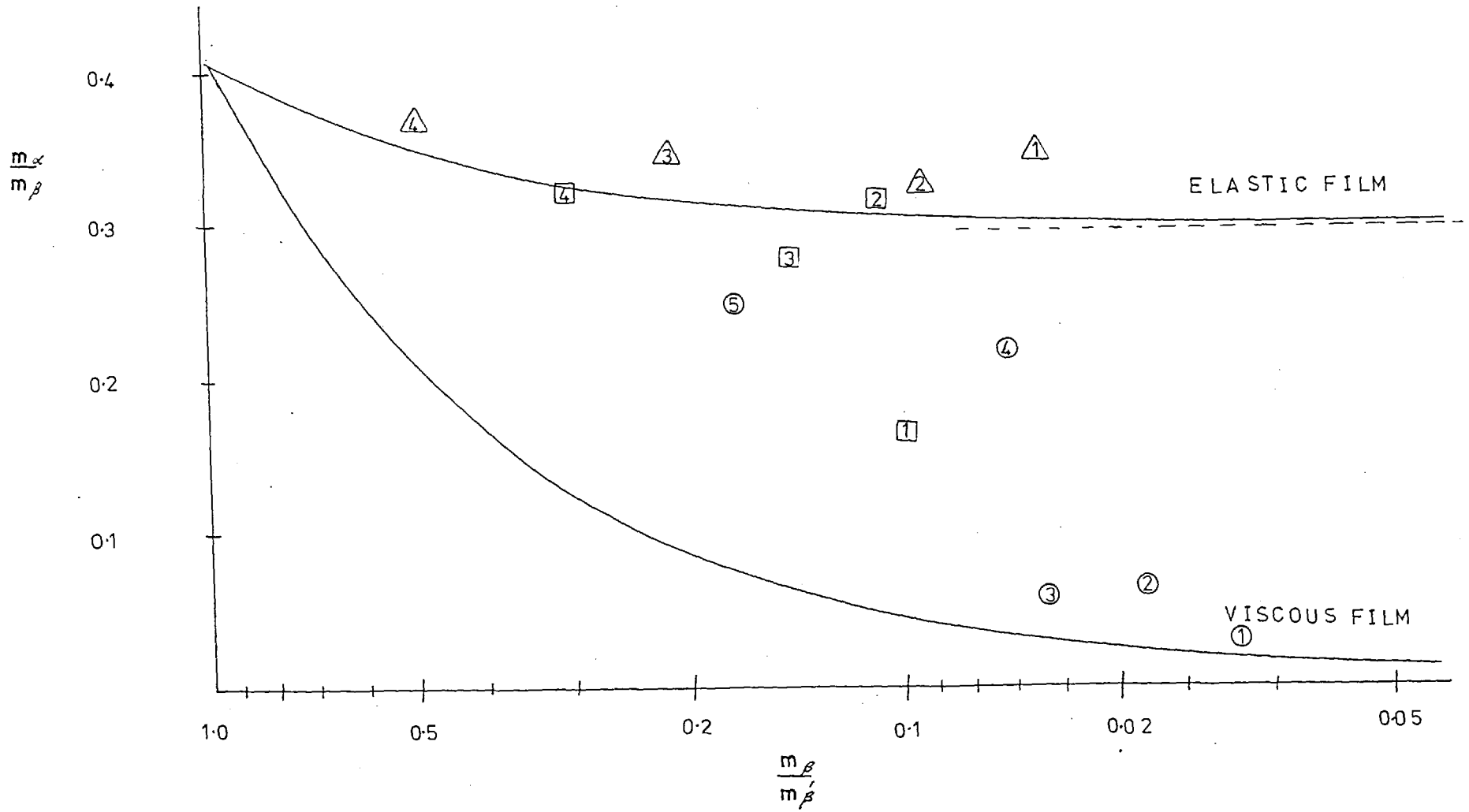
Pmax GPa
1 2 3 4 5
5P4E 1·08 0·82 1·40 1·62
BPBS 0·82 1·24 1·40 1·62
XRM 0·82 0·93 1·08 1·40 1·62
0·4
0·3
0·2
0·1
$\frac{m_\alpha}{m_\beta}$
ELASTIC FILM
VISCOUS FILM
1·0
0·5
0·2
0·1
0·02
0·05
$\frac{m_\beta}{m'_\beta}$

FIG. 7.23

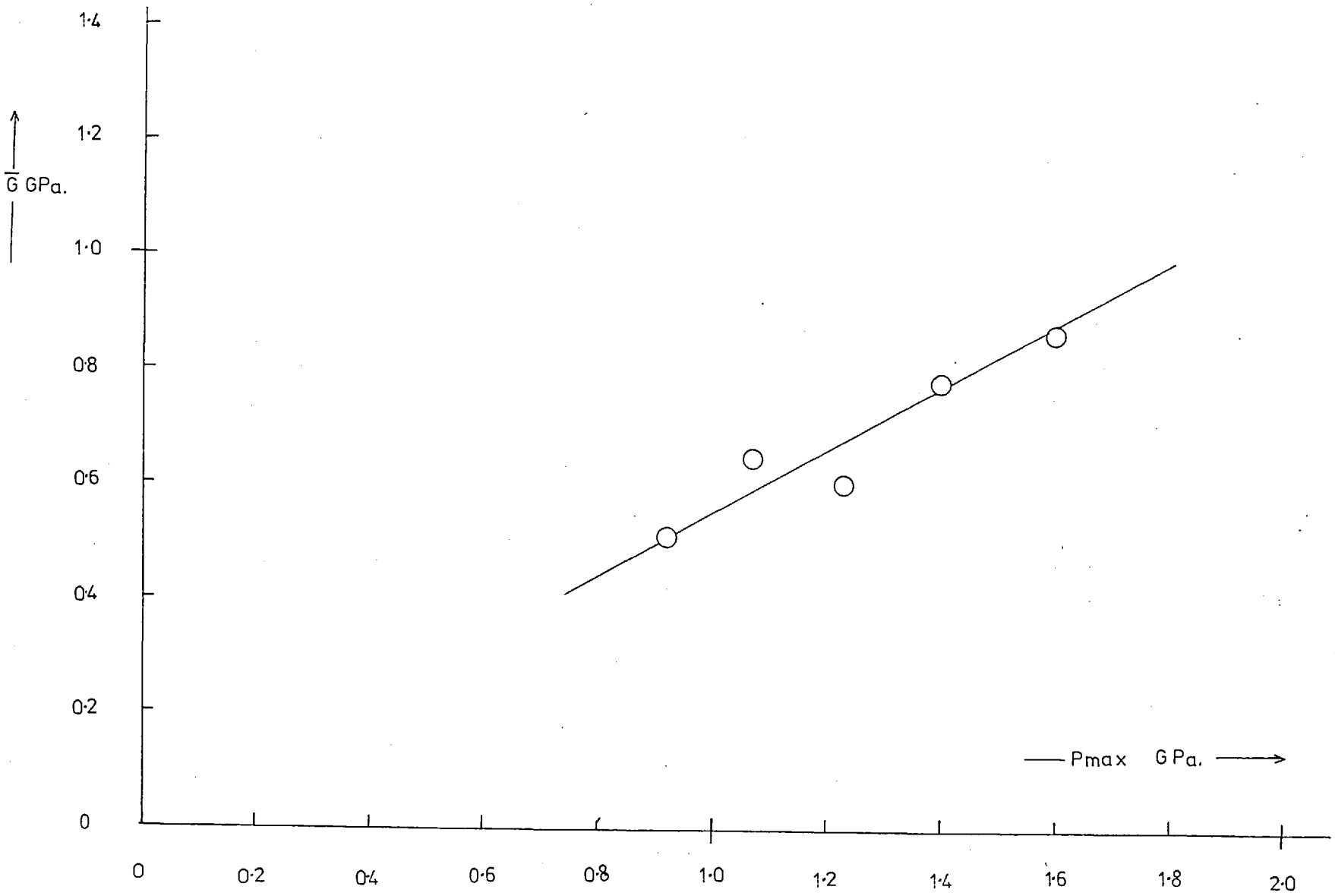
5P4E T = 29°C
$\overline{G}$ GPa.
1·4
1·2
1·0
0·8
0·6
0·4
0·2
0
0
0·2
0·4
0·6
0·8
1·0
1·2
1·4
1·6
1·8
2·0
Pmax GPa.

FIG. 7.24

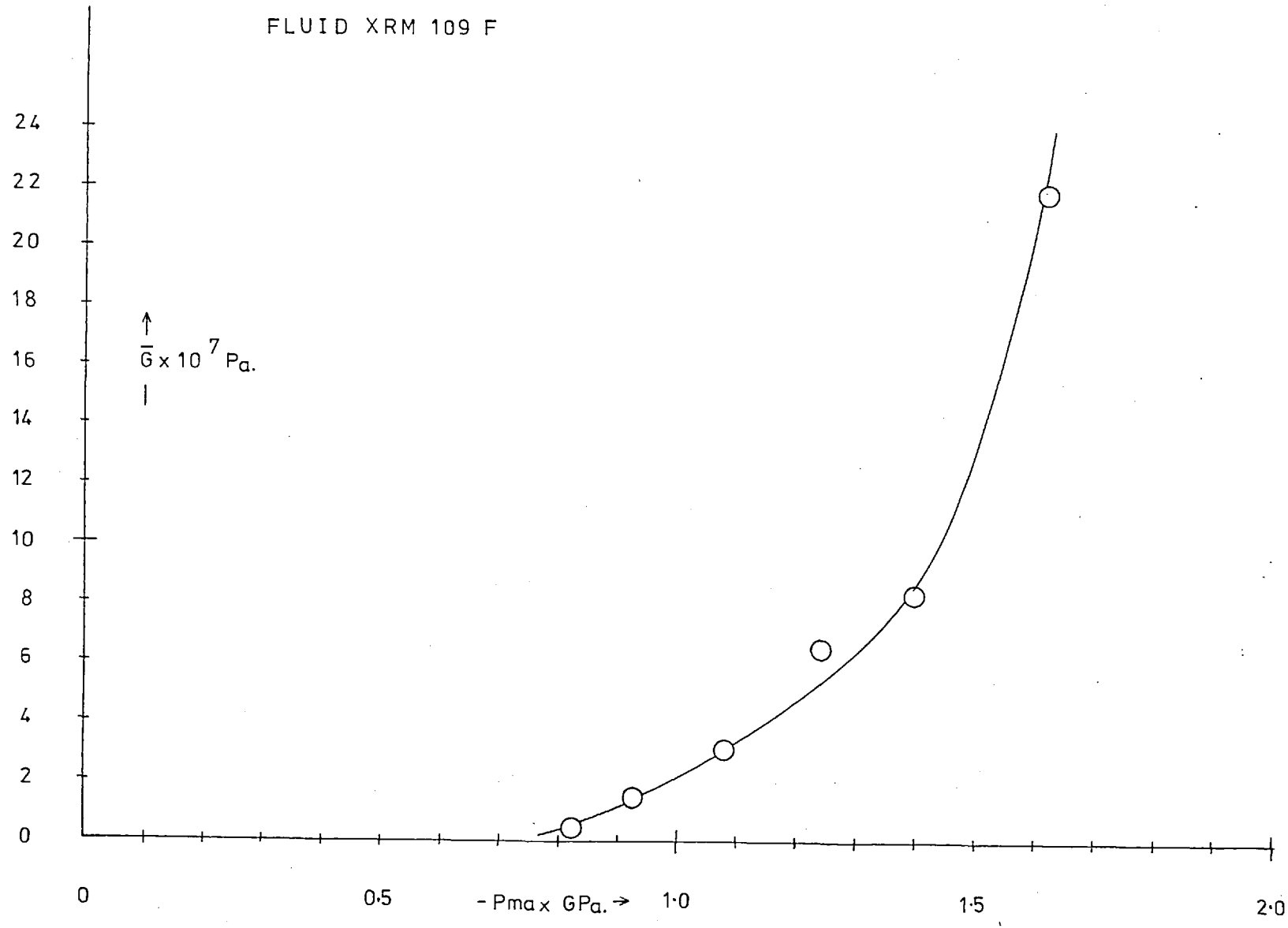
FLUID XRM 109 F
24
22
20
18
16
14
12
10
8
6
4
2
0
$\bar{G} \times 10^7$ Pa.
0
0·5
- Pmax GPa. →
1·0
1·5
2·0

FIG. 7.25

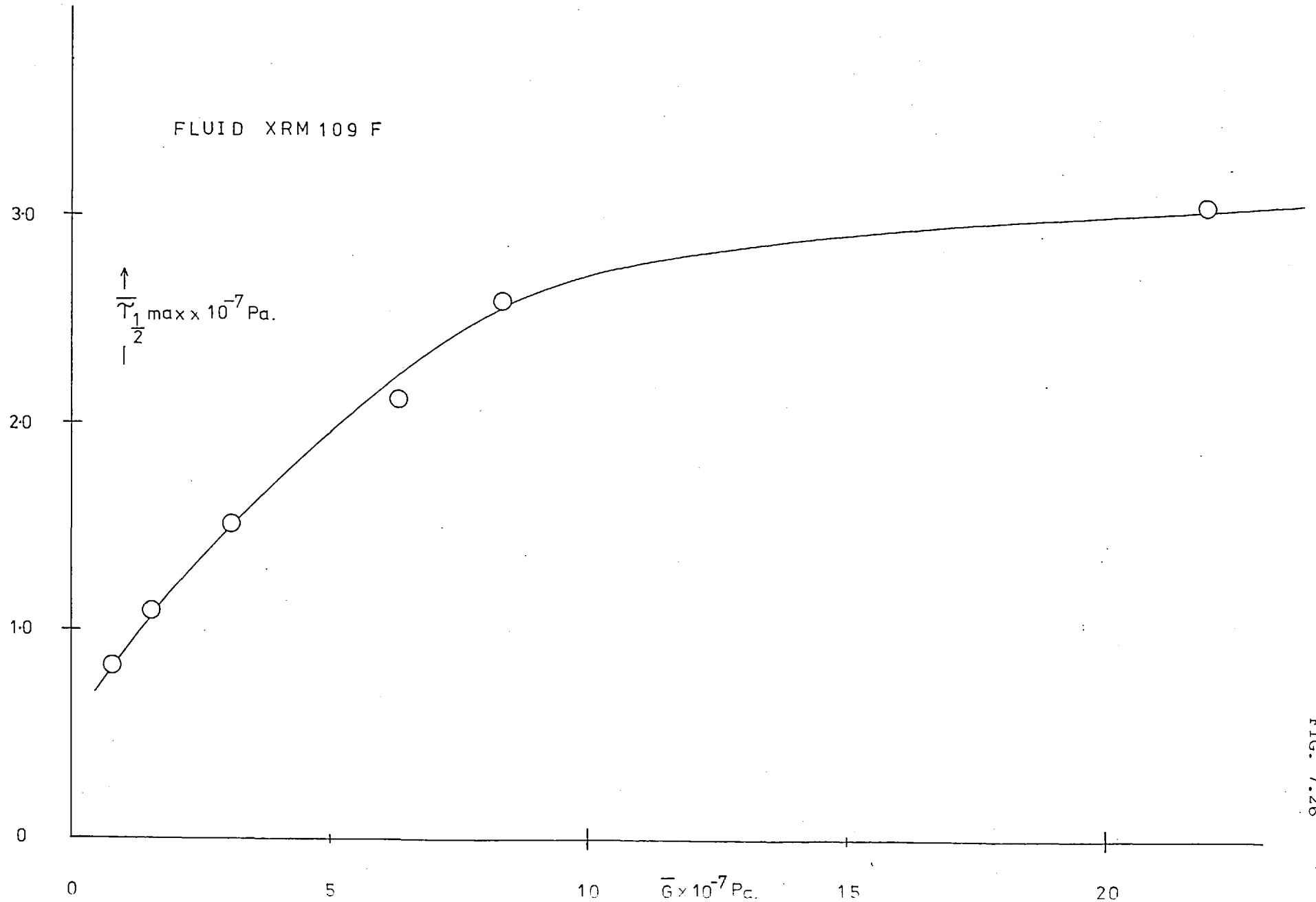
FLUID XRM 109 F
3·0
2·0
1·0
0
$\overline{\tau}_{\frac{1}{2}}$ max x 10^{-7} Pa.
0
5
10
15
20
$\overline{G} \times 10^{-7}$ Pa.

FIG. 7.26

FIG. 7.27

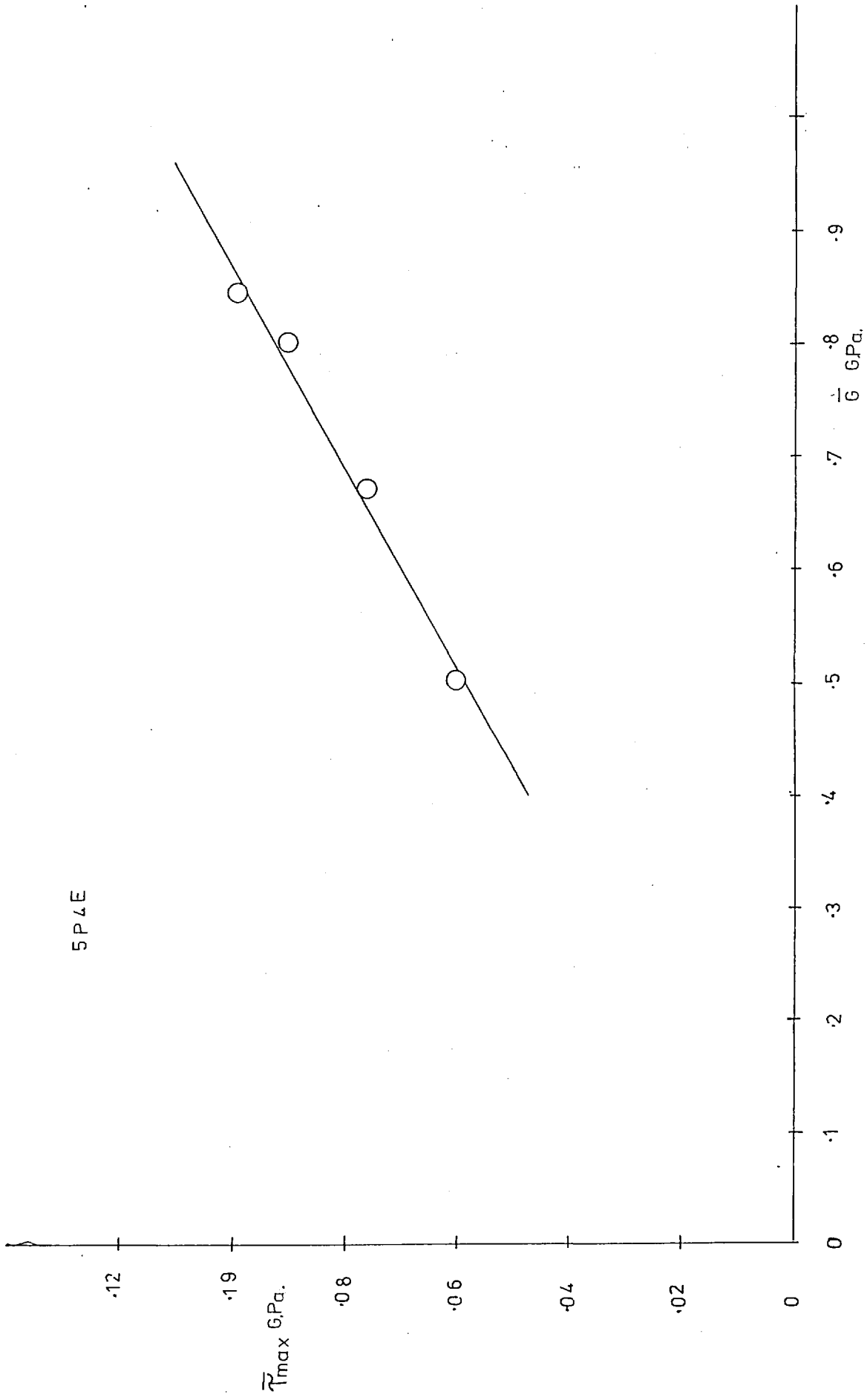
SPLIT
$\bar{\tau}_{max}$ G.Pa.
·12
·1·9
·08
·06
·04
·02
0
0
·1
·2
·3
·4
·5
·6
·7
·8
·9
$\bar{\dot{G}}$ G.Pa.

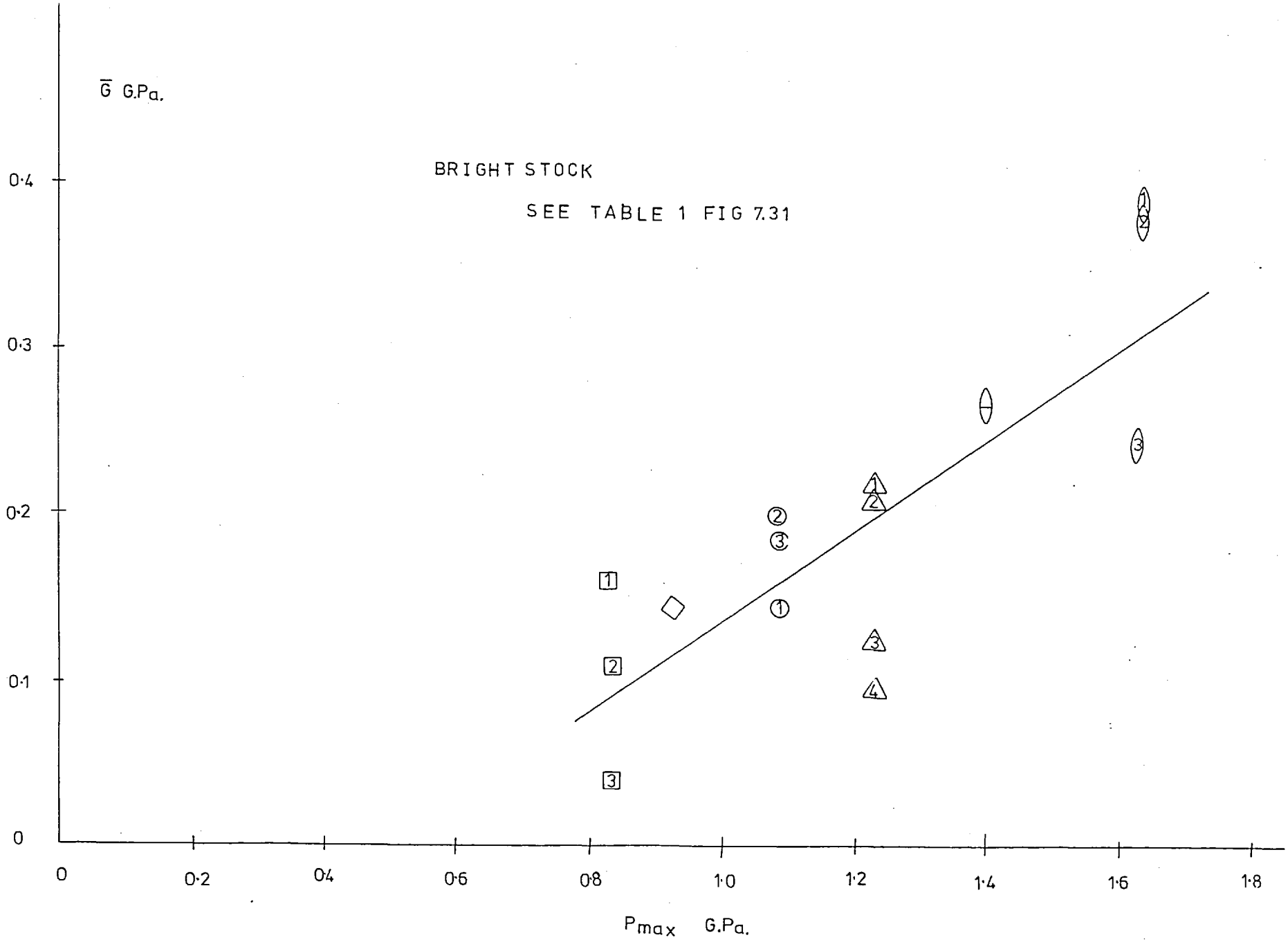
$\bar{G}$ G.Pa.
BRIGHT STOCK
SEE TABLE 1 FIG 7.31
0·4
0·3
0·2
0·1
0
0
0·2
0·4
0·6
0·8
1·0
1·2
1·4
1·6
1·8
P_{max} G.Pa.

FIG. 7.28

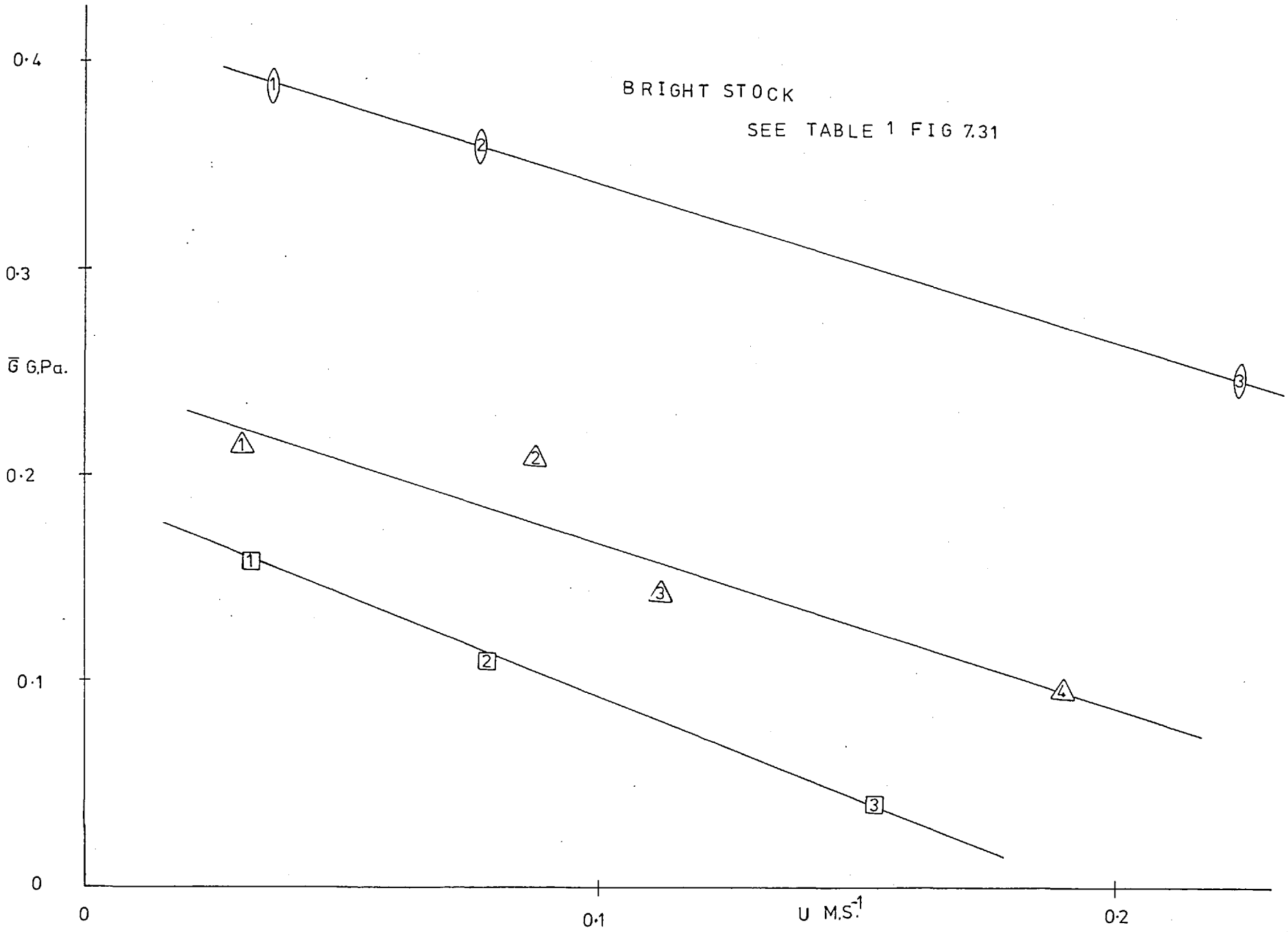
BRIGHT STOCK
SEE TABLE 1 FIG 7.31
0·4
0·3
0·2
0·1
0
$\bar{G}$ G.Pa.
0
0·1
0·2
U M.S.$^{-1}$
1
2
3
1
2
3
4
1
2
3

FIG. 7.29

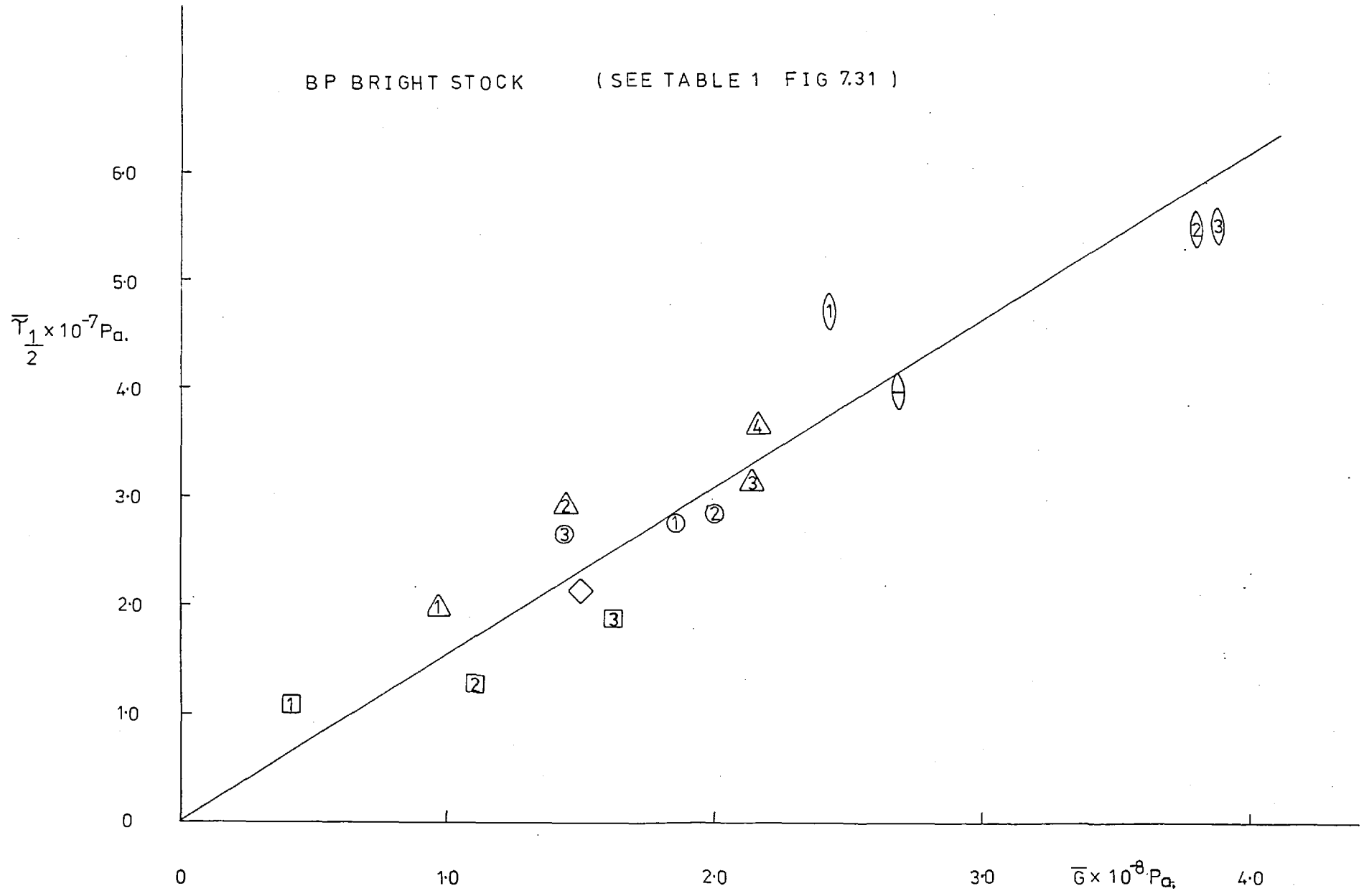
BP BRIGHT STOCK (SEE TABLE 1 FIG 7.31)
$\overline{\tau}_{\frac{1}{2}} \times 10^{-7}$ Pa.
6·0
5·0
4·0
3·0
2·0
1·0
0
0
1·0
2·0
3·0
$\overline{G} \times 10^{-8}$ Pa.
4·0

FIG. 7.30

TABLE 1 BP BRIGHT STOCK $\theta = 30^{\circ}C$

SYMBOL	LOAD NEWTONS	MATERIALS	$U \times 10^2$ M.S.$^{-1}$	$h \times 10^7$ M.	$\left[\frac{I}{N}\right]_{\frac{1}{2}}$	$\overline{\tau}_{\frac{1}{2}} \times 10^7$ Pa.	$\overline{G} \times 10^{-9}$ Pa.	Pmax. G.Pa.
[1]	20·3	1"ST./ SAPPH.	15·30	12·20	0·020	1·09	0·040	0·820
[2]	"	"	7·81	7·80	0·024	1·28	0·110	"
[3]	"	"	3·34	4·60	0·035	1·89	0·16	"
◇	29·3	"	7·75	7·80	0·035	2·15	0·150	0·925
①	4·7·4	"	14·80	12·10	0·039	2·77	0·186	1·08
②	"	"	7·87	7·80	0·040	2·87	0·200	"
③	"	"	3·36	4·60	0·038	2·70	0·143	"
△1	21·2	1 t/c./SAPPH.	18·98	14·00	0·024	1·95	0·097	1·24
△2	"	"	11·20	10·00	0·036	2·96	0·142	"
△3	"	"	7·83	7·82	0·038	3·12	0·215	"
△4	"	"	3·01	4·25	0·045	3·68	0·216	"
⬭	30·20	"	7·85	7·80	0·043	3·99	0·269	1·40
⬭1	48·30	"	22·50	16·00	0·044	4·75	0·243	1·62
⬭2	"	"	7·72	7·80	0·051	5·51	0·379	"
⬭3	"	"	3·67	4·80	0·051	5·56	0·388	"

FIG. 7.31

FIG. 7.32

TABLE OF MATERIAL PROPERTIES USED IN THE COURSE OF THIS WORK

Material	Modulus of Elasticity	Poisson's Ratio
Sapphire	285 GPa	0.47
Steel	211 GPa	0.30
Tungsten carbide	686 GPa	0.25
Glass	77 GPa	0.30

FLUID PROPERTIES

BP Bright Stock

This fluid was supplied by B.P. and was described as a paraffinic cylinder stock. The following data was supplied with it.

At Atmospheric Pressure

Temperature	Viscosity	Density
100°C	0.0448 Pa sec	863 kgM^{-3}
37.7°C	1.079 Pa sec	898 kgM^{-3}
20°C	4.500 Pa sec	910 kgM^{-3}

At 21°C

Pressure	Viscosity
28 MPa	15.85 Pa sec
42 MPa	22.40 Pa sec
77 MPa	200.0 Pa sec

FIG. 7.32
(Contd)

5P4E

This fluid was supplied by Monsanto Corporation and is a 5 phenyl 4 ether. The following data was supplied with it.

Viscosity	Pressure	Temperature
0.419 Pa sec	0.103 MPa	37.7°C
5.536 Pa sec	70 MPa	37.7°C
0.0180 Pa sec	0.103 MPa	100°C
0.028 Pa sec	45 MPa	100°C
0.047 Pa sec	70 MPa	100°C

Pour point 44°C

Bulk modulus 3.22 GPa

For general properties see Gunderstone and Hart "Synthetic Lubricants" Rheinhold, 1962

XRM 109F

This is a synthetic paraffinic oil tht has been extensively tested in high temperature lubrication work.

Viscosity	Temperature
0.31 Pa secs	37.7°C
0.028 Pa secs	100°C
0.004 Pa secs	204°C

FIG. 7.32
(Contd)

Santotrac 50

This fluid was supplied by Monsanto Corporation and is a traction fluid.

Viscosity	Temperature
4.55 Pa sec	-17.7°C
0.0298 Pa sec	37.7°C
0.0048 Pa sec	100°C

Further details may be obtained from Monsanto Corporation.

CHAPTER 8

DISCUSSION OF RESULTS

8.1 INTRODUCTION

This chapter is devoted to the analysis and discussion of the results and derived parameters presented in the previous chapter.

8.2 FILM THICKNESS RESULTS

The variation of film thickness with rolling speed is shown for each of the test fluids on log-log plots in figures 7.1 to 7.4. It may be seen that they all have gradients of approximately 0.7.

Each of these sets of results is re-plotted in the form log h versus log ($\eta_o U$) in fig. 7.5 in order to give approximate estimates of the pressure viscosity (α' values) coefficients of each of the test fluids as explained in Section 6.1.

An error of $\pm 10\%$ in these α' values is expected since the film thickness plots were not to be parallel and so the calculated α' values depend upon the $\eta_o U$ point for comparison (see diagram, Section 6.1).

The film thickness equation for point contact used in the above work is a modification of the Dowson and Higginson formula for elasto-hydrodynamic film thickness in line contact, i.e.

$$\frac{h_{min}}{R} = 1.6\left(\frac{\eta_o U}{E'R}\right)^{0.7} (\alpha' E')^{0.6} \left(\frac{W}{E'R}\right)^{-0.13}$$

h_{min} is the minimum film thickness

R is the radius of relative curvature given by $\frac{1}{R} = \frac{1}{R_1} + \frac{1}{R_2}$ where R_1 and R_2 are surface radii.

η_o is the viscosity in the inlet at atmospheric pressure

U is the mean rolling speed

E' is the reduced Young's modulus given by

$$\frac{2}{E'} = \frac{1 - \sigma_2^2}{E_2} + \frac{1 - \sigma_1^2}{E_1}$$

where σ_1, σ_2 and E_1, E_2 are the Poisson's ratios and the Young's moduli of the surfaces 1 and 2.

α' is the pressure viscosity coefficient defined by the relationship

$$\eta(P) = \eta_o \exp(\alpha' P)$$

W is the load per unit width of contact

From his experimental results, Foord(1) has provided an empirical formula for the film thickness h_o at the centre of a point contact, i.e.

$$\frac{h_o}{R} = 0.86 \left(\frac{\eta_o U}{E'R}\right)^{0.667} (\alpha' E')^{0.6} \frac{N}{E'R^2}$$

where N is the total normal load. Other experimenters (Westlake(2), Gentle(3)) have found different values of the exponents for different fluids and so the above formula cannot be used as a general film thickness relationship except as an approximation.

The main difference between point and line contact is the existence of side leakage in the inlet, causing the film thickness to be lower than for a comparable line contact.

Both the formulae assume isothermal Newtonian behaviour of the lubricant in the inlet region to the contact, together with an exponential viscosity variation with pressure (c.f. $\eta(P) = \eta_o \exp(\alpha' P)$.

There would therefore seem to be the following possible reasons for the difference in log h versus log ($\eta_o U$) slopes for different fluids.

(1) The inlet side leakage is not accounted for specifically in the film thickness formula.

(2) Non Newtonian behaviour of fluids in the inlet region such as time dependent viscosity effects could reduce film thickness.

(3) A more complex variation of viscosity with pressure in the inlet region than $\eta(P) = \eta_o \exp \alpha' P$ is possible.

(4) A more complex dependence of film thickness upon pressure viscosity coefficient is conceivable.

Jackson(4) has found that the variation of film thickness for different ball sizes in point contact is not accurately predicted by the above formula.

The main object of this part of the work was to obtain film thicknesses for the various experimental conditions, so that the traction data could be analysed and so the slight variations of film thickness plots was not important.

8.3 DESCRIPTION OF TRACTION CURVES

Figs. 7.6 to 7.17 show typical sideslip traction curves for the fluids over a wide range of conditions. All the curves show an initial steep gradient m_β followed by a non linear part with the gradient reducing with increased slide/roll ratio. Figs. 7.7 to 7.14 show that, only at high loads and low rolling speeds, do the traction curves for XRM 109F and B.P. Bright Stock approach a near plateau region.

From figs. 7.15, 7.16, 7.17 and 7.18 it is clear that the traction curves for 5P4E and Santotrac 50 may best be described in terms of an initial gradient m_β followed by a non linear part leading to a plateau region with no roll over with increased slide/roll ratio.

Figs. 7.8, 7.9, 7.10 and 7.17 all show some variation in the traction maximum that is much more pronounced at low loads and low rolling speeds regardless of which ball (1" tungsten carbide or 1" steel) was used. The variation of the traction maximum with rolling speed does not seem to depend upon the maximum theoretical Hertz pressure, i.e. the maximum theoretical Hertz pressure varied by

0.82 GPa to 1.08 GPa for a 1" steel ball on sapphire

and

1.24 GPa to 1.62 GPa for a 1" tungsten carbide ball on sapphire

None of the traction curves obtained showed any "roll over" after the traction plateau was reached. Similar behaviour was observed by Gentle(3) at lower maximum Hertz pressures 0.4 to 0.6 GPa. This was not expected to be the pattern at pressures of 1.6 GPa since other workers have found a "roll over" in line contact traction at comparable maximum Hertz pressures.

It is suggested that three factors contribute to the near plateau shape of the traction curves obtained.

(1) All the traction experiments were conducted over a very small range of slide/roll ratios which were themselves small, i.e.

$$\left|\frac{\Delta v}{U}\right| < 3 \times 10^{-2}$$

This meant that the variation of traction force with slide/roll ratio was greatly obscured by the magnification of the slide/roll ratio scale. Also the ratio never even approached a value for which any large reduction of the traction force would be expected.

(2) The idealised Hertz pressure distribution in line contact is quite different from that in point contact. Fig. 8.1 shows the variation of pressure that elements of oil are subjected to in their passage through a point contact and a line contact. It is clear that in a line contact, nearly all the oil is subjected to the same pressure profile.

In point contact, however, the pressure distribution varies from flow line to flow line. The result of this is that in a point contact, the traction phenomena observed are averages in two dimensions (rather than one in line contact) with the concomitant increased masking of distinct traction effects. However, for the same mean pressures in line and point contact, one could still expect to see similar average effects.

(3) It is generally agreed that the fall off in traction for high amounts of sliding is a temperature effect and so it is suggested that, for comparable mean pressures in line and point contact, some of the heat is convected away from the contact by side leakage from within the contact. This point is difficult to justify since the side leakage in point contact is very small compared with the flow through the contact in the rolling direction. As shown by Wolveridge and Archard(5), the time constant for the conductive component of heat transfer is

$$\frac{h^2}{\pi^2 K \rho c}$$

FIG. 8.1

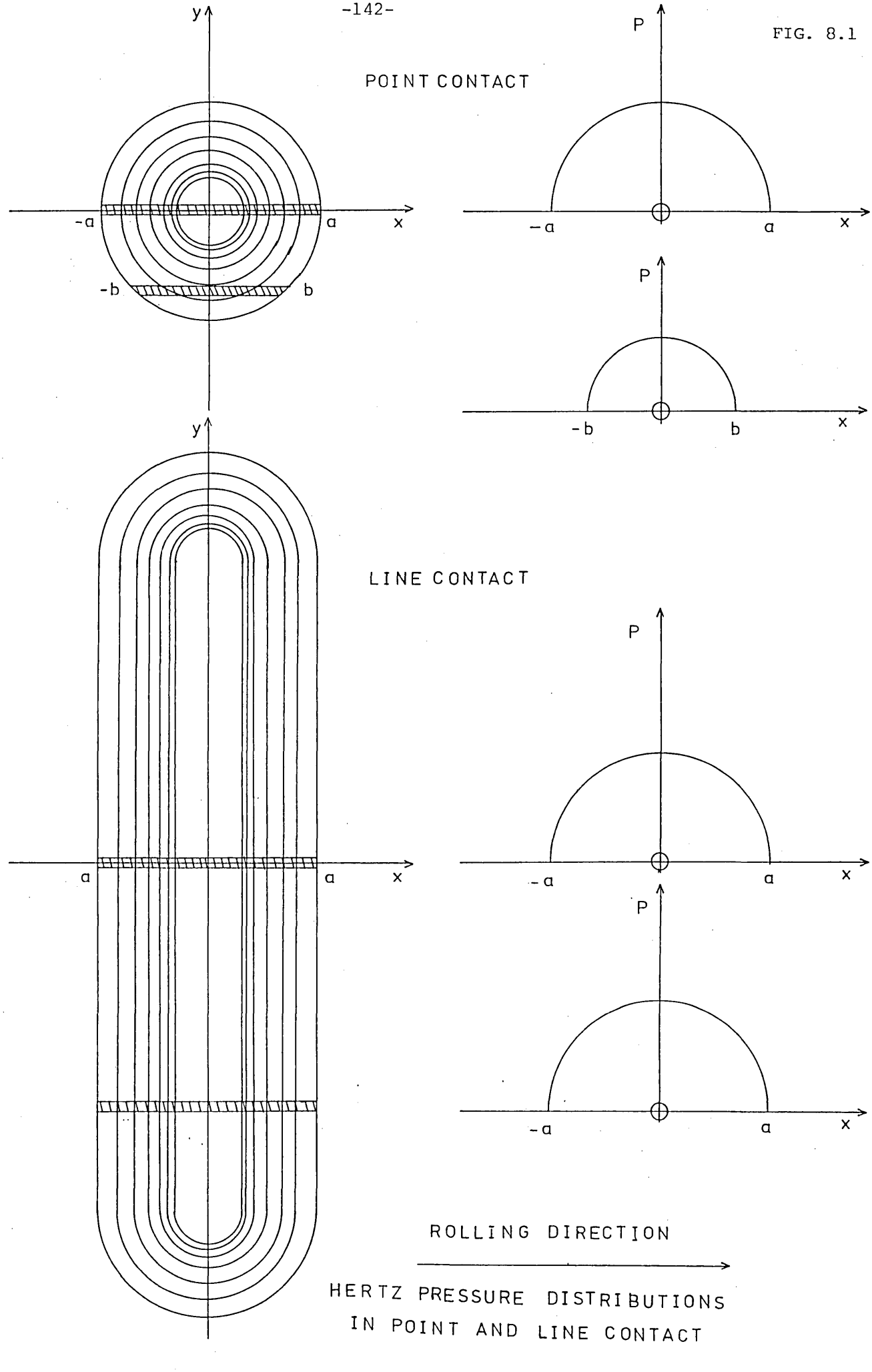

HERTZ PRESSURE DISTRIBUTIONS
IN POINT AND LINE CONTACT

where h is the film thickness

K is the thermal conductivity

c is the specific heat

ρ is the density

Approximate values of these in the above experiments are

$h = 10^{-6} M$

$K = 0.13\ JM^{-1}S^{-1}K^{1}{}^{\circ}C^{-1}$

$c = 2.1 \times 10^{3} Jkg^{-1}C^{-1}$

$\rho = 10^{3} kgM^{-3}$

which gives $\frac{h^2}{\pi^2 K\rho c} = 1.6 \times 10^{-7}$ seconds.

Since transit times in these experiments were 10^{-4} to 10^{-3} seconds, all heat dissipation was by conduction rather than convection, and so convection by side leakage would seem to be out of the question.

8.4 INTERPRETATION OF THE TRACTION MAXIMUM

It was decided to see if the limiting shear stress model would give a consistent interpretation of the traction maxima. These results were divided into two parts:

(a) 5P4E and Santotrac 50

(b) XRM 109F and B.P. Bright Stock

(a) For 5P4E and Santotrac 50 it was easy to distinguish a near plateau region of traction coefficient $\frac{T}{N}$ versus sideslip/roll ratio $\frac{\Delta V}{U}$ which was interpreted in terms of:

$$\bar{\tau}_{max} = \frac{T_{max}}{\pi a^2}$$

For 5P4E it was found that the maximum traction coefficient fell with increased rolling speed far more markedly at lower temperatures and low loads (10 N, 25°C) than at higher temperatures (60°C) and loads (47 N) whereas Santotrac 50 showed almost no variation of traction maximum with rolling speed, temperature or load (see fig. 7.18).

It was proposed that the fall of traction maximum with rolling speed was due to hydrodynamic lift around the inlet zone to the contact area which was reducing the effective load on the deformed contact zone and so reducing the mean limiting shear stress of the film.

Since hydrodynamic lift is predominantly dependent upon inlet viscosity η and rolling speed U and since the viscosities of Santotrac 50 and 5P4E at 25°C and 60°C are:

	25°C	60°C	
Santotrac	3.02	0.073	Pa secs
5P4E	0.053	0.013	Pa secs

one would expect this effect to be far more pronounced at low temperatures with 5P4E than Santotrac 50, and less so at higher temperatures for either fluid.

A similar effect was seen by Klemz, Gohar and Cameron(6) who measured the reduction in local stresses consequent upon a thick lubricant film.

Hamilton and Moore(7) in 1971, using a manganin pressure transducer, found significant changes in pressure distribution with rolling speed. Several attempts have been made to calculate the pressure distribution from other more easily measured physical properties.

Kannel, Bell and Allen(8) used the film shape measured by an x-ray technique to find the pressure distribution. Ranger(9) used the film shapes, measured optically by Wymer(10), for a tapered steel roller on a glass disc, and by the inversion of the elasticity equation obtained pressure distributions for the contacts (see fig. 8.2). It is clear from fig. 8.2 that the pressure distribution changes considerably with increased rolling speed.

By an iterative solution of both the elasticity and Reynold's equations, Ranger(9) was able to show that the pressure distribution in a point contact varies with rolling speed in a similar way to that in a line contact (see fig. 8.3). He also showed that the pressure distribution was changed more for low loads than high loads with all other variables kept constant.

Fig. 7.19 shows that the derived mean limiting shear stress for 5P4E is a nearly linear function of Hertz pressure for low rolling speeds where large changes in the pressure distribution were not expected. Fig. 7.20 also shows the mean limiting shear stress of Santotrac 50 to be a linear function of Hertz pressure.

If, at this stage, the limiting shear stress is taken to be proportional to pressure then the simplest explanation for the fall in traction coefficient with rolling speed for 5P4E is that the mean pressure within the constriction is reduced by hydrodynamic effects outside it.

Ranger only dealt with low viscosity fluids with low pressure viscosity α' coefficient and low Hertz pressures, and so can only be used as qualitative data.

FIG. 8.2

Variation of pressure distribution with rolling speed in line contact from Ranger(9)

Curve	Rolling Speed MS^{-1}
A	0.251
B	0.508
C	1.270
D	1.270
E	2.540

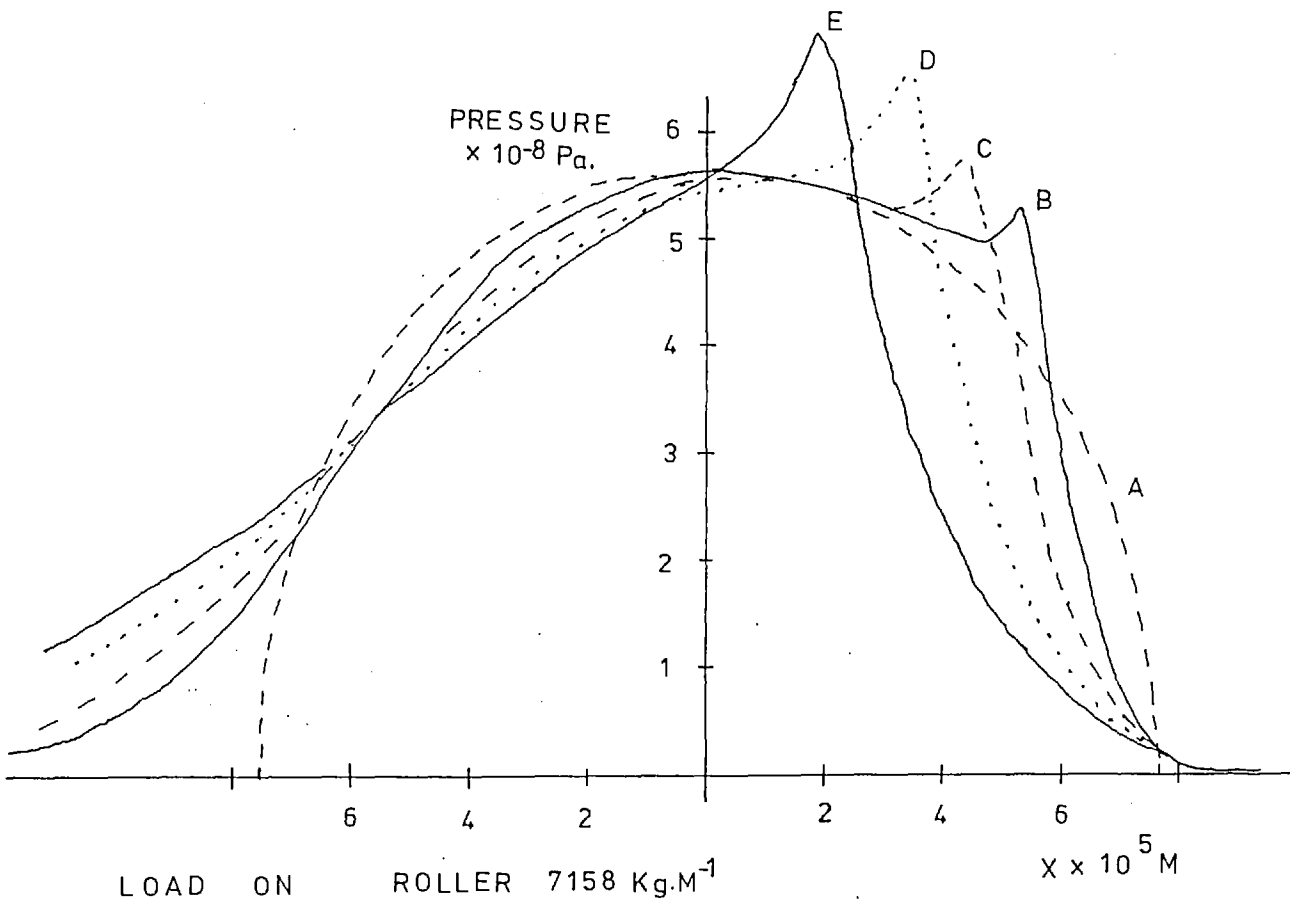

FIG. 8.3

Variation of pressure distribution with rolling speed calculated by Ranger(9) for a 1" steel ball rolling on glass for an oil of inlet viscosity 0.5 Pa secs.

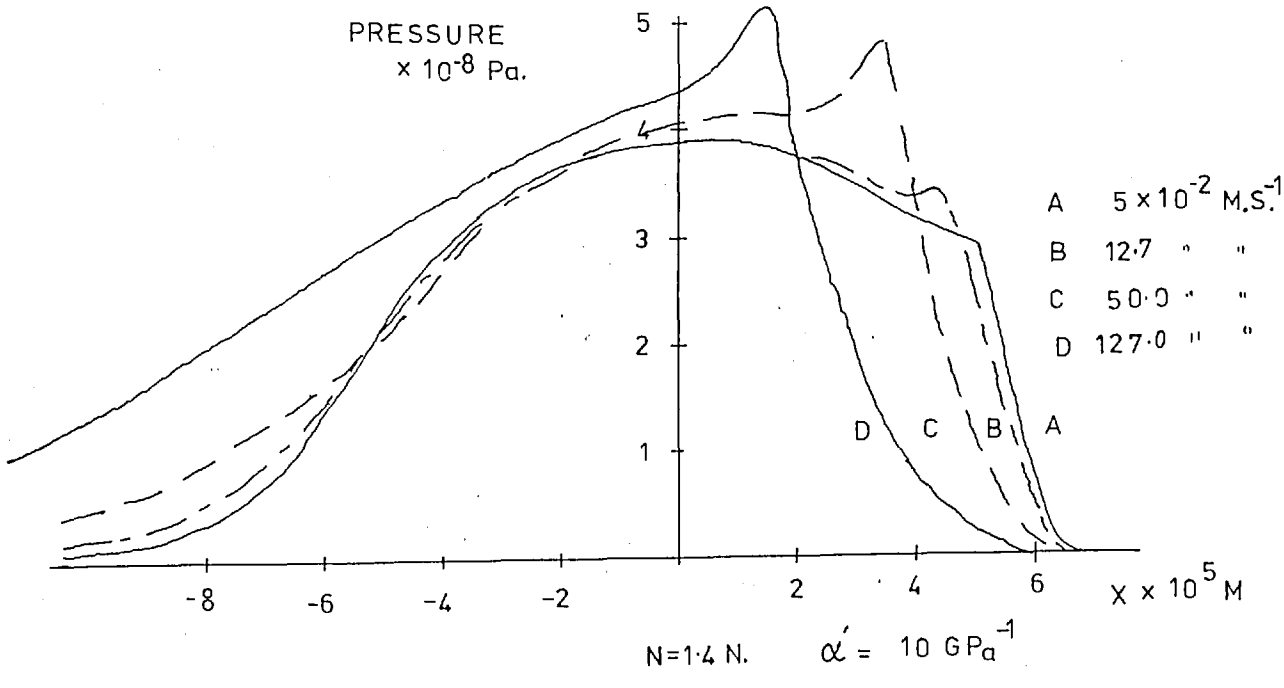

From a direct application of the Kapitza(11) solution for the half Sommerfeld conditions of Reynold's equation for a rigid sphere rolling on a flat plate, it can be shown that the hydrodynamic lift is a significant fraction of the normal load, provided that the distance of closest approach is taken to be the central e.h.d. film thickness.

$$F = \frac{6\pi U\eta}{5}\sqrt{\frac{2R_o^3}{h}}$$

where F is the hydrodynamic lift

U is the mean rolling speed

η is the viscosity

R_o is the radius of the ball

h is taken to be the central film thickness

For typical experimental conditions such as found in fig.7.18, Chapter 7

for $U = 0.44\ MS^{-1}$

$\eta = 3.02$ Pa sec (5P4E)

$\theta = 25^{o}C$

$h = 5.1 \times 10^{-6} M$

$R_o = 1.27 \times 10^{-2} M$ (1" ball)

then $F = 4.5$ N

This lift would reduce the mean contact pressure by 45% with a consequent reduction in limiting shear stress of 45% (assuming τ_{max} proportional to P). Experimentally the traction force fell to nearly zero and so this calculation can only be used as qualitative evidence for a modification of pressure distribution with rolling speed. This must also depend upon the degree of flooding in the inlet, the pressure

FIG. 8.4

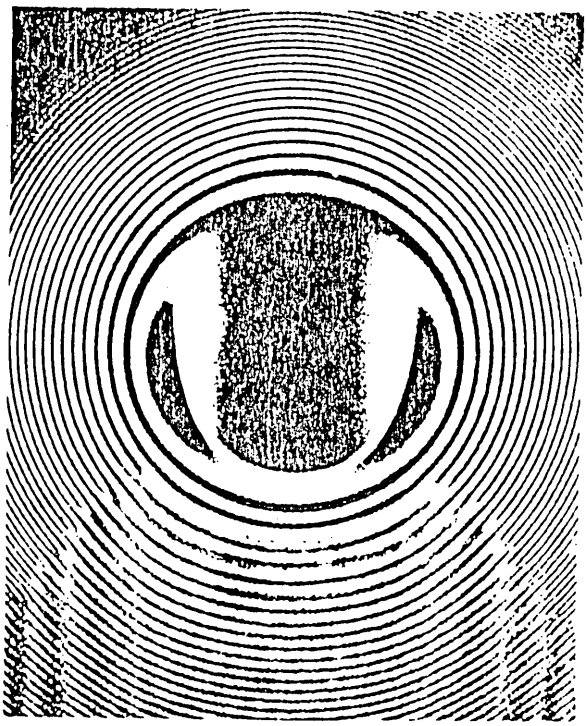

a) 5LB 3RD BLACK

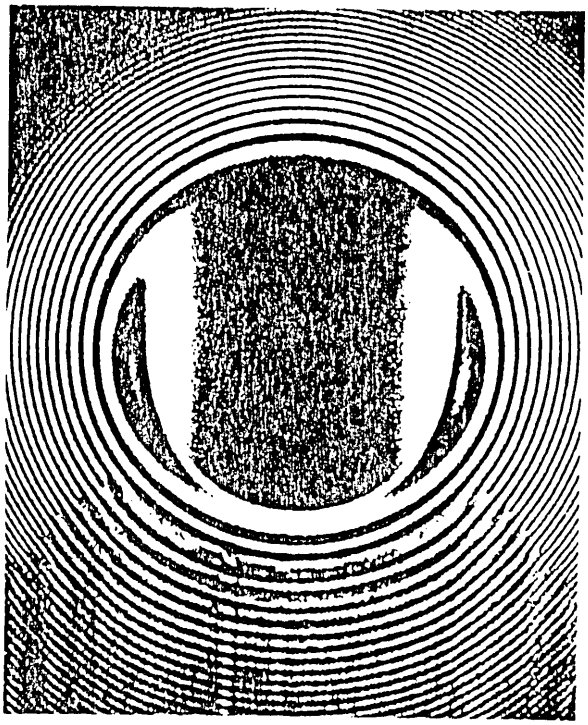

b) 10LB 3RD BLACK

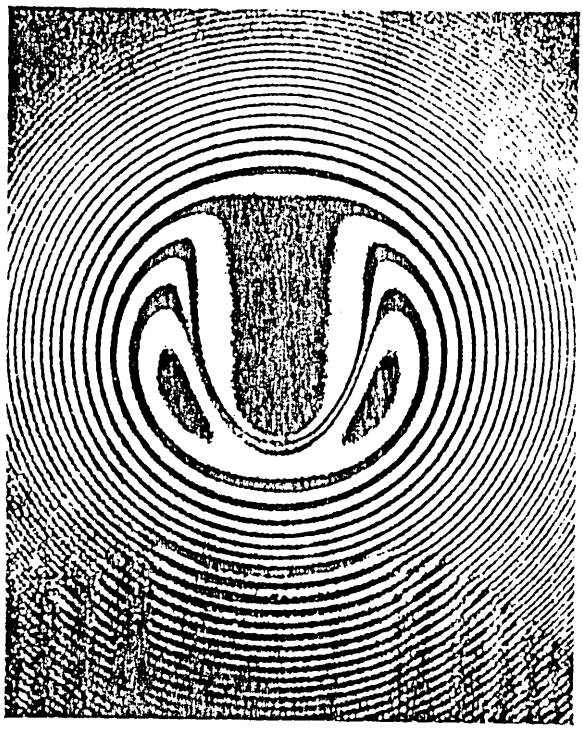

c) 5LB 10TH BLACK

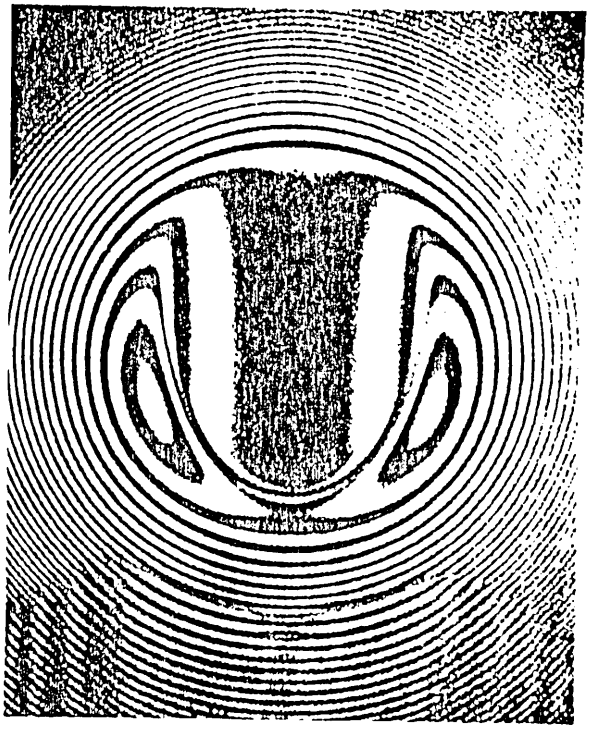

d) 10LB 10TH BLACK

ROLLING CONTACTS LUBRICATED WITH 5-PHENYL-4-ETHER (from Foord(1))

FIG. 8.5

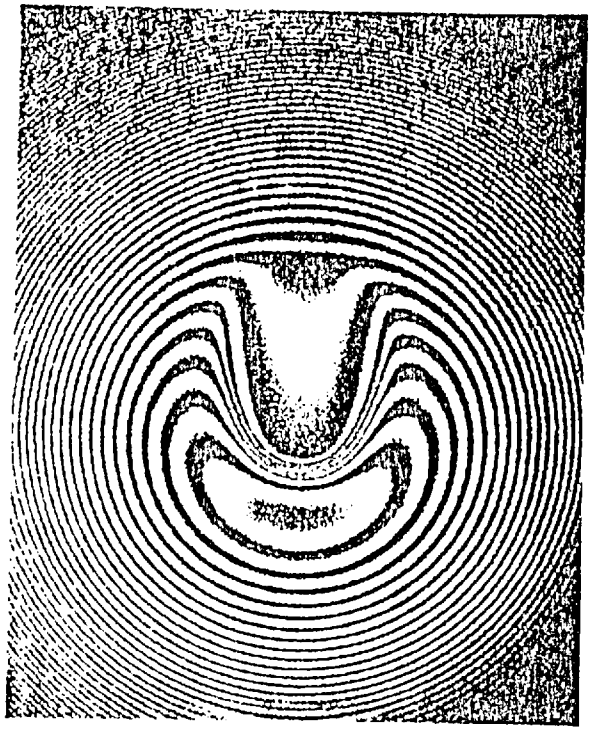

e) 5LB 20TH BLACK

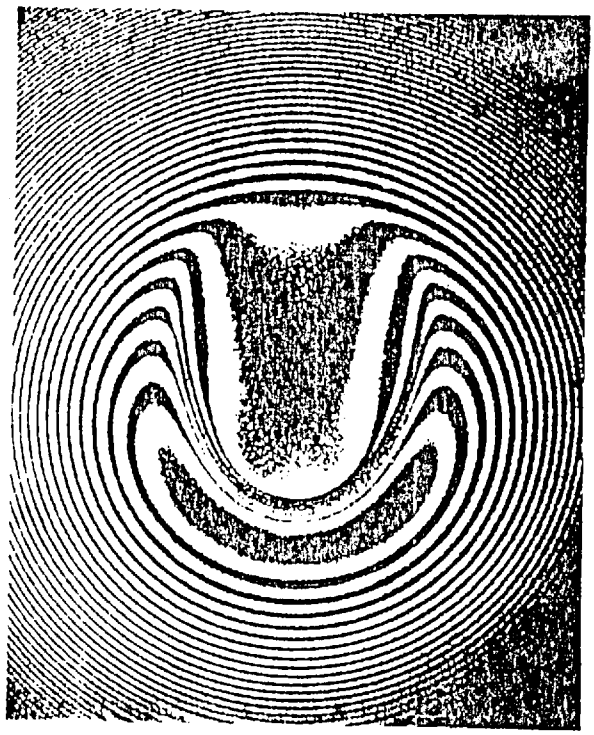

f) 10LB 20TH BLACK

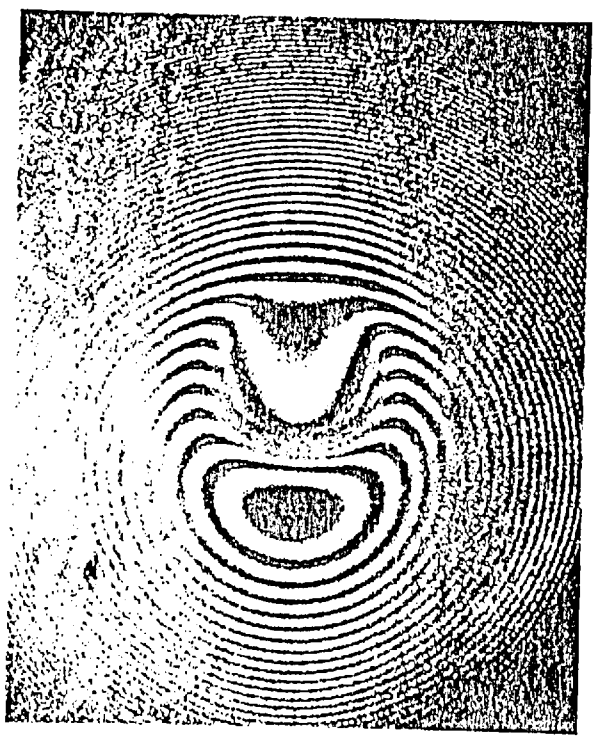

g) 5LB 30TH BLACK

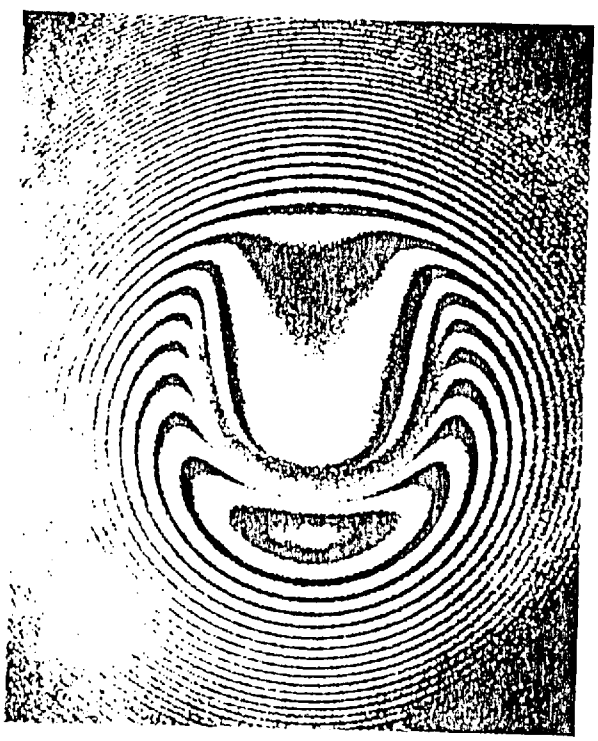

h) 10LB 30TH BLACK

(from Foord(1))

viscosity coefficient of the fluid, and the detailed geometry of the surfaces close to the deformed area. It is surprising that the Kapitza formula provides such a close estimate.

A sodium lamp was used to observe the film shape under identical conditions to those above, and it was found that the central contact area had been reduced nearly to zero and Newton's rings were seen with only minor deviations in the centre of the contact. This effect has been photographed by Foord(1) with 5P4E (see figs. 8.4 and 8.5). Uncertainties in the refractive index of the fluid under these conditions precludes any exact analysis of these interferograms which do provide overwhelming evidence for changes from the theoretical Hertzian pressure distribution (Pmax = 0.82 GPa) to a far broader low pressure distribution where limiting shear stress effects would not be expected to manifest themselves.

This reduction in traction coefficient with rolling speed is of supreme practical importance since it determines the power transmission capabilities of traction drives.

(b) Bright Stock and XRM 109F

From figures 7.7, 7.8, 7.9, 7.10, 7.11, 7.12, 7.13 and 7.14 it is clear that no such pronounced traction plateaux were found for Bright Stock and XRM 109F as for 5P4E and Santotrac 50, except at high pressures. These results were therefore described in terms of $\bar{\tau}_{\frac{1}{2}}$ as used by Hirst and Moore(12) where

$$\bar{\tau}_{\frac{1}{2}} = \frac{T}{\pi a^2} \frac{1}{2} \quad \text{(see fig. 5.1)}$$

The results of the variation of $\bar{\tau}_{max}$ and $\bar{\tau}_{\frac{1}{2}}$ with maximum Hertz pressure for various material combinations and 5P4E, XRM 109F and Santotrac 50 is shown in figures 7.19 and 7.20. The striking characteristic of all these plots is that they are nearly continuous from one ball and plate material combination to the next. If the flattening off of traction curves were a thermal effect, then since the thermal properties of the bearing materials vary widely, significant discontinuities in the limiting shear stress pressure plots would have been expected.

TABLE OF THERMAL PROPERTIES OF BEARING MATERIALS

	Thermal Conductivity $K(JM^{-1}K^{-1}S)^{-1}$	Specific Heat $C(Jkg^{-1}{}^{o}C^{-1})$
Steel	50	480
Tungsten carbide	17.1	125
Glass	1.1	670
Sapphire	38.5	717

This finding is further evidence for the traction plateau being a limiting shear stress of the e.h.d. film, rather than a thermal, effect and it also demonstrates that the limiting shear stress is not strongly temperature dependent.

Further evidence of limiting shear stress behaviour of fluids at high pressures has been provided by Paul and Cameron(13) from experiments performed in a modified high pressure impact microviscometer. The limiting shear stress versus pressure data for 5P4E has been integrated over a contact, assuming a Hertzian deformation and pressure profile.

The results of these calculations are plotted in figure 7.19 and are found to be lower than those derived from the traction experiments.

This was thought to be due partly to the difference in the definition of limiting shear stress behaviour in the two types of equipment. There are advantages and disadvantages in analysing the plateau region in terms of limiting shear stress effects or deciding on some other point (Hirst and Moore(12)) where the traction curve departs "significantly" from a straight line. There is also the possibility that the limiting shear stress in the experiments of Paul and Cameron had not quite been reached and that further experiments be performed at higher rotational speeds to decide this.

8.5 CONCLUSIONS OF "TRACTION MAXIMUM" ANALYSIS

It would seem that the limiting shear stress of a fluid is a unique property of that fluid. It is predominantly a function of pressure and to a far lesser extent of temperature. It is only under the extreme pressures encountered in elastohydrodynamic traction that the flow and deformation properties of fluids lead to such high shear stresses as to permit the manifestation of this behaviour. It has been known for many years that polymers such as polymethylmethacrylate (P.M.M.A.) exhibit similar pressure dependent yield stress behaviour (Rabinowitz et al.(14)).

For P.M.M.A.

$$\tau_{max} = 50\left(\text{Lim shear stress at st.p.}\right) + KP \text{ MPa}$$

where $K \simeq 0.25$ and may vary from 0.1 to 0.3 for other polymeric materials.

From the experimental results of figs.

for Santotrac 50 $\quad \bar{\tau}_{max} = 0.066 \text{ Pmax}$

$= 0.1 \text{ P}$

and 5P4E $\bar{\tau}_{max} = 0.06\ P_{max}$

$= 0.09\ P$

where P is average Hertz pressure.

It would seem that this similarity is no coincidence and that fluids in elastohydrodynamic traction are exhibiting yield stress behaviour.

This model fits the experimental data remarkably well if the approximations that are inherent in the analysis are considered. The strong agreement with the more refined experiments of Paul(13) lends further credence to this hypothesis.

8.6 ANALYSIS OF THE INITIAL SLOPES OF THE TRACTION CURVE

This part of the work was divided into two parts as described in Chapter 5, i.e.

8.61 Sideslip traction tests with zero spin.

8.62 Sideslip traction tests in forward and reverse with different amounts of spin in the contact to measure those forces arising from spin alone.

8.61 Sideslip traction test results and analysis

These results were analysed assuming that the fluid was behaving (i) viscously with a mean effective viscosity $\bar{\eta}$, and (ii) elastically with a mean effective shear modulus $\bar{G}$.

(i) Viscous analysis

For this equation (25), Chapter 6

$$\bar{\eta} = \frac{G_s h}{2U} \tan\left(\frac{\pi}{2}\,\frac{m_\beta}{m_{\beta'}}\right)$$

was used to obtain mean effective viscosities.

(ii) Elastic analysis

Equation

$$\bar{G} = \frac{\pi h P_{max}}{4a}\left(\frac{m_\beta m_\beta'}{m_\beta' - m_\beta}\right)$$

was used to determine mean effective shear modulus of the film.

For both of the above analyses values of $\bar{\eta}$ and $\bar{G}$ were found for a range of rolling speeds at peak Hertz pressures (1 to 2 GPa) where elastic behaviour of the film might have been more likely.

In all cases the values of $\bar{G}$ were far less dependent upon rolling speed than the values of $\bar{\eta}$. The values of $\bar{\eta}$ and $\bar{G}$ were quite high for very low rolling speeds because at low rolling speeds m_β was of the same order as m_β' leading to overcorrected values of $\bar{\eta}$ and $\bar{G}$ but as the rolling speed was increased $\bar{\eta}$ fell quite steeply, but $\bar{G}$ tended to flatten off.

Other tests were performed when the transit time through the contact of the fluid was varied by changing from a 1" ball to a 0.65" ball and maintaining the same maximum Hertz pressure. Some of the results are plotted in fig. 7.22. They show that either the fluid was behaving in a linear time dependent viscous manner or that the fluid was exhibiting elastic solid behaviour, independent of the transit time.

It was decided that no further information as to which rheological model to choose could be gleaned from these tests and that spin tests be performed for a range of conditions on the three fluids:

1. 5P4E polyphenyl ether
2. B.P. Bright Stock
3. XRM 109F, a synthetic paraffin

8.62 Distinction of elastic from viscous behaviour

As discussed in Sections 6.61 and 6.62, the gradients of the spin and sideslip traction curves m_α, m_β together with the dry traction gradient, m_β', were expected to relate in the manner

$$\frac{m_\alpha}{m_\beta} = 0.404 \frac{m_\beta}{m_\beta'} \text{ for viscous behaviour}$$

and

$$\frac{m_\alpha}{m_\beta} = \frac{1}{1 - 0.28 \frac{m_\beta}{m_\beta'}} \text{ for elastic behaviour}$$

The results for 1, 2 and 3 above were plotted in fig. 7.23 in a manner designed to highlight these differences.

It may be seen from fig. 7.23 that 5P4E appears to behave elastically for all the experimental conditions imposed. XRM 109F, however, only starts to show significant elastic behaviour at pressures in excess of 1.4 GPa and the B.P. Bright Stock shows elastic behaviour at pressures in excess of 0.82 GPa.

8.7 MEAN EFFECTIVE ELASTIC MODULUS VARIATION WITH MAXIMUM HERTZ PRESSURE

Different ball materials and normal loads N were used to vary the maximum Hertz contact pressure over a wide range and the results of these tests are presented in figs. 7.24, 7.25 and 7.28. 5P4E (see fig. 7.24) shows a roughly linear relationship between elastic modulus $\bar{G}$ and

peak Hertz pressure Pmax. Fig. 7.25 for XRM 109F shows very low values of derived mean effective shear modulus up to 1.4 GPa, beyond which point it appears to increase considerably with pressure. The results for Bright Stock are shown in fig. 7.28, and although there is considerable scatter, a roughly linear relationship can be seen. One of the problems in the analysis of all the elastic moduli results was that the values $\bar{G}$ did fall with increased rolling speed (see fig. 7.29) in a similar manner to the way in which the maximum traction coefficient $\frac{T_{max}}{N}$ and $\frac{T_{\frac{1}{2}}}{N}$ also fell with increased rolling speed.

8.8 THE CORRELATION BETWEEN LIMITING SHEAR STRESS AND ELASTIC SHEAR MODULUS

It was thought that, assuming both elastic modulus $\bar{G}$ and limiting stress $\bar{\tau}_{max}$ or $\bar{\tau}_{\frac{1}{2}}$ were linear functions of pressure, then if this variation were simply a result of modification to the pressure distribution inside the e.h.d. contact, then there should be a better correlation between them than between $\bar{G}$ and pressure for different loads and rolling speeds.

This was indeed the case as is best illustrated by fig. 7.30 for the Bright Stock for a wide range of conditions.

A good correlation is also found for 5P4E (see fig. 7.27). In both of these cases, the gradients of the plots were about 0.15

i.e. $\bar{\tau}_{\frac{1}{2}} = 0.15\ \bar{G}$ (Bright Stock)

$\bar{\tau}_{max} = 0.11\ \bar{G}$ 5P4E

The graph of $\bar{\tau}_{\frac{1}{2}}/\bar{G}$ for XRM 109F (see fig. 7.26) starts off very steeply because at low pressures the values of $\bar{\tau}_{\frac{1}{2}}$ were thought to be mostly a result of viscous shearing rather than the limiting shear stress of an

elastic solid. At higher pressures the curve tends to a straight line of approximate gradient 0.1

$$\text{i.e. } \bar{\tau}_{\frac{1}{2}} = 0.1\ \bar{G}$$

which is similar to those obtained for 5P4E and the Bright Stock.

This type of relationship between limiting shear stress and elastic shear modulus is reminiscent of the Frenkel(15) critical shear strength model for a perfect crystal. By considering the shear displacement of two planes of atoms past each other, Frenkel was able to show that the lattice became unstable when

$$\tau = \frac{G}{2\pi} = 0.16\ G$$

Very poor agreement has been found for this relation with existing plastics, and steels and polycrystals of aluminium, because of lattice imperfections and dislocations.

It is suggested that the close agreement between this relation and the practical observations of limiting shear stress and elastic shear modulus is no coincidence. Because of the way in which EHD films are formed, a shearing and possibly ordering process and the continuous replacement of the molecular structure in the EHD contact and because of the small dimensions of the contact, imperfections, normally leading to the breakdown of the Frenkel shear strength model, are far less likely to occur in an EHD film.

8.9 ALTERNATIVE EXPLANATIONS OF THE RESULTS

In this section, pressure, temperature, film thickness and visco-elastic fime effects will be considered in the light of this and other experimental work.

8.91 Temperature effects

Isothermal Newtonian film thickness theories give good agreement with experiment and so apart from adiabatic heating, the heating resulting from shearing was so low that temperature effects could be excluded.

Adiabatic heating would lead to a lower viscosity in the inlet half of the contact than the outlet, and so lead to a spin force in the opposite direction to that measured, (see fig. 1.8).

8.92 Pressure effects

This would seem the most promising alternative explanation of the spin traction force. Increased rolling speed certainly does lead to a movement of the centre of pressure towards the inlet region with the consequent higher mean viscosity in the inlet region, leading to a traction force in the direction measured (see fig. 1.8).

It is doubtful whether this model could predict the consistent value of 0.3 for the ratio $\frac{m_\alpha}{m_\beta}$ and since there is such poor correlation between pressure viscosity coefficients and traction parameters, it is thought unlikely that pressure effects play a significant role in this part of the experiments.

8.93 Film thickness anomalies

It is well known from experimental interferometric and theoretical analyses that the film thickness towards the outlet region of an e.h.d. contact is about 20% less than in the inlet region. This would result in a traction spin force for Newtonian behaviour in the opposite direction to that predicted for elastic solid film behaviour. In none of the

experiments was a spin force observed in such a direction, and so this film thickness effect was ignored (see fig. 1.8).

8.94 Viscoelasticity and time effects

While the physics of crystalline solids and dilute gases is quite well understood, a physical picture of the grey area between these two extremes is far from understood. The consequence is that most models rely on poorly defined parameters. After early attempts to treat liquids by Van der Waal's theory of condensed gases had failed, most modern theories have been based upon a model of a quasi-crystalline structure of liquids. X-ray investigations (Prins(16,17), Debye(18)) have shown the structure of liquids in microscopic regions is similar to that of a crystal. They found that there is a tendency for particles in the immediate vicinity of a central particle to occupy sites which correspond to those of a crystal lattice. This tendency, however, decreases rapidly with distance from each microcrystal. One would therefore expect any liquid to possess some elastic properties associated with the deformation of these microcrystalline structures within the liquid. Barlow et al.(19) have been able to measure high frequency elastic shear moduli and relaxation times of liquids that confirm their viscoelastic behaviour.

As discussed in Chapter 1, there are two distinct viscoelastic models for fluid behaviour that have been proposed as alternative explanations of the anomalous shear behaviour of fluids in elasto-hydrodynamic traction. These are the viscoelastic shear and the compressional viscoelastic models. In this section it will be shown that these two models are by no means mutually exclusive on the basis of traction and viscometry results.

Viscoelastic shear model

The simplest form of this model is that of a fluid that is characterised by a "short time scale" elastic shear modulus G_∞ and a long time scale viscosity η_o. The Maxwell relaxation time for such a fluid is given by

$$\text{relaxation time } t' = \frac{\eta_o}{G_\infty}$$

(see Section 1.42).

It is this time that determines whether, for a given time scale of shear experiment, viscous or elastic behaviour will be observed.

If $t' \gg t$ elastic behaviour will be observed,

but if $t' \ll t$ viscous behaviour will be seen,

where t is the time scale of the experiment, i.e. the contact transit time as in the e.h.d. case.

8.95 Compressional viscoelasticity

This approach is concerned with the variation of viscosity with time after a pressure step. There are two relationships for this variation, one of which is based on experimental work of Paul(20) and the other suggested by Fein, which is based on free volume.

(a) Nearly linear viscosity/time

Paul(20) found that

$$\eta \simeq 10^6 \, t^{1.30} \text{ Pa secs}$$

for $t > 2 \times 10^{-2}$ secs and a pressure of 1 GPa at 20°C with B.P. Bright Stock.

(b) The viscosity increases almost instantaneously to a value corresponding to the reduction in free volume and then increases relatively slowly as the rates of molecular diffusion processes necessary to accomplish structural re-arrangements become increasingly slower.

In all of the traction tests at pressures in excess of 1 GPa BP Bright Stock showed elastic behaviour with mean elastic shear moduli of the order of 5×10^{8} Pa for contact transit times of 10^{-4} to 10^{-3} seconds. If Paul's relationship for viscosity/time behaviour is approximated to $\eta = 10^{6}t$ Pa secs., then $\frac{\eta}{G} = t \times 2 \times 10^{-3}$ secs.
where t is the transit time through the contact. In this case the relaxation time of the fluid would always be far less than the transit time. Thus viscous behaviour would be expected for any transit time. The traction forces arising from spin were in the opposite direction to that predicted by linear time dependent viscous behaviour (see fig. 1.8). It is clear that Paul's relationship cannot be used for times less than 2×10^{-2} secs. Paul(20) suggested that the extrapolation of his results to shorter times was extremely speculative. Temperature effects might well have reduced the viscosities measured after 2×10^{-2} seconds.

Assume, however, that the viscosity of BP Bright Stock rises in a very short time (nanoseconds) to 10^{5} Pa secs. Next it increases in a roughly linear manner with time. Then for times of 6×10^{-2} secs and greater, good agreement would be found with Paul's results(20). The shear relaxation time for BP Bright Stock as /GPa is then

$$\frac{\eta}{G} = \frac{10^{5} + 10^{6}t}{10^{8}} \approx 10^{-3} \text{ secs}$$

This would mean that for contact transit times smaller than 10^{-3} secs one would expect to observe elastic behaviour for BP Bright Stock at 1 GPa and 20°C.

8.96 Conclusions

(1) Elastic behaviour of fluids under the special conditions of e.h.d. traction has been observed and the derived elastic shear moduli are found to rise in a roughly linear manner with pressure.

(2) Fluids exhibit limiting shear stress behaviour in e.h.d. traction that is a linear function of pressure. This is not unlike the behaviour of high polymers such as polymethylmethacrylate in magnitude and quality.

(3) The limiting shear stress correlates well with the derived mean elastic shear modulus. It corresponds closely to the manner predicted by the Frenkel shear strength model which was derived for simple crystals. It may be equally applicable to molecular bundles riding over one another, rather than single atoms beyond shear strains of

$$\frac{1}{2\pi} = 0.16$$

(4) These fluid films are viscoelastic. However, under the conditions of these experiments (where elastic behaviour has been observed) the viscous component has always been sufficiently high for elastic behaviour to predominate. It has been inferred that the viscosity of these fluids rises almost instantaneously to a certain value and then continues to rise far more slowly with time. It is this initial viscosity rise that determines whether or not elastic behaviour is observed.

(5) The rolling speed effects on traction coefficient for low loads and high viscosity fluids must be considered in the choice of an ideal tractant. This should have sufficient atmospheric viscosity and a high pressure/viscosity coefficient to provide a thick enough e.h.d. film to prevent wear, large compared with surface roughness. It must also have a high limiting shear stress.

8.97 Further work

There is a need for further traction work to be performed with simple fluids that are chemically well defined so that elastic and limiting shear stress effects may be more closely related to chemical structure. Unfortunately, most simple fluids have very low viscosities and so a very high speed traction rig would be required to obtain thick enough e.h.d. films.

From a more practical point of view, it would be of use to obtain a general relationship between mean contact pressure and viscosity, rolling speed, geometry and pressure viscosity coefficient, etc. so that hydrodynamic effects could be minimised in traction drives.

More definite information on the variation of viscosity with time after a pressure step would clearly be of interest.

8.10 REFERENCES

1. FOORD, C.A., Ph.D. Thesis, London University 1968

2. WESTLAKE, F.J., Ph.D. Thesis, London University 1970

3. GENTLE, C.R., Ph.D. Thesis, London University 1972

4. JACKSON, A., Private communication

5. WOLVERIDGE, P.E. and ARCHARD, J.F., "Temperature distributions in elastohydrodynamic films: A new approach", C9/72, Elastohydrodynamic Lubrication 1972, Leeds Symposium, Inst. Mech. Engrs.

6. KLEMZ, B.L., GOHAR, R. and CAMERON, A., "Photoelastic studies of lubricated line contacts", Tribology Group 9th Annual Convention, Douglas, Isle of Man, May 1971, (Inst. Mech. Engrs. Lond.)

7. HAMILTON, G.M. and MOORE, S.L., 1971, Proc. Roy. Soc., London (A), 322, 313

8. KANNEL, J.W., Bell, J.C. and ALLEN, C.M., "Methods for determining pressure distributions in a lubricated rolling contact", Trans. ASLE, 1965, V. 8, p. 250

9. RANGER, A.P. Ph.D. Thesis, London University, 1974

10. WYMER, D.G., Ph.D. Thesis, London University, 1972

11. KAPITZA, P.L., "Hydrodynamic theory of lubrication during rolling", Zhurn. Tekh. Fiz., 1955, V. 25, p. 747

12. HIRST, W. and MOORE, A.J., "Non-Newtonian behaviour in EHL", Proc. Roy. Soc., London (A), 337, 101-121, 1974

13. PAUL, G.R. and CAMERON, A., "The ultimate shear stress of fluids at high temperatures measured by a modified impact micro viscometers", to be published

14. RABINOWITZ, S., WARD, I.M. and PARRY, J.C.S., J. Mat. Sci., 5, 29,(1971)

15. FRENKEL, J., (1926), Z. Phys., 37, 572

16. PRINS, J.A., Physica 1, 1171, (1934)

17. PRINS, J.A., Physica 2, 1016 (1935)

18. DEBYE, P. and MENKE, H., Physic Z, 31, 797, (1930)

19. BARLOW, A.J., ERGINSLAV, A. and LAMB, J., "Viscoelastic relaxation of supercooled liquids", Proc. Roy. Soc., London (A), 289, 481 (1967)

20. PAUL, G.R., "Time dependent viscosity following a pressure rise measured on an impact viscometer", ASLE/ASME Lubrication Conference, Montreal 1974, Paper 74LC-5B-1

21. FEIN, R.S., "Possible role of compressional viscoelasticity in concentrated contact lubrication", Trans. ASME, Series F., J. Lub. Tech. 127-131 (1967)

A P P E N D I X

ELASTOHYDRODYNAMIC FILM THICKNESSES AT EXTREME PRESSURES

There has recently been disagreement on the effect of load on elastohydrodynamic film thicknesses at pressures beyond 7×10^8 NM^{-2}, which was the approximate limit of earlier experiments. This disagreement which concerns a departure from established theory has been heightened by the fact that it is based on results from rather novel techniques. Work carried out by the author, Gentle, C.R. and Cameron, A. has been presented in a paper to "The American Society of Mechanical Engineers".

This paper describes an extension of well characterised optical interferometric measurements on rolling point contacts to pressures of over 2×10^9 NM^{-2}. The central film thickness is found to fall off with load at a rate which agrees well with theory. In view of this, the results from other techniques are considered and in one case reproduced.

It is concluded that the theory is essentially correct as far as it goes and possible causes of the disagreements are advanced in terms of thermal and surface roughness effects.

A photocopy of this paper is presented with this appendix.

Printed in U.S.A.

Paper No.
74-Lub-27

an ASME publication

$3.00 PER COPY $1.00 TO ASME MEMBERS

C. R. Gentle
Royal Military College of Science, Shrivenham, Swindon, Wilts, England

R. R. Duckworth
A. Cameron
Imperial College, London, England

Elastohydrodynamic Film Thicknesses at Extreme Pressures

There has recently been disagreement on the effect of load on elastohydrodynamic film thicknesses at pressures beyond 7×10^8 Nm^{-2}, which was the approximate limit of earlier experiments. This disagreement which concerns a departure from established theory has been heightened by the fact that it is based on results from rather novel techniques. This paper describes an extension of well-characterized optical interferometric measurements on rolling-point contacts to pressures of over 2×10^9 Nm^{-2}. The central film thickness is found to fall off with load at a rate which agrees well with theory. In view of this, the results from other techniques are considered and in one case reproduced. It is concluded that the theory is essentially correct as far as it goes and possible causes of the disagreements are advanced in terms of thermal and surface roughness effects.

Introduction

In rolling element bearings one of the most important parameters is the thickness of the elastohydradynamic lubricant film generated between the bearing surfaces, since this governs the operation and life of the bearing. Consequently, a great deal of work has been carried out on measurement of ehd film thicknesses with a view to testing various theories of film formation, and more lately as a method of comparing lubricants. The problems involved in studying bearings directly have mostly been avoided by simulating the real situation with disk machines, crossed cylinders or ball and plate rigs. Three main techniques have evolved over the years: capacitance measurements [1, 2],[1] optical interferometry [3, 4, 5] and X-ray transmission [6, 7]. The first two of these have generally been limited to a maximum Hertz contact pressure of about 7×10^8 Nm^{-2} and over this range all three methods have been in broad agreement with each other (2) and with ehd theories [8, 9, 10]. However, pressures in real bearings are well above this range typically and so there has recently been an attempt to extend the techniques to pressures of over 2×10^9 Nm^{-2}. Unfortunately a marked discrepancy between various techniques and theories now becomes apparent. On the one hand optical interferometry of pure rolling point contacts by Gohar [11] showed no anomalous behaviour of central film thickness up to over 3.5×10^9 Nm^{-2} peak Hertz pressure. A double logarithmic plot of h against W produced accurate straight lines which fell slightly, with slope -0.11. Measurements were also made of the minimum film thickness in the contact, which proved to be more scattered but indicated rather greater sensitivity to load.

On the other hand recent interferometric measurements in pure sliding [12] have indicated greatly increased influence of load on central film thickness at high pressures. Simultaneous measurement of the minimum film thickness showed even greater dependence on load. This supported X-ray evidence [7, 13] that h_m was smaller than h_c by up to an order of magnitude as opposed to the earlier view supported by Gohar [11] that the ratio was more like 50 to 75 percent. Unfortunately the work of Gohar was only on a straight mineral oil whereas the other work referred to rather more exotic lubricants, so a direct comparison was not possible.

The work described here was initiated with the main aim of resolving the disagreement about central film thickness by reproducing the technique of Gohar on fluids of the type used in references [7, 12, 13]. As will be seen the disagreement is not a result of the lubricant properties and so the report goes on to describe further work which was carried out on the problem. It is concluded that the film thickness measured in pure rolling optical interferometry relates well to the film thickness considered in smooth-surface e.h.l theories. Reasons are given why the techniques of [7, 12, 13] might be expected not to give good agreement with theory either for central or minimum film thickness.

Experimental Techniques

The apparatus used was a sophistication of earlier devices such as those of Foord, et al. [5] and Gohar [11]. The principal difference was that the transparent lubricated element in this case was an artifieial sapphire disk. When loaded against a 1-in-dia tungsten carbide ball, pressures of up to 20×10^8 Nm^{-2} could be generated in the point contact for a normal load of only 135 N. The

[1] Numbers in brackets designate References at end of paper.

Contributed by the Lubrication Division of THE AMERICAN SOCIETY OF MECHANICAL ENGINEERS for presentation at the ASME-ASLE Joint Lubrication Conference, Montreal, Canada, October 8-10, 1974. Manuscript received at ASME Headquarters July 8, 1974. Paper No. 74-Lub-27.

Copies will be available until June, 1975.

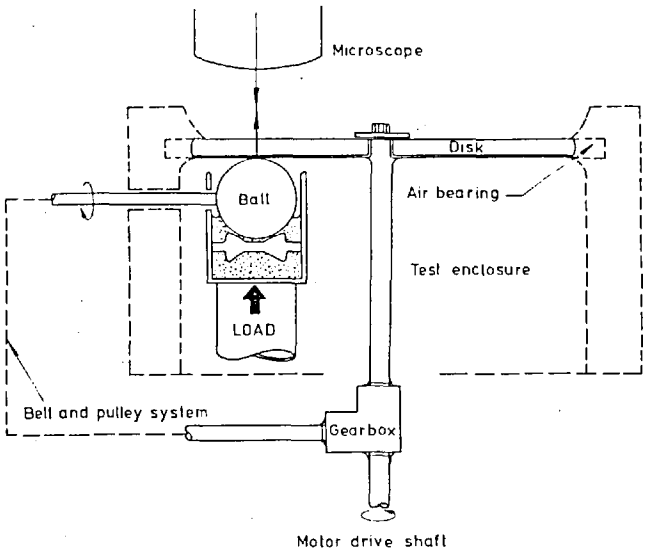

Fig. 1 Film thickness apparatus

experimental rig is shown schematically in Fig. 1. The sapphire disk is supported in an air bearing and is rotated by a variable speed electric motor. The tungsten carbide ball, which sits on rollers in a small lubricant reservoir, is also driven by the same motor, via a gearbox and pulleys with toothed belts. The rotational speed is measured digitally with a magnetic transducer and toothed wheel, and the accuracy of speed control and measurement is generally better than one percent. The ball and its drive shaft could be moved in or out along a radius of the disk, thus altering the surface velocity of the disk through the point contact. A position was chosen to give equal surface speeds to the ball and the disk at their contact ie pure rolling. The idea of this arrangement is that by moving the ball through this position along a radius the amount of sliding between ball and disk is varied. By using this in conjunction with measurement of the resulting force on the ball, it would be possible to obtain a continuous traction curve for the test fluid. However, this was not the concern of this set of experiments and apart from pure rolling, the only other situation used was that of total sliding which was achieved by decoupling the disk and holding it stationary against the rotating ball.

The film thickness of lubricant between the rotating elements was measured using chromatic or white-light interferometry. For this reason the underside of the optically polished disk was coated with a 200 Å partially reflecting layer of chromium. For pure rolling a vacuum-deposited layer is adequate but the imposition of sliding necessitates a sputtered coating to give sufficient adhesion with the crystalline sapphire surface. The contact was observed from above using a long working distance stereoscopic microscope adapted so that one branch could be used for illumination. Chromatic interferometry was chosen in preference to monochromatic since generally four times as many data points can be taken in each interferometric order, one for each distinguishable color. Although the thickness range is smaller for chromatic interferometry it was felt that this increased accuracy was more important for a study of possible departures from theoretical behavior, and outweighed the disadvantages.

The main disadvantage was that the minimum film thickness could not easily be measured in the narrow constriction at the contact exit or in the side lobes since the resolution was not as good as monochromatic interferometry. This limits the data mainly to central film thickness.

The data to be recorded was the series of motor speeds required to give films of specific interferometric color and hence known thickness and this was taken using the following experimental technique. Firstly, the motor was turned slowly so that the ball revolved in the lubricant reservoir of about 5-ml capacity and became coated before being loaded gradually against the disk by means of a hydrostatic air piston. This procedure minimized the danger of scratching the disk surface. The speed was then increased and the apparatus was run for a minute or so to ensure even spreading of the lubricant on a track around the disk. When the contact was seen through the microscope to have attained a steady film thickness, the temperature of the lubricant was measured by a trailing thermocouple and the experiment itself was commenced. The speed was reduced and then slowly built up and recorded at each of the successive chosen thicknesses. As a check, the speed was also recorded again as it was decreased. Throughout the run the temperature was monitored for signs of frictional heating. The possibility of lubricant starvation was ruled out by observing the inlet boundary and making sure it did not come too close to the contact to allow adequate pressure buildup, as governed by Wedeven's criterion [14].

Results

(a) Pure Rolling. The fluids used in the tests were:

1 a synthetic paraffin as used in [12, 13]
2 naphthenic mineral oil base stock
3 fluid 2 plus 10 percent *W* paraffinic heavy resin.

The central film thickness/speed results are displayed in Fig. 2, being taken for at least eight set film thicknesses. Owing to uncertainties in the correct value of refractive index to apply to the fluids at the elevated temperature and pressure inside the contact, the film thicknesses have been left as optical central film thickness. The relationship is:

optical thickness = actual thickness × refractive index

and in each case the refractive index is about 1.5 at ambient conditions. Refractive index is related to density of the fluids and therefore increases with pressure and decreases with temperature. Normally, this change can be neglected but in this case the maximum pressure could raise the index by 20 percent, while the contact temperature, particularly in sliding, could lower it by as much. In general, the two effects act to cancel each other out and the overall variation is probably less than 10 percent for central film thickness. For minimum film thickness, where pressures are lower and temperatures higher it is more difficult to estimate. The results cover a range of optical thickness from about $2\text{-}8 \times 10^{-7}$ m, corresponding to a range of actual thickness of approximately $1.3\text{-}5.3 \times 10^{-7}$ m.

The data plots are straight lines on double-logarithmic axes, which are displaced to the right as the load is increased. This represents a fall in film thickness at constant speed for an increase in contact pressure, and may be studied in the following manner. At a chosen rolling speed approximately in the center of the graph, say 0.1 ms^{-1}, a line is drawn parallel to the ordinate. The points at which this line intersects the experimental lines are read off and may be plotted as in Fig. 3 against the maximum Hertzian stress in the contact. Once again double-logarithmic axes are chosen since theory indicates that

Nomenclature

h_{cla} = film thickness between rough surface centerline averages
h_m = minimum film thickness
P_{max} = maximum Hertz contact pressure
W = point contact load
h_c = central film thickness
$U = \frac{1}{2}(u_1 + u_2)$ = rolling speed or average surface speed
a = film thickness/load coefficient

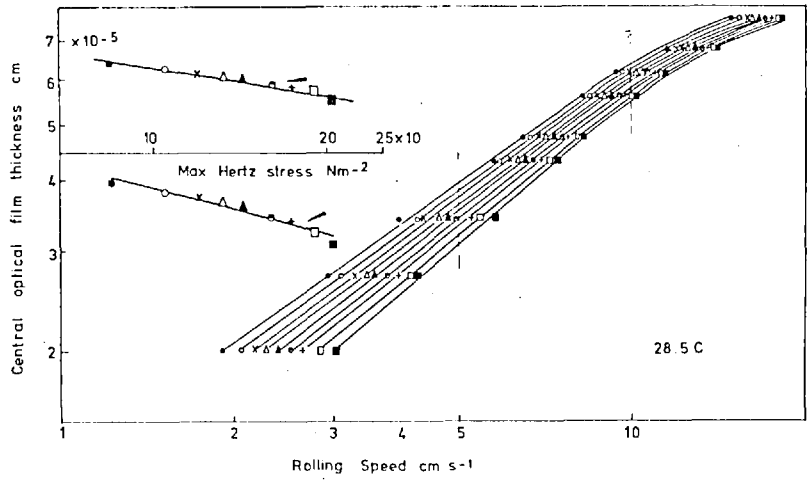

Fig. 2 Central optical film thickness/film speed results

$$h \alpha W^{-a}$$

or

$$h \alpha P_{max}^{-3a} \text{ since } P_{max} \alpha W^{1/3}$$

If this relationship is true, then a straight line should be obtained. As will be seen the points obtained by the aforementioned technique fall remarkably well on straight lines. Certainly there is a small divergence at the lowest and at the highest pressures. Now the random errors associated with the measuring technique are much smaller than would be caused by actually maintaining a fixed rolling speed and trying to detect a change in film thickness interferometrically as the load is changed. But there are two sources of error which could easily account for this small divergence. First, the pressure in a point contact depends on the cube root of the load and so a constant inaccuracy in measuring and applying the load would mean inaccuracy in the low pressure is 27 times greater than that at high pressure for the three-fold pressure range used here. The calculated lowest pressure might be in error by up to 10 percent. The second source of error is the unavoidable heating of the fluid in the inlet which is difficult to detect using a trailing thermocouple but which could easily lower the film thickness, particularly at high loads. However, even without taking these sources of error into account it cannot by any stretch of the imagination be said that the results show any anomalous trends. It is difficult to compare the absolute magnitudes of film thickness with theoretical estimates since data such as pressure-viscosity coefficient is not accurately available. A partial comparison can be made simply on the basis of the slope a. The experimental slopes are given along with those predicted by Dowson and Higginson [8] and Archard [9] and are not greatly different although they do vary from fluid to fluid and with the rolling speed.

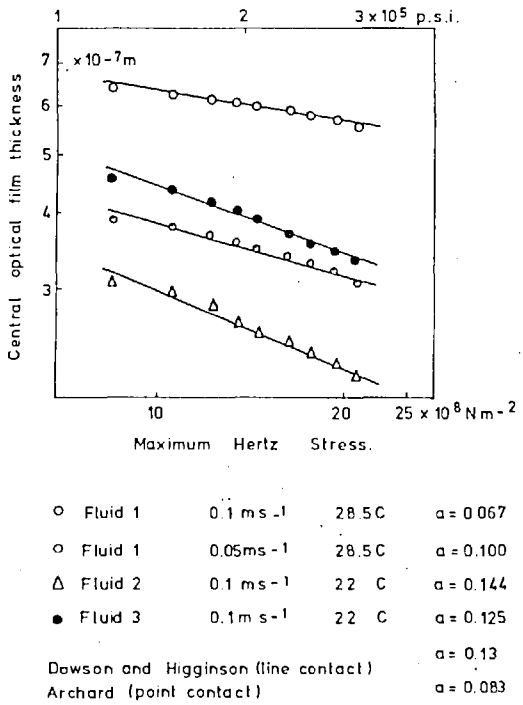

Fig. 3 Film thickness/maximum Hertzian contact pressure results in pure rolling

Some comments can be made about the minimum film thickness in spite of the fact that detailed results were not taken. As the rolling speed was increased from zero, the first color seen in the central area was yellow, indicating an optical thickness of 2×10^{-7} m. As the speed was increased further, this yellow moved to the sides and exit region of the contact and was replaced by red at the center, corresponding to 2.7×10^{-7} m. In this situation h_m was 75 percent of h_r. This occurred at all pressures. For the maximum central film thickness observed, 7.6×10^{-7} m, the side lobe color was a first order blue/green indicating optical thickness of 4×10^{-7} m, a little more than 50 percent of h_r. This also occurred at all pressures. Hence, although the actual variation of minimum film with load was not recorded, it appears that h_m was between 50 and 75 percent of h_r throughout.

From this work it can be concluded that the results of Gohar, that ehd theory is adequate in pure rolling even at high loads, are probably correct in general and not just for the fluids he chose. But this is hardly a satisfying point at which to leave the matter since the discrepancy between these results and other methods has still not been resolved.

(b) Pure Sliding. The obvious next stage was to try and generate the anomalous results by reproducing one of the other methods. As mentioned earlier it was a simple matter to operate the experimental rig in total sliding by decoupling the disk from the drive shaft and holding it stationary, so it was possible to repeat the experiments of [12] using a synthetic paraffinic fluid (XRM-109F). The results are shown in Fig. 4 and compared with the original data. Clearly the experiment has proved to be reproducible and indicates that any disagreement about the data from optical interferometry must have been caused by one technique using pure rolling and the other using pure sliding, since this was the only difference.

There are at least two phenomena associated with sliding in elastohydrodynamic contacts which would account for this reduced film thickness at high loads. Both of them reduce the effective viscosity of the lubricant as it enters the contact; firstly, there is shear thinning and secondly, there is frictional heating.

As pointed out in [12] the fact that all fluids seem to exhibit this lowered film thickness makes it unlikely that shear thinning is the answer, since it is known that the fluids have widely varying responses to shear stress of the magnitude found here.

Lee, Sanborn, and Winer in [12] also rule out the effect of frictional heating. Their argument is that they could achieve the same load dependence data by starting with the highest loads as they could be starting with the lowest loads. The last readings in each set might be expected to be affected most by the contact area and lubricant warming up, so frictional heating would make the order of the results irreversible. This reversibility was also observed in the experiments described here. However, an alternative explanation is possible; that the frictional heating causes a very rapid increase in the temperature of the small amount of lubricant which actually passes into the contact. To get some idea of the quantities involved, for a pressure of 2×10^9 Nm $^{-2}$ and sliding speed of 0.1 ms $^{-1}$, the power dissipation in the Hertz contact is approximately 0.25 W. The volume of lubricant passing through this region per second is only 5×10^{-6} ml. So potentially there is enough heat available inside the contact to produce a temperature rise in the contact of the order of hundreds of deg C. Winer, et al. are at present studying this situation under an infrared technique [15] and do seem to find a temperature rise of this magnitude. However this temperature rise of the lubricant inside the contact is not important to the formation of the film since this is governed by the inlet region. It will only have an effect if the stationary sapphire disk becomes hot outside the contact area and warms the lubricant in the inlet. Greenwood and Kauzlarich [16] have indicated that only a small rise in inlet temperature can have large effects on the film thickness, even though the temperature might be impossible to measure with thermocouples since the rise occurs so close to the contact. To check what order of temperature rise in the inlet would produce the fall-off of film thickness at high load sliding it is therefore necessary to use a circuitous method. It was decided to run a series of tests in pure rolling at elevated temperatures to see what temperature rise of the lubricant would produce a reduced film thickness equal to that in the sliding experiments. These experiments were carried out for the high loads only. Owing to the three-fold range of pressure, there is an increase in load of about 27 from the lowest to the highest. Since the frictional heating is more or less proportional to the load it follows that the heating only becomes a problem for the highest loads. This would agree well with the observed dependence of film thickness reduction with load. The results are given in Fig 5. The maximum temperature rise needed to explain the central film thickness results is about 8 C, which does not seem unreasonable at a distance of only about 10^{-4} m from the contact where temperature rises may be in hundreds of degrees Centigrade almost immediately after sliding commences.

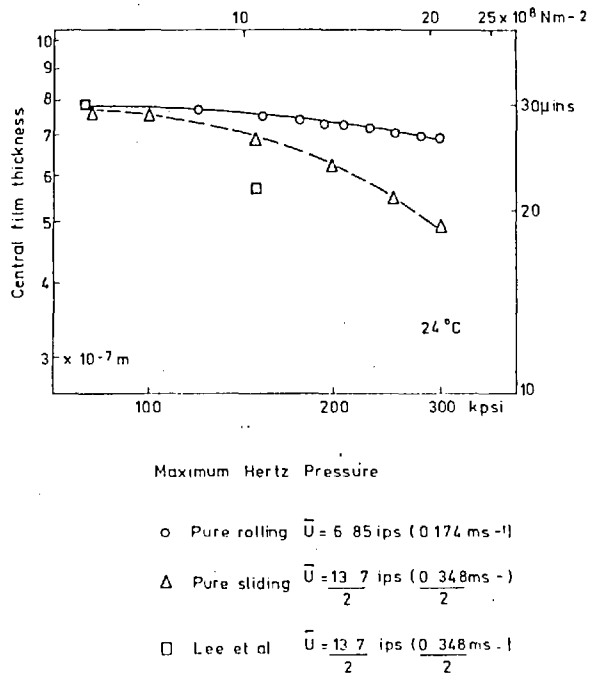

Fig. 4 Film thickness/maximum Hertzian pressure results in pure sliding

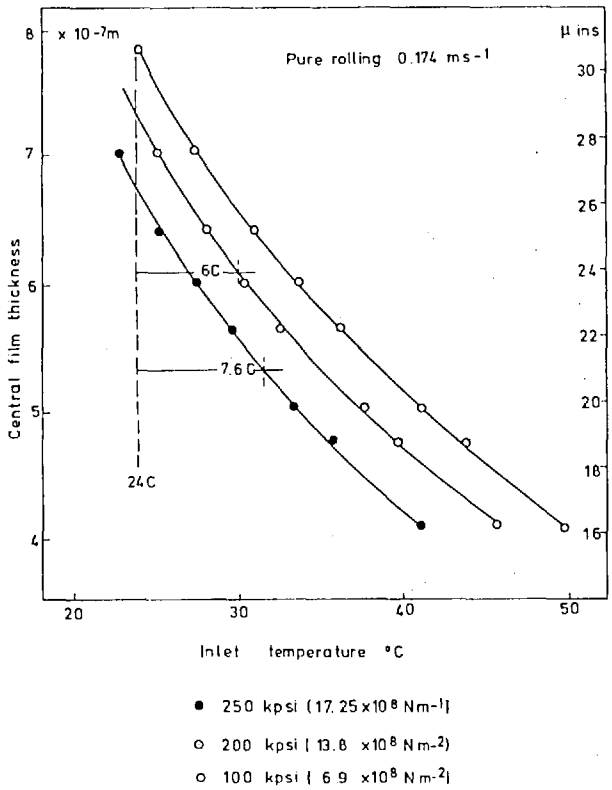

Fig. 5 The effect of inlet temperature rise on film thickness results

Discussion of X-ray Measurements

Having found a fairly satisfactory explanation of the difference in film thickness measurements between optical studies of pure rolling and pure sliding, it is disappointing to find that it cannot apply to the X-ray results of [7, 13]. These studies have been carried out in pure rolling and so frictional heating could not account for the increased load dependence. To find a true explanation one must look for some other difference between the optical technique and the X-ray technique. The most obvious one is that the two sets of optical results here have generally been taken at much lower rolling speeds than the X-ray data. It is possible that inlet shear heating [16] could be responsible at these high speeds, but the speeds have been covered at lower pressures in optical experiments without any fall-off in film thickness of the order of magnitude found here. It is felt that the significant diffrence lies in the fact that the X-ray examination takes place along the contact whereas the optical study is performed normal to the contact. This means that the X-ray method always observes the minimum film thickness, as opposed to the optical results which produce a contour map. So far this minimum value has simply been taken to be the minimum value of the elastohydrodynamic film in the

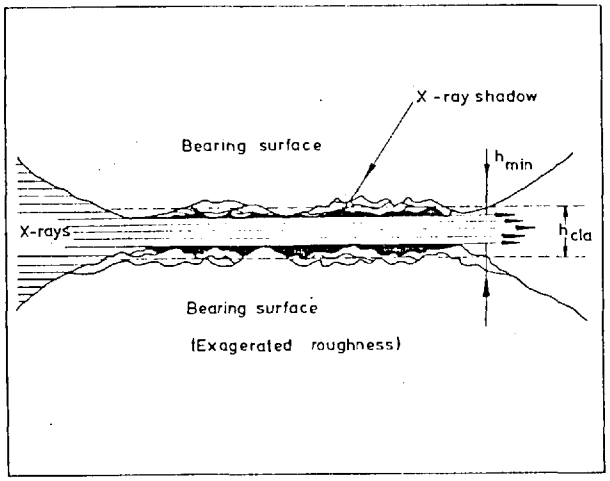

Fig. 6 Surface roughness effect (section through constriction)

constriction near the contact exit, and has been compared against theoretical predictions based on smooth surfaces. However, this does not take into account the fact that both rolling surfaces are quite rough compared with the film thicknesses generally encountered here. The surface finish in these optical measurements is generally better than 125 Å rms while in the X-ray case [13] it is from 250 Å to 500 Å rms. Now since the optical measurements are made normal to the surface, what is observed is an interference color corresponding to an average separation of the two surfaces; ie., optical interferometry measures essentially the separation of two perfectly smooth surfaces and superimposed on this, although not observed, are the roughness peaks and valleys. This is why optical measurements in pure rolling agree well with theory since the predicted film thickness relates to the separation of smooth surfaces and small roughnesses have little effect.

The calibration technique used in determining what thickness corresponds to each interference color is of course of vital importance. The method employed was to load the ball against the plate to achieve a dry, static, Hertzian contact. A color interferogram was made of the "Newton's rings" pattern in air surrounding the contact area. By comparing this against Hertz's equation for the separation of a smooth ball and plate of known materials it was possible to obtain an accurate calibration for the average optical thickness between the surfaces at any radius. The effect of small surface roughnesses is simply to reduce the fringe visibility, and does not affect the calibration. For example, if a green interference color is observed, it could represent a uniform film thickness caused by separation of smooth surfaces, or it could represent the average separation of rougher surfaces with corresponding interference colors ranging from blue through green to yellow.

The X-ray technique, however, measures the minimum overall separation of the rough surface peaks and does not "see" the valleys at all, as illustrated in Fig. 6. This fact is not overcome by the calibration technique, which also measures the minimum separation of peaks, using a mechanical method involving the use of a fine screw thread separator and a dial gage. The two separation measurements are, therefore, self-consistent, the dial gage indicates zero separation for zero X-ray transmission. Nevertheless, the calibrated film thickness is not truly representative of what is generally understood by the term "film thickness," ie., the separation of two smooth surfaces on which are superimposed the roughnesses. Consequently, the experimental results may be expected to yield estimates of film thickness which are less than the predicted ones which relate to the separation of the surface center lines, h_{cla}. This idea can be tested by estimating the height of peaks which are present in sufficient numbers to be opaque to the X-rays and cast a complete shadow. Obviously, there may be occasional peaks which are an order of magnitude higher than the rms roughness value but so long as they are rare they will be unimportant. Designers generally allow for peak heights of about four times the rms value being common. So for the results in [13] one might expect the X-ray estimate of film thickness to be 2000 Å too small for each surface, ie., 4000 Å too small altogether, when compared with theory. For large film thicknesses this difference is not particularly important, but for small film thicknesses it is crucial. This fact is readily illustrated by adding 4000 Å to each experimental film thickness value as in Fig. 7 taken from [13]. The logarithmic method of plotting causes the high pressure (low film thickness) results to be raised by much more than the low pressure (high film thickness) results. Clearly the excessive fall of film thickness with load, observed by the X-ray method, is now largely eliminated and it is reasonable to draw straight lines through the modified points. The slopes of these lines vary from −0.28 to −0.42. This implies values of a in the range 0.09 to 0.14 which now compare well with the values in Fig. 3. The values of a taken from the unmodified data and assuming initial linearity at low pressures were considerably higher. So this explanation of the difference between X-ray data on h_m and the values predicted by theory, fits the facts very well. However, it should be stressed that it is not only the extreme pressure results which are affected, they are just affected most on a logarithmic scale since they represent the lowest film thicknesses. The low pressure film thicknesses are raised by the same amounts, numerically, due to the suggested modification and so one must examine whether the film thickness/speed results are thrown out by the modification and invalidate it.

In fact Parker and Kannel [13] found that their film thickness data for h_m fell below the theoretical values by a few thousand angstroms so this modification actually makes their data fit the theory much better. The exception to this is the data of [13] relating to a synthetic paraffinic oil (fluid 1) containing an organic phosphonic antiwear additive, which was found to fit the theory quite well anyway, without the modification. This is an extremely

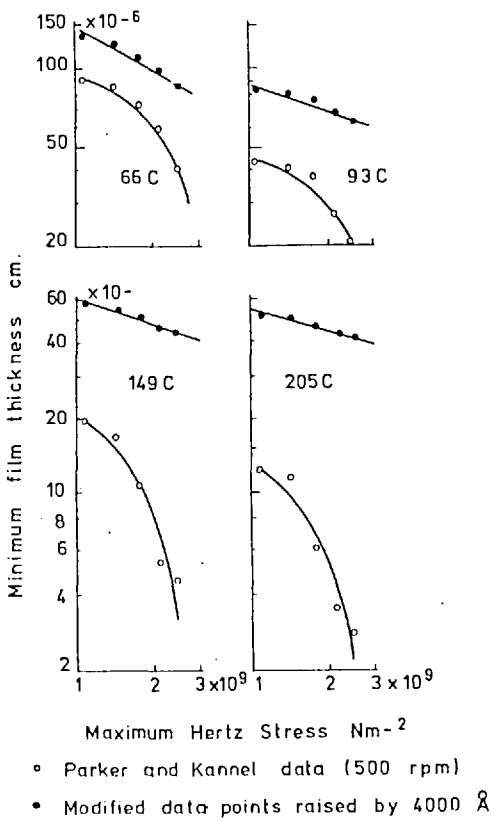

Fig. 7 Surface roughness effect on the X-ray data

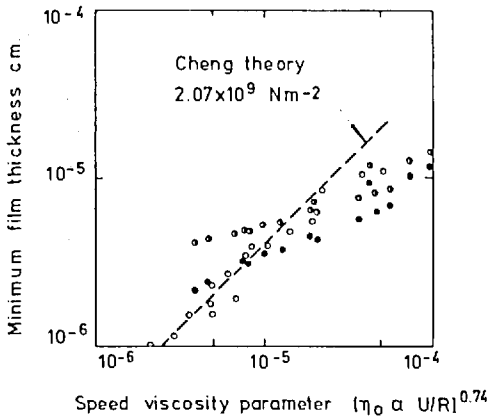

- ○ Synthetic paraffin + additive
- • Synthetic paraffin data + 2000 Å
- • Synthetic paraffin data + 4000 Å

Fig. 8 Modified X-ray data compared with theory

interesting situation since it can be used to add weight to the idea of surface roughness modifying the X-ray film thickness data, as follows. Gentle and Day [17] investigated the action of this additive using elastohydrodynamic and chemical techniques. They showed that this particular additive forms residual surface films on a steel ball immersed in the lubricant. At a temperature of 150 deg C, a film of up to 3000 Å in thickness was formed, and remained when the ball was removed from the lubricant. It appeared from [17] that these films were, however, too fragile when subjected to shear to withstand passing through ehd contacts when the underlying surface was of the smoothness used in optical or capacitance techniques. Cameron and Westlake [18] had already pointed out that experimental evidence for the effect of additives on film thickness in rolling contacts came not from the optical or capacitance methods but from techniques which use rougher surfaces. It seems likely therefore that the residual films, although fragile, could withstand rolling ehd contact conditions if they were sheltered in the roughness valleys. Any residual film on the roughness peaks would be swept away by the inlet shear and the result would be a surface where the roughness valleys were filled in by a semi-solid residual film of the additive. In the case of the X-ray data on the additive-containing fluid, the surfaces become essentially very smooth and the center line average corresponds to the average peak height used in the modification. Consequently, the theoretical predictions of elastohydrodynamic film thickness should for this case be reckoned from this new, higher, smooth surface rather than from the actual center line. Since this new surface is at the peak height which is "observed" by the X-rays, it is to be expected that the X-ray data does agree with the theory quite well. In addition if an estimate of the residual film thickness is made and added to the data of film thickness versus speed for the base lubricant, then the data for the additive-containing fluid should be reproduced. Fig. 8 shows the original results for the additive-containing fluid together with data points for the base fluid which have been modified by two estimates of the residual film. As will be seen, the modified results fall within the range of the original results. The high slope found in the results of (13) for the base fluid is lowered to the value for the additive-containing fluid since, once again, the modification of adding a constant film thickness has more effect at lower film thicknesses. In fact the new slope is rather lower than predicted by theory, evaluated by Parker and Kannel, and the data starts to tail off at high values of the speed-viscosity parameter. However this phenomenon is quite common and is generally accredited to inlet shear heating (16) or more recently to a critical shear stress (19), neither of which is taken into account in the theory.

One further point which ought to be mentioned while discussing these X-ray results is that the residual film idea explains only the data for crowned disks (13) and offers no explanation for the data on crowned cone disks.

Conclusions

The findings of Gohar [11] that central film thickness decreases uniformly with load, even up to very high pressures, have been confirmed using the technique of optical interferometry on a rolling elastohydrodynamic contact. Data on the variation of minimum film thickness, although approximate, pointed to the fact that nothing startling was occurring there either. This has been substantiated by Johnson and Roberts [20]. As a result it was necessary to find why there should be a discrepancy between this data and that from optical sliding measurements and X-ray measurements.

Firstly, the optical sliding central film thickness data was reproduced for one fluid, which showed that the discrepancy here must be due to the sliding itself. It was suggested that the cause of this was frictional heating in the contact raising the temperature of the inlet very quickly. So quickly, in fact, that the order of the results becomes irrelevant. Experiments at elevated temperature in rolling showed that an inlet temperature rise of less than 8 C was necessary to explain the results. In view of this, it is suggested that values of h_m obtained in sliding should not be compared against isothermal theory.

Secondly, the X-ray data was examined, bearing in mind the effect of looking along the rougher surfaces used here. It was found that the roughness peaks gave a false interpretation of the film thickness being observed by the X-rays when compared against the value used in theory.

Modification to take account of this made the data of [13] fit theory quite well. Some evidence was also found for additives forming residual films which cling to the valleys of rough surfaces and make them effectively very smooth.

In conclusion, it seems that optical interferometry offers the best method of examining elastohydrodynamic theory even up to extreme pressures, and finds that the isothermal theory fits rolling data quite well. On the other hand X-ray data is probably of more use in practical situations since it detects the real minimum film thickness and can study the effects of additives for rougher surfaces which are generally found in bearings and are not suitable for interferometry.

Acknowledgments

The work was partly supported by the Science Research Council. The fluids were supplied by Mr. R. L. Johnson of NASA—Cleveland Research Center who has been very helpful in coordinating all this film thickness data.

References

1 Dyson, A., Naylor, H., and Wilson, A. R., "The Measurement of Oil Film Thickness in Elastohydrodynamic Contacts," *EHL Symposium, Proceedings of the Institution of Mechanical Engineers*, 180 (Pt. 3B), 1965-66, p. 119.

2 Spidle, R. W., and Archard, J. F., "Experimental Investigation of Elastohydrodynamic Lubrication at Point Contacts," Paper C2/72, *EHL Symposium, Institution of Mechanical Engineers*, April 1972.

3 Cameron, A., and Gohar, R., "Optical Measurement of Oil Film Thickness Under Elastohydrodynamic Lubrication," *Nature*, Vol. 200, 1963, pp. 458–459.

4 Archard, J. F., and Kirk, M. T., "Lubrication at Point Contacts," *Proceedings of the Royal Society of London*, A 532, 1961, p. 52.

5 Foord, C. A., Wedeven, L. D., Westlake, F. J., and Cameron, A., "Optical Elastohydrodynamics," *Proceedings of the Institution of Mechanical Engineers*, 184 (Pt. 1, No. 28), 1969–70, p. 487.

6 Sibley, L. B., and Orcutt, F. K., "Elastohydrodynamic Lubrication of Rolling-Contact Surfaces," *ASLE Trans.*, Vol. 4, 1961, pp. 234–249.

7 Kannel, J. W., and Bell, J. C., "Interpretations of the Thickness of Lubricant Films in Rolling Contact I. Examination of Measurements Obtained by X-rays," TRANS. ASME, Series F, JOURNAL OF LUBRICATION TECHNOLOGY, Oct. 1971, p. 478.

8 Dowson, D., and Higginson, G. R., "New Roller-Bearing Lubrication Formula," *Engineering*, London 1961, 192, p. 158.

9 Archard, J. F., and Cowking, E. W., "Elastohydrodynamic Lubrication at Point Contact," *EHL Symposium, Proceedings of the Institution of Mechanical Engineers*, 180 (Pt. 3B), 1965-66, p. 47.

10 Cameron, A., and Gohar, R., "Theoretical and Experimental Studies of the Oil Film in Lubricated Point Contact," *Proceedings of the Royal Society of London*, A 1966, 291, p. 520.

11 Gohar, R., "Oil Film Thickness and Rolling Friction in EHD Point Contact," ASME/ASLE Lubrication Conference, 1970, Paper No. 70-Lub-2.

12 Lee, D., Sanborn, D. M., and Winer, W. O., "Some Observations of the Relationship Between Film Thickness and Load in High Hertz Pressure Sliding Elastohydrodynamic Contacts," TRANS. ASME, JOURNAL OF LUBRICATION TECHNOLOGY, Vol. 95, No. 3, July 1973, pp. 386-390.

13 Parker, R. J., and Kannel, J. W., "Elastohydrodynamic Film Thickness Between Rolling Disks with a Synthetic Paraffinic Oil to 589 K," National Aeronautics and Space Administration, Technical Note, TN D-6411.

14 Wedeven, L. D., L. D. Evand, D., and Cameron, A., "Optical Analysis of Ball Bearing Starvation," ASME/ASLE Lubrication Conference, 1970, Paper No. 70-Lub-19.

15 Winer, W. O., et al., verbal presentation at "Limits of Lubrication Conference," Imperial College, London, 1973.

16 Greenwood, J. A., and Kauzlarich, J. J., "Inlet Shear Heating in EHL," TRANS. ASME, Vol. 95, Series F, No. 4, pp. 417-426.

17 Gentle, C. R., and Day, R. S., "Effect of Some Antiwear Additives on the EHL of a Point Contact," Tribology Convention, Institution of Mechanical Engineers, 1972, Paper C81/72.

18 Cameron, A., and Westlake, F. J., "Optical EHD Fluid Testing," ASME/ASLE Conference, 1971, Paper 12.

19 Adams, D. R., and Hirst, W., "Frictional Traction in Elastohydrodynamic Lubrication," *Proceedings of the Royal Society of London*, A 332, 1973, pp. 505-525.

20 Johnson, K. L., and Roberts, A. D., "Film Thickness Variation with Load in EHL Contacts," *Wear*, 27, 1974, pp. 391-393.

Printed in U. S. A.